MACHETE

Martian Autonomous Critter-Housing for Extra Terrestrial Exploration

C. Akkermans	1356119	R.J. Grandia	4084993
F.D. Andriessen	1517619	B.F. Lagaune	4065174
S. Butter	4080173	M.R. van Reijen	4019156
R.J. Crone	1506870	N.M. van Schoote	4103947
G. Galatis	4085000	B. Walgaard	1534572

Final Report

Design Synthesis Exercise

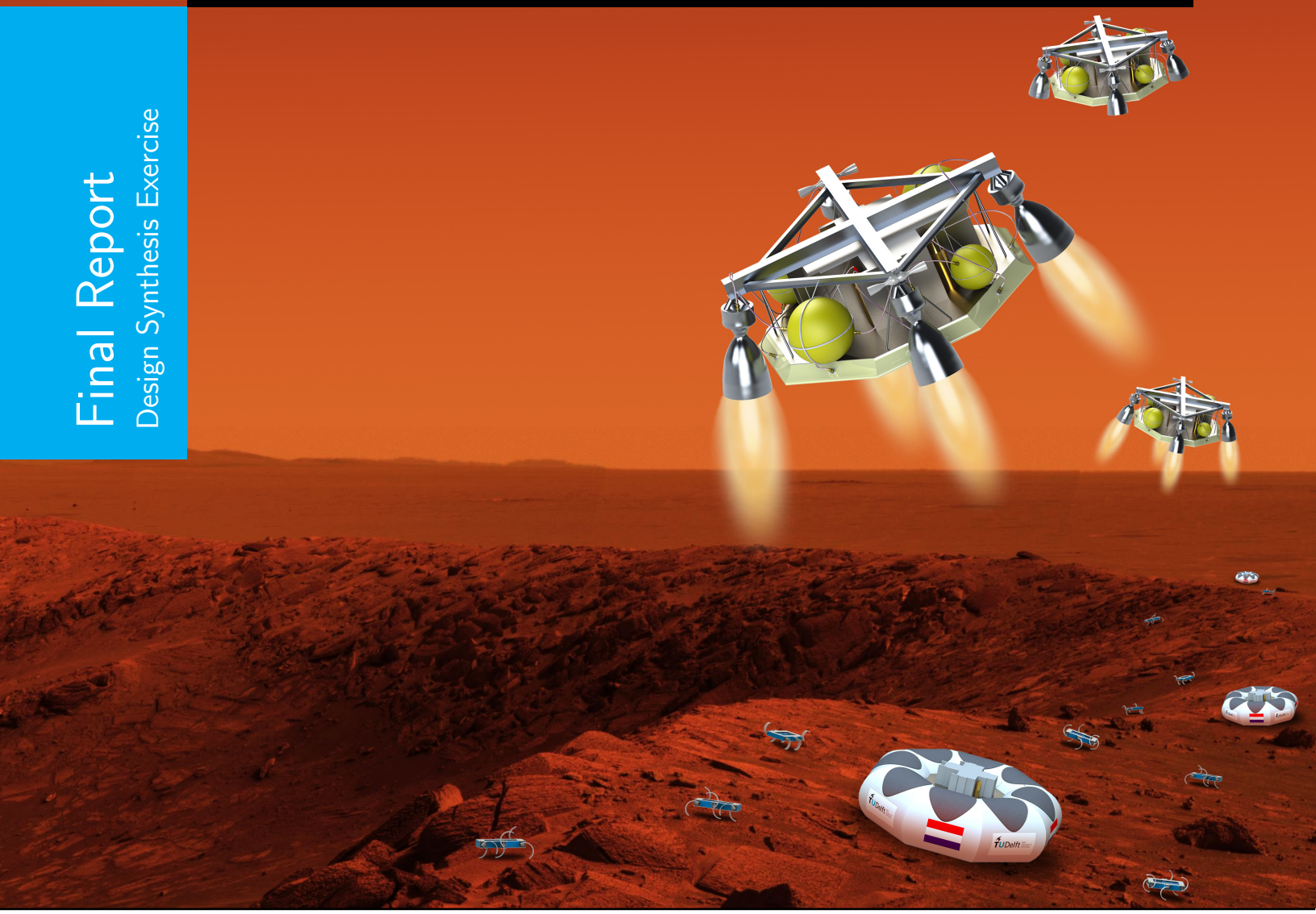

TU Delft Delft University of Technology

Aerospace Engineering

January 28, 2014

Preface

On 11 November 2013 group N08 received their assignment from their tutor Professor Chris Verhoeven. The mission: Design a system capable of landing a swarm of Zebros on the Martian surface. At first there was some confusion since most of the group members expected they where going to design a VTVL vehicle, but soon ideas started forming on how to achieve the new mission goal.
This project proved to be challenging on many levels, from the system engineering side to engineering and programming side this project combined a lot of the courses from the bachelor program. We had a well balanced team with a great skill in internal communication, this especially contributed to the projects progress and the final product that we achieved to create. Our team would like to thank Chris Verhoeven for his input on the project and the opportunities he created for us. We would also like to thank our two coaches Abhishek Bhat and Thomas Scholcz for their critical view on the technical aspects of the project during the reviews and weekly meetings. Without the help of professor Coen de Visser and professor René van Paassen the simulation model would not have been as far and solid as it is today. We would like to thank Barry Zandbergen for helping us out with his advise and the book provided on rocket propulsion. From the space department we want to thank Steven Engelen for his critical view on our findings, and from the Zebro team we want to thank Eric Smit for the detailed information on the Zebros. At last we want to thank the Technical University of Delft for providing us with the needed resources to perform the research and documenting on the project. This DSE project has been a great learning experience for all of us.

C.(Christ) Akkermans
F.D.(Frerik) Andriessen
S.(Sjoerd) Butter
R.J.(Robert) Crone
G.(Giorgos) Galatis
R.J.(Ruben) Grandia
B.F.(Bastiaan) Lagaune
M.R.(Marc) van Reijen
N.M.(Nathan) van Schoote
B(Bart).Walgaard

Summary

In order to put man on Mars, the planet needs to be explored to find suitable living areas. The following report contains the detailed design of the next generation of autonomous planetary exploration landers, capable of hosting and deploying multiple payloads, a swarm of Zebro's. Zebro's are six legged scavenger robots approximately the size of a text book. They were recently developed at the faculty of Electrical Engineering at the Technical University of Delft.

This report presents the work that has been done in ten weeks by a group of ten students for their Bachelor graduation project at the faculty of Aerospace Engineering of the Technical University of Delft. The mission need statement is:

"Safely land a swarm of Zebro robots on the Martian surface."

In this project, a systems engineering approach has been taken, consisting of identification and quantification of system goals, creation of alternative system design concepts, performance of design trades, selection of the best design, and verifying that the design has been made properly. Also recommendations on validation procedures are given.

This system is referred to as the Martian Autonomous Critter Housing for Extra Terrestrial Exploration or MACHETE. This revolutionary concept is an evolution of the traditional planetary lander vehicle that deploys a single rover. The MACHETE is completely autonomous, suitable landing sites are chosen on the spot utilizing advanced sensors. As to its capabilities it is not restricted to one single payload, but it is designed to deploy 28 Zebro's per lander, each of which can carry their own payload. This makes this a very flexible mission. The landers are known as the Clustered Autonomous Extraterrestrial Ship for the Allocation of Robots or CAESAR and up to eight CAESAR's can be hosted in the MACHETE. During the last stage from CAESAR to Martian surface the Zebro's will be protected by the Landing And Deployment System or LADS.

As discussed with the customer, the MACHETE is sized such that the launch, interplanetary transfer, and hypersonic re-entry vehicles similar to that of the Mars science laboratory mission can be used. Consequently, for these phases, the technical feasibility is ensured and the development costs are minimized.

The mission is clustered after the MACHETE stage, as opposed to after the CAESAR stage, because the former provides higher mission reliability. Furthermore, when landing eight systems in parallel instead of in series, more accurate and efficient landing spot determination can be performed. These advantages outweigh the mass penalty, which is in the order of few percent.

Based on the above mission profile and customer demands, several top level requirements can be outlined. The swarm has to be deployed within a 1 km precision on the Martian surface. This mission has to be performed autonomously and should protect the payload from launch till deployment.

The attitude determination and control system department has designed a system comprising of sensors and a description of the actuators needed. By constructing a simulation in Simulink®, the feasibility of the designed controllers was demonstrated. This simulation showed it is possible to use the designed systems to reach the landing zone. After arriving at the landing zone, the actual deployment and hazard avoidance of the LADS was done using a flash LiDAR system.

The propulsion and parachute department has designed the steerable supersonic parachute and thruster systems. An AGAS, the US army's Affordable Guided Airdrop System, based parachute system with a ringsail parachute was selected as starting point. This system has been proven in Martian like atmospheric conditions. In order to determine the achievable distance using the guided parachute, a simulation was performed. From the simulation it is concluded that in the worst case scenario 2 km can be traversed. However, 1 km wind drift is estimated. Together with the 3.25 km entry uncertainty, this means that using a parachute alone would not meet the 1 km precision requirement. For the rocket stage, the selected propellant

combination of nitrous oxide and ethane provides both high performance and is eco-friendly. It was verified that there should be no major technical hurdles in designing an engine which is capable of throttling to the required low power levels. The combination of a fairly novel propellant combination and deep throttling, however, will probably lead to a significant development process.

The structural design department has designed a system to carry all the payload and systems within the aeroshell. The MACHETE in the aeroshell has been designed to have 12 vertical beams supported by 16 horizontal rods holding the eight CAESAR's in place. After safely releasing the 8 clusters, the structure of the CAESAR's has been designed to have enough structural integrity to resist the differential thrust from the rockets engines. The 28 Zebro's per CAESAR are packed in four columns of seven. They are held in place with a magnesium shell laying on top of an octagonal raster of I-beams covered by a magnesium plate. The rockets and fuel tanks have their own square shaped structure composed of aluminium I-beams.

The touchdown department designed the final phase of the mission; the landing. After release from the CAESAR at 30 m from the Martian surface, the LADS will begin a four second free fall. The inflation of the octagonal shaped vented airbags begins 1 second after release. In the remaining three seconds, four Cool Gas Generation tanks inflate the 5 m^3 airbag to a pressure of 12 kPa. Directly after impact the airbag will be entirely vented by means of eight 0.4 m^2 vents located on each section of the airbag. Vent control will be done using either a series of strain gages located on the bottom of the airbag or a radar/motion sensor on top of the airbag. With this system the LADS can cope with 0.5 m high rocks and slopes up to 10 deg. Spectra 75 fibre is selected as the airbag material, as it provides the best puncture resistance under the low Martian atmospheric temperature. Also, it is shown that Zebro's can adequately crawl on this material after deployment.

The power and command & data handling department has created a system that is capable of providing enough power over the duration of the mission. This department was also tasked with providing an interface between the different subsystems and a way of transferring the collected data to Earth. By choosing Lithium Iron Phosphate batteries the power demand was satisfied without a significant mass penalty. Communication will be handled via both the MRO and MO using an UHF antenna and directly to Earth using an X-band low gain antenna. To protect the electronic systems from bit flips, a triple voting algorithm is implemented.

With the presented design, it is found that within the limits of currently off-the-shelf and demonstrated technologies, it is possible to land a swarm of 224 Zebro's on Mars. With a total system mass of 3052 kg entering the atmosphere, and a total Zebro mass of 896 kg, the achieved payload ratio is 29%.

For the validation it is recommended that parachute deployment is tested in a supersonic windtunnel. The parachute control performance can be tested at high atmospheric altitudes. The release sequence of the CAESAR's requires thorough simulation. A full scale CAESAR demonstrator is recommended to validate the beacon communication together with the control system performance. Full scale airbag test should be performed to validate inflation time, airbag puncturing, and vent system performance.

Contents

List of Figures

List of Tables

List of symbols

α	Coefficient of thermal expansion	$\mu \cdot K^{-1}$
α_d	Parachute thrust steering angle	rad
χ_a	Aerodynamic heading angle	rad
$\dot{m}$	Mass flow	$m \cdot s{-}1$
η_w	Parachute winch motor efficiency	-
γ	Specific heat ratio	-
γ_a	Aerodynamic pitch angle	rad
$\hat{m}_{ctrl1}, \hat{m}_{ctrl2}$	Unit vector of the pitch and roll, and yaw control moment	-
$\hat{z}_b$	Unit vector in the z direction of the body axis	-
$\mathbb{T}_{21}$	Transformation matrix from frame 1 to 2	-
μ_a	Aerodynamic bank angle	rad
ϕ	Body roll angle	rad
ϕ_T	Main thruster orientation angle	rad
ψ	Body yaw angle	rad
ρ	Atmospheric density	$kg \cdot m^{-3}$
ρ_{mat}	Material density	$kg \cdot m^{-3}$
σ	Stress in a beam	MPa
σ_y	Material yield strength	MPa
τ	Shear stress in a beam	MPa
τ_{par}	Parachute response time	s
τ_{yaw}	Settling time for the yaw control	s
θ	Body pitch angle	rad
ζ	Damping ratio	-
A	Cross sectional area of a beam	m^2
A_T	Matrix transforming individual thrust levels to resulting forces and moments	-
A_{vent}	Vent area	m^2
b	Beam width	m
$C(s)$	Transfer function for the PD controller	-
C_D, C_L, C_{st}	Drag, lift, and parachute steering coefficient	-
c_g, c_p	Center of gravity, and pressure location w.r.t. geometrical center	m
d	Beam diameter	m
D_0	Parachute canopy reference diameter	m
d_i	Distance from thruster #i to geometrical center	m
d_i^*	Moment arm for thruster #i around the center of gravity	m
d_{cable}	Cable length	m
E	Young's modulus	GPa
e_{ctrl1}	Angular error between F_{ctrl} and $\hat{z}_b$	deg
e_{ctrl2}	Angular rate error	deg
E_{gr}	Glide ratio	-
F	Force applied to a beam	N
$F(s)$	Transfer function for the filter	-
F_D	Parachute drag force	N
F_T	Total thrust force	N
F_w	Parachute wire force	N
F_{aero}	Force due to aerodynamics	N
F_{ctrl}	Desired control force in the body frame	N
F_{ctrl}^m	Desired control force in the Martian reference frame	N
F_{st}	Parachute steering force	N
$F_{T,i}$	Thrust force for thruster #i	N

g_E, g_M	Gravitational acceleration on Earth, and on Mars	$m \cdot s^2$
h	Beam height	m
$H(s)$	Simplified transfer function for the equations of motion	-
i	Number assigned to a thruster	-
$I_{a,ii}$	Area moment of inertia about a certain axis	m^4
I_{ii}	Mass moment of inertia about a certain axis	$kg \cdot m^2$
Isp	Specific impulse	s
J	Torsion constant	m^4
k	Discharge coefficient	-
k_d	Derivative control term	-
k_p	Proportional control term	-
L	Lift force	N
l	Beam length	m
L_{cable}	Cable loss	dB
l_{cable}	Cable loss per meter	dB
L_{fs}	Free space loss	dB
M	Moment applied to a beam	$N \cdot m$
m	Mass	kg
M_T	Total moment due to thrust force	$N \cdot m$
M_{aero}	Moment due to aerodynamics	$N \cdot m$
M_{ctrl1}	Attitude control magnitude	$N \cdot m$
M_{ctrl2}	Yaw rate control magnitude	$N \cdot m$
M_{ctrl}	Total control moment	$N \cdot m$
M_{nit}	Molar mass of nitrogen gas	$g \cdot mol^{-1}$
m_{nit}	Mass of nitrogen gas	kg
n	Buckling mode	-
P	Airbag pressure	kPa
P_w	Parachute winch power	W
P_{atm}	Airbag pressure	kPa
P_{nit}	Pressure of nitrogen gas	kPa
Q	Pressure ratio	-
R_i, R_o	Beam inner radius, beam outer radius	m
R_u	Universal gas constant	$J \cdot (mol \cdot K)^{-1}$
S	Aerodynamic reference area	m^2
s	Laplace parameter	Hz
s_i	Length of beam segment i	m
T	Torsion applied to a beam	$N \cdot m$
t	Simulation time	s
t_1	I-beam horizontal flange thickness	m
t_2	I-beam shear web thickness	m
T_s	Settling time	s
t_w	Parachute winch time from minimum to maximum	s
T_{atm}	Mars atmospheric temperature	K
T_{nit}	Temperature of the nitrogen gas	K
t_{wall}	Wall thickness	m
V	Velocity	$m \cdot s^{-1}$
v	Airbag volume	m^3
v_{nit}	Volume of nitrogen gas	m^3
W	Weight	N
w_f	Filter cut-off frequency	$rad \cdot s^{-1}$
w_n	Natural frequency	$rad \cdot s^{-1}$
$X(s)$	Transfer function of reference signal	-
$Y(s)$	Transfer function of output signal	-
y_n	Distance from the neutral axis	m

List of abbreviations

ADCS	Attitude Determination and Control System
AGAS	Affordable Guided Airdrop System
CADH	Command and Data Handling
CAESAR	Clustered Autonomous Extraterrestrial Ship for the Allocation of Robots
CECE	Common Extensible Cryogenic Engine
CGG	Cool Gas Generator
COPV	Carbon fiber Overwrapped Pressure Vessels
CPU	Central Processing Unit
CR	Carbon Reduction
DGB	Disk Gap Band
DoF	Degree of Freedom
EDL	Entry, Descent, and Landing
EDLD	Entry, Descent, Landing, and Deployment
EOM	Equations of Motion
EPIRB	Emergency Position Indication Radio Beacon
EPS	Electrical Power Subsystem
ESA	European Space Agency
ESTEC	European Space Research and Technology Centre
FBD	Functional Breakdown Diagram
FBS	Functional Breakdown Structure
FEM	Finite Elements Method
FFD	Functional Flow Diagram
FPGA	Field Programmable Gate Array
F-RAM	Ferroelectric Random Access
GB	Gigabyte
HDA	Hazard Detection and Avoidance
HR	Hazard Reduction
HRN	Hazard Relative Navigation
HTP	High Test Peroxide
ILS	Instrument Landing System
IMU	Inertia Measurement Unit
LADS	Landing And Deployment System
LIDAR	Light Imaging Detection and Ranging
LMDE	Lunar Module Descent Engine
LS-DYNA	Livermore Software (nonlinear) transient DYNAmics
MACHETE	Martian Autonomous Critter-Housing for Extra Terrestrial Exploration
MER	Mars Exploration Rover
MIPS	Millions of Instructions Per Second
MMH	Mono-methylhydrazine
MO	Mars Odyssey
MPF	Mars Pathfinder
MRO	Mars Reconnaissance Orbiter
MSL	Mars Science Laboratory

NASA	National Aeronautical and Space Administration
NDB	Non-Directional Beacon
NOFBX	Nitrous Oxide Fuel Blends
NPO	Nitrous Oxide Propane
NSD	NASA Standard Detonator
PCADH	Power, Command, And Data Handling
PCM	Phase Change Material
PD	Proportional Derivative
RAMS	Reliability, Availability, Maintainability, and Safety
RP-1	Kerosine
RPL	Rate Power Level
S/C	Spacecraft
SD	Sustainable Development
SDS	Sustainable Development Strategy
SMAD	Space Mission Analysis and Design
SPCGG	Solid Propellant Cool Gas Generator
SPGG	Solid Propellant Gas Generator
TBD	To Be Determined
TLS	Transponder Landing System
TRN	Terrain Relative Navigation
UHF	Ultra High Frequency
VA	Venting Area
Vectran HT	Vectran High Tenacity
VL1	Viking Lander 1
VL2	Viking Lander 2
WEB	Warm Electronics Box
Zebro	Zes Benige Robot

1 Introduction

Ever since the manned missions to the moon in the 1970's, man has been eager to put a man on Mars. So far that dream has not turned into reality; only missions carrying robots have visited Mars. These robotic missions, however, suffered from the fact that they are fragile and limited in range. While quite a few of the missions were highly successful relative to their design mission, they only covered little ground on Mars.

One method to improve the exploration range considerably, would be to send a swarm of robots to the Martian surface. Swarms of robots can easily cover large amounts of surface area and offer the opportunity to explore interesting terrain features like caves. Because the fate of no single individual robot is detrimental to the whole of the mission, operation with higher risks can be performed with potentially a higher pay-off. Therefore, the mission need statement for this study is:

"Safely land a swarm of Zebro robots on the Martian surface."

It is assumed that the mission will follow a similar pattern as the Mars Science Laboratory mission up to the point of its atmospheric entry. Central is the requirement to use off-the-shelf technologies while also pushing technological boundaries. Technologies chosen are thus required to have at least been demonstrated experimentally.

After exploring various possible post atmospheric entry landing scenarios in the baseline report [25], the most promising ones were worked out in the midterm report [26]. In addition, the midterm included identification of and downselecting the large number of subsystem design options. Based on the selected design options in the midterm report, initial mass and size estimations were obtained.

In this report, the mission design is further detailed. In order to obtain a more precise estimation of the required propellant masses and various other primary design parameters, a detailed simulation of the rocket powered landing phase was constructed. By constructing the simulation in Simulink®, the feasibility of the designed controllers is demonstrated. In addition the simulation allows for detailed sensitivity analysis.

To be able to make a distinction between the different phases of the mission, three names have been defined that allow a clear distinction to be made between the different mission phases. When the ship enters the Martian atmosphere it is called the Martian Autonomous Critter Housing for Extra Terrestrial Exploration or MACHETE. While descending it will split into eight Clustered Autonomous Extraterrestrial Ships for the Allocation of Robots or CAESAR. These eight CAESAR's will then navigate toward the landing spot where they will drop the Landing And Deployment System or LADS. This system will absorb the ground impact and deploy the swarm of Zebro robots.

The report is divided in three main parts: project outline, technical design, post design operations.

The first part gives an overview of the project and the overall design approach. It starts with Chap. 2 on systems engineering and project management, where the different functions of the system are defined and a functional mission overview is given. Chapter 3 then explains the sustainability approach taken. After this, Chap. 4 gives a short recapitulation of previous work, which can be found in more detail in the baseline and midterm reports[25] [26]. Ending part one is then Chap. 5 with the overview of used assumptions, requirements and constraints throughout the entire project.

The second part gives the technical design of the MACHETE, CAESAR, and LADS. It goes through the detailed design results of the five departments in the following order. This part starts with Chap. 6 about the attitude determination and control system, responsible for the stability and orientation of the system, and continues with Chap. 7 about the parachute and propulsion system. In Chap. 8 the lightweight primary structure of the system is discussed and in Chap. 9 the vented airbag and deployment system used for the LADS is described. In Chap. 10 the power and command & data handling system is discussed. Finally, Chap. 11 gives an overview of the complete system.

The third part is about the post design operations, this start with Chap. 12 which lists all requirements and whether they are met by the design. After this in Chap. 13 a risk assessment of the whole mission is given and then in Chap. 14 the possible continuation of this project is described together with a cost estimation. Finally, in Chap. 15 conclusions are drawn regarding the entire project and recommendations for a future project are given.

Part I: Project outline

The first part of this report will deal with the project outline. The project outline will provide the reader with an overview of the approach taken in designing this challenging mission to the Martian surface. The result of various system engineering tools are presented and a resource breakdown is given.

Next, the reader is informed on the used sustainability approach during project. During the project it was not only attempted to come up with a sustainable system design, but also the sustainability of the design process itself was examined.

Following the sustainability approach, a recapitulation of the previous work is presented. This final report builds on two previous works; the baseline report [25] and the midterm report [26]. In order to get the reader up to speed on the work described in these reports, all important decisions and trade-offs made during the writing of these reports are explained.

Finally the starting point for the design is laid down in the assumptions, requirements and constraints. Using the boundaries and guidelines laid out in this chapter, the final design was constructed. Lastly some considerations on the possible landing sites on Mars are given. While no final landing site is given, there are a few assumptions made on the landing site, which see their effect in the eventual selection of a landing site.

2 Systems engineering and project management

This chapter will inform on the functions that the system will perform in a systematic manner and give an overview of the resources that were available for the project. It will start by showing the functional breakdown structure (FBS) and functional flow diagram (FFD) of the system after which resource allocation and budgeting is given.

2.1 Functional breakdown structure

The FBS shows the different functions that the system has to perform divided in four different groups. The groups are (1) provide deceleration and control power, (2) provide control and navigation, (3) provide Zebro protection and deployment, and (4) provide power and command and data handling. The FBS can be found in Fig. 2.1.

2.1.1 Provide deceleration and control power

Power is required to control the body in order to slow down through the Martian atmosphere and to navigate towards a predetermined location. Slowing down through the Martian atmosphere is important for the first phase of the mission, where the MACHETE has just entered the atmosphere at Mach 1.5 and control power must be provided throughout the mission to navigate to a beacon with a precision of 1 km.

2.1.2 Provide control and navigation

In order to control the attitude of the body and navigate it towards the beacon a control system must be present that gathers sensor input and from this calculates the required response for navigating towards the beacon.

2.1.3 Provide Zebro protection and deployment

The Zebro's, which are the payload for this mission, must be protected from loads occurring during different stages of the mission. Also the must be activated and allowed to get out of the structure after touchdown.

2.1.4 Provide power and command & data handling

Electrical power is required for operation of several systems. Every control system requires it as well as some motors that are considered in the design. Furthermore it is important that during the mission data is collected and transmitted to Earth for analysis of mission performance.

2.2 Functional flow diagram

In the functional flow diagram the order in which the system has to perform its different functions is shown. The FFD can be found in Fig. 2.2. This functional flow diagram has been made with the final design in mind and as such shows the actual function that every part of the lander will have to perform to fulfill the mission. The first stage of the mission is where the MACHETE enters the atmosphere inside the aeroshell and the supersonic parachute is deployed. After reaching an altitude of 2.5 km the eight CAESAR's will be deployed and they will navigate to their separate landing locations around the beacon where they will drop the LADS. The LADS will with the help of an airbag absorb the impact from touchdown and deploy the Zebro swarm.

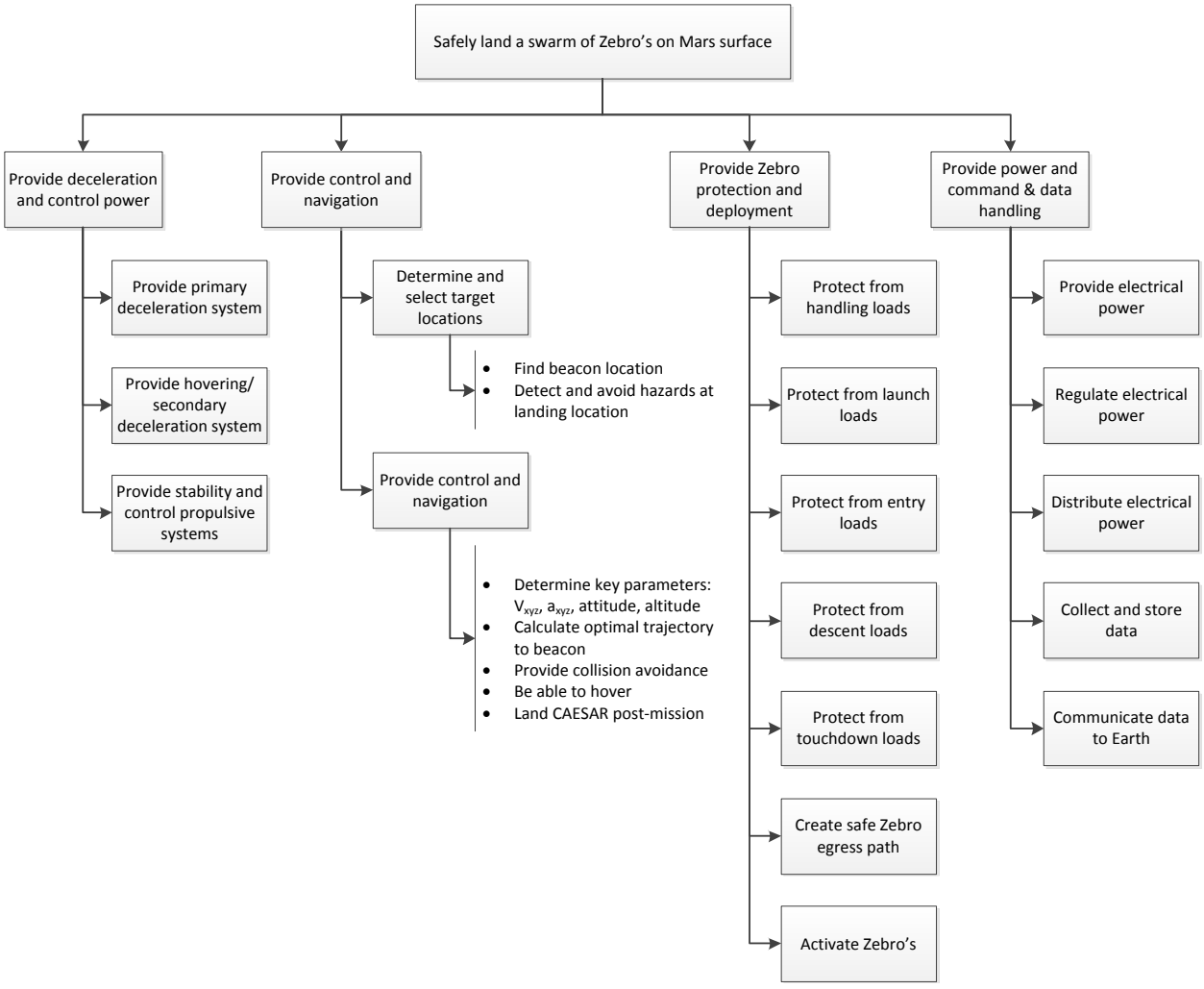

Figure 2.1: Functional breakdown structure

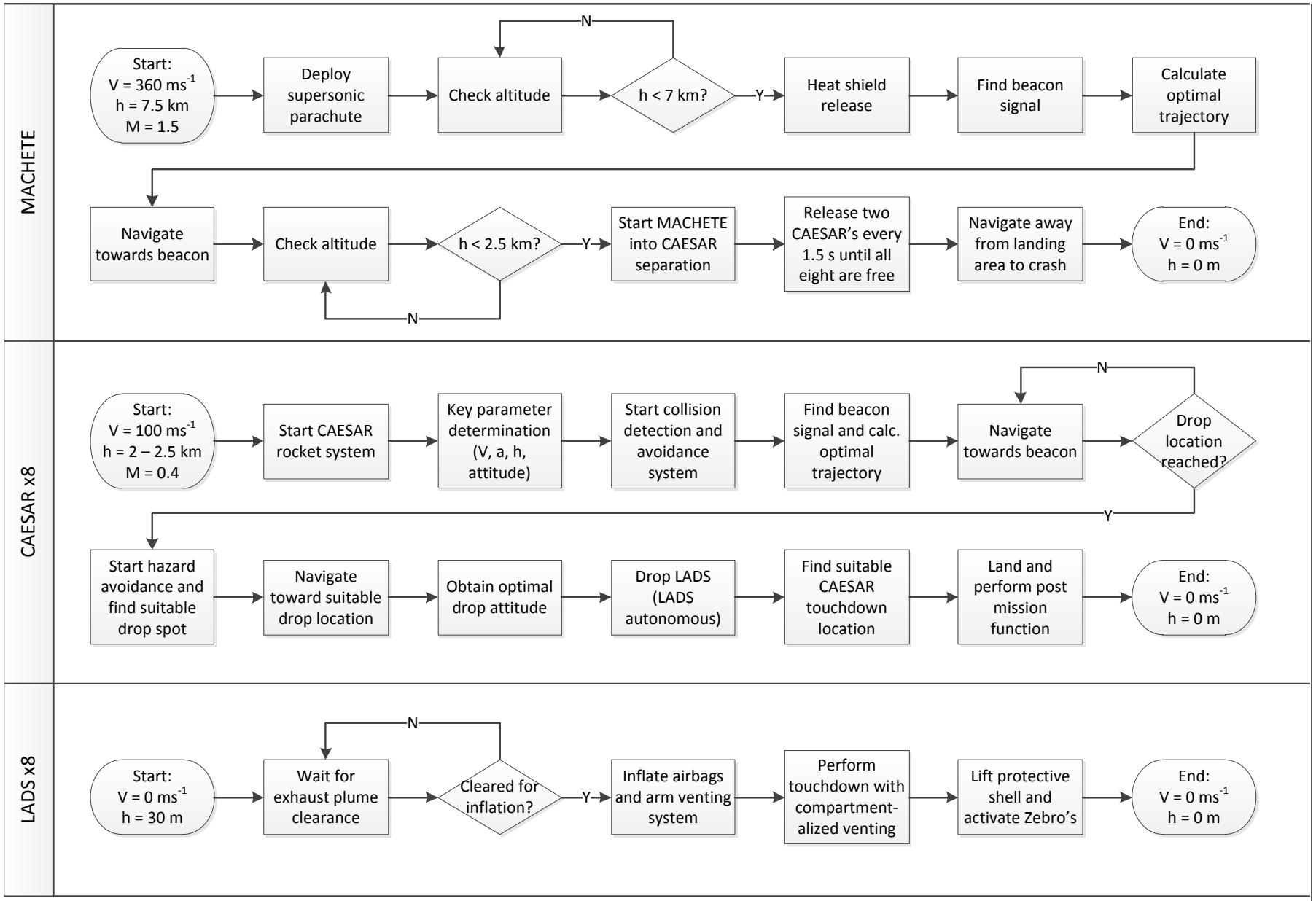

Figure 2.2: Functional flow diagram

2.3 Resource allocation and budget breakdown

This section will inform on how to effectively distribute available resources to reach the mission goals. Also a preliminary budget breakdown on the mission will be given along with a supporting description.

2.3.1 Resource allocation

Different kinds of resources are available during this project. To optimize the design and engineering aspects of the mission an effective distribution of these resources is essential.

The team consists of ten members which have ten full time weeks to complete the project. In order to investigate and structure the tasks to be done in these ten weeks three different tools are used. First a work break-down structure is made, this to get an overview of all the tasks to be done. The results from the work break-down structure can be categorized in the work flow diagram, this will help to identify which tasks can be done simultaneously and thus enable concurrent engineering. Finally, all the tasks will be displayed on a time-scale in the Gantt chart, the third tool. By identifying the tasks that need to be performed in the work flow diagram and work break-down structure and estimating the total amount of time to finish a task in the Gantt chart, human resources are effectively distributed to finish the tasks in the available time. By effectively noting down the task each team member is working on on the white board, a clear overview of tasks being done and task that still need attention is made.

Other resources taken into consideration are the available work space or workstations available. For this project, one table for ten persons is available. Two computers are available at the project table and every group member has a laptop at his disposal. Presentations and meetings can be held in a designated conference room.

The project made use of the knowledge resources within the TU Delft. For example, the Zebro team is part of the TU Delft Robotics Institute and the tutors are experienced in the fields of flight performance, propulsion and aerodynamics. When required, other knowledge resources are found within the broad spectrum of the TU Delft faculties.

2.3.2 Budget breakdown

The budget for this project is available only on request and will be given per idea separately. Ideas that are useful for promotion of continuation of the project are likely to be granted as long as they are in the order of magnitude of a hundred euro. Note that an estimation of the required budget for continuation of this project can be found in Sect. 14.5 based on reference missions.

3 Sustainable development strategy

In the proceeding section the team's specified goals and means to integrate sustainable development into its project will be presented.

The achievement of the total sustainable development of the system is of prime importance to the team. Providing a sustainable system that will be capable of a peaceful space exploration, will provide a long term socio-economic benefit [19, 24]. It will provide society with the technology that will raise the living standards of the citizens, but will also provide economic growth in its production phase. The initial conceptual design, up until the production and post function of such a system, will require a strong co-operation amongst the efficient use of environmental resources of terrestrial and space applications [48]. It will have to focus on the tri-fold concept of the interlinking concepts of the environmental, economic and social impact of the project.

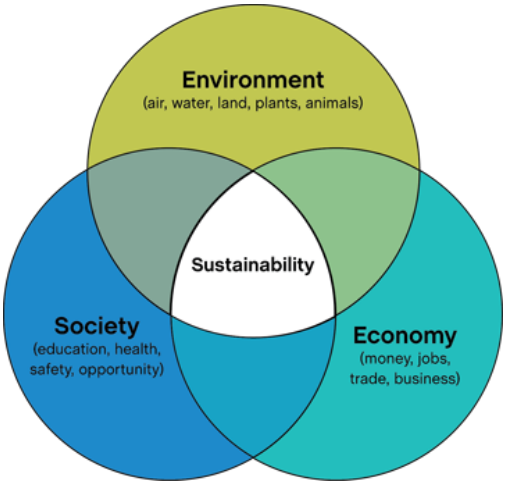

Figure 3.1: Tri-fold concept of the interlinking between the environmental, economic, and social impact. [48]

This system will be conceived and manufactured on Earth, but it will be operational in space. Based on the above mentioned research and design profile the sustainability actions can be sub-categorized in two main branches: terrestrial sustainable goals and extraterrestrial sustainable goals.

The terrestrial goals can be outlined as:

- *Transportation*
  Fuel emission is kept to a minimum by optimization of the systems mechanical structure.
- *Manufacturing*
  During manufacturing the use of more sustainable modes of production are needed. The inter-linkage of design, material and process must be such that environmental degradation is minimalised.
- *During design*
  The use of resources during the project design phase must be optimal; e.g. digital storage of information instead of paper copies.

While the system will be operating in an extraterrestrial environment, different sustainability standards must be set on the system itself.These requierments can be derived from the definition of sustainability:

"Sustainable development is development that meets the needs of the present without compromising the ability of future generations to meet their own needs.[1]"

Based on the above definition the post mission management of the system must ensure that it can be used either to support the operation of the Zebro mission, or to be used from a Earth based ground control to receive post mission data.

Mars exploration is under the microscope of the scientific community. Discovering the secrets of this planet will provide them with more clues on the lifelong questions of Earth's history. The discovery of any clues, as to the existence of past or present life forms on the planet will have a great impact on our understanding of our Earth. Reflecting back on to the definition of sustainability it is concluded that during production the system should not be contaminated with any terrestrial organisms that may corrupt the ability of future generations to explore the probability of the existence of life on Mars [55, 62]. Therefore, any form of contamination must be avoided. Also the lander design should be such that further (manned) Mars missions will not be endangered by the remains of it, and the remaining structure should not form a hazard for future man on Mars.

One other condition that can be linked with the above definition of sustainability, is the aspect that human interaction with the lander will occur. It is thus important to take this event under consideration, and design the lander such that it will not pose any threats to human explorers if handled.

3.1 Plan of approach

For sustainable development a strategy and a list of actions that meet the mentioned needs must be created. Meeting the actions that are listed below will ensure that the project is meeting its minimum requirements for sustainability [56].

- *Governance*
  will ensure that the mission statement will be in accordance with the sustainability development plan throughout the project.

- *Action plan*
  The action plan will include milestones, baseline figures and reports on the sustainability development of the project.

- *Reporting*
  This action will demonstrate progress by monitoring the process for emissions produced, chemicals that will be implemented or any biological contamination of the system or sub-systems. Reporting will also be used to estimate and compare if targets have been met. Also during this action the outline of specific, acceptable values will be set.

- *Division of sustainable planning*
  The sustainability plan will be sub-divided into sections that will ensure the assessment of the project and its risks for the environment, a section for adoption of the strategies used, as also a plan for compliance and assessment for forward contamination. action, assessment of the post-mission functionality of the system will be investigated in compliance with the needs of the customer or future customers that will utilize the system based on the market analysis.

For the readers that are interested to study in depth the "Sustainability development plan" we recommend them to read the mid-term report of [26].

3.2 Evolution of the Sustainable Development Plan

In the proceeding section the evolution of the sustainable development plan will be presented, from the initial design phase up until the completion of the project. Data will be presented that will allow to track the survivability of the sustainability development plan throughout course of this project. Toward the end of this chapter a conclusion will be drawn as to whether this plan was able to succeed. Proposals will be set while solutions to targets that where not achieved will be provided. As has been mentioned in the

previous sections the sustainability development plan has been divided into two parts, the terrestrial and extraterrestrial. While the plan of approach has been structured in a table format.

In the following tables are a presentation of the sustainable development plan, that will be followed. The column that rates the degree of compliance is a measure that rates to what extent the specific area has achieved its goals. A 10/10 score donates that the sustainable targets of that department have been met, while a score 1/10 donates that no targets have been met. The "weight" column in the table is a measure to identifie the significance of that section. Again 10/10 is most important, while 1/10 is least importance.

Table 3.1: A presentation of the sustainable development plan for the reduction of the carbon emissions produced while the project is in the research and design phase. Note: CR: Carbon Reduction SDS: Sustainable development strategy

Area Of CR	SDS objective	Degree of Compliance	Weight
Management	Set energy saving and carbon reduction schemes of the project team	7/10	3/10
Manufacturing	Meet low emission manufacturing standards	6/10	2/10
Transportation	Provide low carbon emission models for transportation between assembly sites.	6/10	7/10
Team development	Increase team awareness, and support behavioural change	8/10	5/10
Governance	Ensure that sustainability is embedded in each aspect of the project time-line	8/10	6/10

Table 3.2: A presentation of the sustainable development plan for the reduction of the hazards that may arise due to the use of toxic chemicals while the project is in the manufacturing and production phase. Note: HR: Hazard Reduction SDS: Sustainable Development Strategy

Area of HR	SDS objective	Degree of Compliance	Weight
Human hazards	Research chemicals used and potential health hazards	9/10	8/10
Environmental hazards	Research chemicals used and potential environmental damage	9/10	8/10

3.2.1 Paper consumed

Through the printer account it has been measured that the team has consumed 2100 A4 papers, in addition to the papers used as scrap to total amount is around 3100 pieces of A4 paper, according to How Much Information? 2003 filed by the University of California at Berkeley [2] , it has been estimated that a single tree can produce about 80500 sheets of A4 paper thus for the design and production of this project not even 4% of a tree was used as a resource.

Using a conversion factor of 6 GB of data per metric ton of paper [2] . Thus it can be estimated that, In total trees saved: 4.4 rounded 5 trees where saved.

Table 3.3: A Presentation of the sustainable development plan for the extraterrestrial use of the system. Note: SD: Sustainable Development, SDS: Sustainable Development Strategy

Area of SD	SDS objective	Degree of Compliance	Weight
Post mission use	Ensure that the system will have a post-mission function, and safe for future astronauts	7/10	8/10
Forward contamination	Ensure that contamination is minimised	8/10	7/10

Several comments that can be done based on the consumption of paper in correspondence to the use of it throughout out the project. It should be stated that the majority of the consumption of paper was used to print out drafts or original copies of reports required to distribute to staff members or supervisors for reviewing upon request or revision. The second most costly expense to paper was the use of it during the lunch breaks where it would be used as an eating mat, in average 14 A4 sized papers where used daily corresponding to 700 pieces of A4 paper. A solution to this phenomena would be to implement reusable eating mats during lunch breaks. It is suggested that these eating mats be provided by the faculty due to the fact that that they can be used by other students other than this group. As to the copies provided to the staff members and supervisors this expense in paper is unavoidable, the only measure that can be drawn would be to promote further the use of recyclable paper, or promote amongst the staff members the use of e-readers.

3.2.2 CO_2 production

The production of green house gases of the group, mainly CO_2, is done by indirect means. The duration of the project is mainly done on design basis and has little to none interaction with the heavy industry. According to the Environmental Energy Technologies Division of the U.S. Department of Energy [3], the manufacturing cost of one virgin A4 office paper is 17 Wh, while the production of 100% recycled A4 paper corresponds to 12 Wh of energy consumption. According to the U.S. Energy Information Administration in average it takes 0.84 kg of CO_2 to produce 1 kWh. Thus the total production of CO_2 just for paper and assuming a mixed rate between recycled and virgin paper, the CO_2 emissions just for one A4 paper consumption corresponds to 14.8 g of CO_2. Thus in total for paper consumption 45.8 kg of CO_2 was produced.

Carbon emission also was produced indirectly from the use of the personal computer of each group member. In average each personal computer requires 60 W of power to operate, thus per an eight hour work day each computer consumed 480 Wh of energy. To produce 1 kWh, on average it takes 0.84 kg of CO_2. Per day, each computer produced indirectly 403.2 g of CO_2, thus in total for 10 computers that have been used daily (number of group members) for the project duration of 50 days, 8 hours of work per day, has produced a total of 201.6 kg of CO_2.

As a consequence the total amount of CO_2 production for the conceptual design of the product is 247.4 kg.

Other parameters that add an additional CO_2 burden to the environment are the transportation cost of the ship from the manufacturing site to the launch site, and from the surface of Earth to its outer boundary of its atmosphere. This is inevitable but can be minimized with smart planning of the production locations.

3.2.3 Human and environmental hazards

Human and environmental safety is important when chemicals are being used. The lander consists of a power supply and a rocket booster, both containing chemicals. One criteria that the chemicals were chosen upon was the environmental and human hazards that may be caused if mishandled or released in the environment. Following are solutions to the concerns of the group, for any human or environmental hazards that may arise

during the production of the system. It has been investigated that hazards that could be a reflection of bad research and design. Focus is set on the chemicals used for the batteries as also the propulsion system.

Battery Supply ($LiFePO_4$)

The provided technologies that comes with this form of batteries have far superior thermal and chemical stability than other Lithium battery supplies , in consequence provides better safety characteristics than the usual Lithium-ion technology made with different cathode materials. In the case of unfortunate handling during charging or discharging times, Lithium Phosphate cells are incombustible, meaning that under overcharge or short circuit conditions they can withstand high temperatures without decomposing. Other safety advantages of this form of cell chemistry includes that the phosphate based cathode material if abused will not burn and is not prone to thermal runaway. The use of phosphates in the cells chemistry reduces the drawbacks of the cobalt chemistry, particularly on the cost, safety and environmental characteristics. All the above mentioned advantages, that Lithium Phosphate cells have when considering the human and environmental safety aspect as compared to other batteries, makes it a very eco-friendly and human hazard free choice [4].

Thruster fuel (Nitrous Oxide- Ethane)

Nitrous oxide-ethane is an eco-friendly oxidizer-oxidant fuel combination that releases non toxic gases to the environment. To be specific: N_2, CO, H_2O, H_2 and CO_2 are all non-toxic and produce no accumulated deposits or contamination. These two chemicals are relatively safe to handle, though there have been cases in the past where these chemicals have been mistreated resulting in fatalities[66]. As for ethane it poses no known acute or chronic toxicological risk.

3.2.4 Post mission management

After communication with our customer and having done a thorough market survey, it has finally been decided that the most efficient post mission functions that the lander may pursue are:

- Functioning as a power supply for the Zebro's.
- Functioning as a telecommunications hub for the Zebro's.

3.2.5 Forward contamination - Human interaction hazards

Forward contamination for the current mission will be avoided by proposing procedures and restrictions during manufacturing and in the assembly phase.

As for the protection of the human explorer that may come in contact with any of the ships, the MACHETE and CAESAR have been designed such that no sharp edges are present in the structure that may puncture the space suits of future pioneers. Reinforcements and attention stickers will be placed in positions where chemical leakages may occur.

3.3 Conclusion

In this chapter, a strategy and list of actions have been outlined that need to be followed. Governance has been outlined, to ensure that the mission statement is in-line with the sustainability development plan. Milestones have been set through out the project time-line while environmental awareness has been developed through out the team. Observing values of the outcomes of produced CO_2 as also looking upon the total amount of paper consumed, we may draw the conclusion that the team has been as sustainable as it could be with the resources that have been provided to it.

4 Recapitulation of previous work

As the MACHETE vehicle is nearing the end of the design phase this report will build on the work done earlier in order to reduce the content of this document. This work is documented in other reports already delivered to the Delft University of Technology [25, 26]. In order for readers to understand all the aspects of this document this chapter will explain all important decisions and trade-offs made during the project.

4.1 Baseline report

In the baseline report the planning of the project was created. The mission statement was formed and several mission scenarios were constructed according to the assumptions and constraints that were present. A study was performed to identify all theoretical landing and touchdown options, of which only the feasible methods were selected. Another study was done on the possibilities of Zebro deployment after or during landing. After this process different trade-offs were made which lead to a final choice in the mission scenario: A given entry using a heat shield, a super sonic parachute, clustered or non-clustered rocket descent, and an airbag touchdown. The transfer from Earth to Mars was assumed to be similar to the cruise of the Mars Science Laboratory.

4.2 Midterm report

During the writing of the midterm report more precise calculations were possible, giving more information about the clustering versus the non clustering situation. Several conceptual systems existed to perform the task these mission scenarios needed. So for each of the subsystems conceptual designs are made. The subsystems are ADCS, descent and propulsion, structural and deployment, touchdown, and power and command & data handling. For the ADCS sensors are selected and the logic flow for navigation is designed. For flight and propulsion the flight profile is defined and research is done on parachutes and wind drift and a shortlist is created of the possible propellants. For the structural subsystem the optimal way of Zebro stacking and attachment is chosen and material selection is done. For the touchdown system vented airbags are selected and the shape, fabric and gas generation systems of these airbags are designed. Finally for the power and command & data handling subsystem memory, battery, CPU, and antennas have been chosen. Several mass iterations have been made. This is a continuous process that also takes place during the final report. A preliminary design of the subsystem logic has also been made, together with a system layout.

4.3 Clustered and non-clustered landing trade-off

In the period between the wrapping up of the midterm report and the start of the final design phase, the landing scenario trade-off has been made. This trade-off could have been completed in an earlier stage but the customer wanted the team to keep the options open for as long as possible in order to be able to make a detailed trade-off.

In Table 4.1 the different criteria for trade-off are stated and marked with an 'X' for the scenario with preferable characteristics. For instance: the scenario with high reliability gets the 'X', but the scenario with the highest risk does not get it, this is reserved for the scenario with the lowest risk. It should be well understood that this trade-off is about whether or not the powered descent phase will be clustered. For clarity: If in this section the clustered scenario is chosen this means that after deployment of the parachute MACHETE will split up in clusters which will all have their individual landing systems (communication between them is possible). If the non-clustered scenario is chosen this means that MACHETE will not split up after deployment of the parachute, and will separate as a whole dropping the clusters by itself after it has descended to the required altitude.

Table 4.1: Trade-off table of clustered and non-clustered descent

Criterion	Clustered	Non-clustered
Landing reliability	X	
Post landing functionality	X	
Sustainable impact		X
Landing time	X	
Risk of maneuver at start		X
Mass of landing system		X
Redundancy	X	

- **The landing reliability** is higher for the clustered scenario. When MACHETE has to drop the clusters itself, it has to translate horizontally while doing this, for the clusters not to land on each-other. Because the clustered descent systems can operate individually and only have one landing to deal with they do not have to move horizontally, which results in an insignificant horizontal velocity, dramatically reducing the possibility of tip-over of the airbags during landing.
- **Post landing functionality** is increased for the clustered scenario where instead of one lander there are now eight landers that can also create a communication grid by functioning as a relay between sub-swarms of Zebro's that are separated too far from each other to communicate directly.
- **The sustainable impact** of clustered rockets is compromised due to an eight-fold of landers that will eventually be discarded and scattered over a small area, opposed to just one big lander. However, when this is compared to the hundreds of Zebro's that will be scattered everywhere in a large area this criterion becomes less relevant.
- **Landing time** is decreased for the clustered scenario because the landings can take place parallel in time, which also leaves more time for accurate landings.
- **Risk of maneuver at start** of the descent phase is present for the clustered scenario. After parachute separation the clusters need to split up which could lead to them getting entangled in the parachute or colliding into each other. When well designed, the risk of this maneuver is estimated to be low.
- **The mass of the landing system** of all the clustered systems is of course larger than that of one individual lander. The difference is smaller than one would expect: 3352 kg for clustered to 3136 kg for non-clustered, based on the last iteration in the midterm report.
- **The redundancy of the landing system** for the non-clustered system is non-existent. If it fails the whole mission has failed. The clustered system will still function if one of the clusters fails. Of course if this happens it means less Zebro's will land on the Martian surface, but the remaining Zebro's can still function as a swarm.

The most important part of our mission consists of getting a swarm of Zebro's safely on Mars. The clustered system has significantly higher reliability and redundancy at the cost of a minor mass increase and a slightly higher risk at the beginning of the descent phase. This is why a clustered descent phase is chosen.

To clarify what the Entry, Descent, and Landing (EDL) phases consist of for the final design:
Aeroshell → Parachute descent → Clustered rockets descent → Airbags

5 Assumptions, requirements and constraints

In this chapter all assumptions, requirements, and constrains regarding the MACHETE project are listed. The assumptions and requirements segments are divided into a general mission section and a design section where each technical subsystem is discussed separately. Ultimately, the project constraints and the constraints regarding astrodynamics are presented.

5.1 Assumptions

Assumptions made during the project that made it possible to work towards a final design. Some of the assumptions are purely for mathematical reasons, others are made to create a working system.

5.1.1 Assumptions parachute and propulsion

- The flight path angle is -15 degrees at parachute deployment.
- For speed of sound calculation, a 100% CO2 atmosphere is assumed.
- Vacuum specific impulse is assumed in all rocket engine related calculations.
- Propellant tank pressure is constant.
- Rocket engines can be throttled between 100% and 0% of rated power level without efficiency losses.

5.1.2 Assumptions ADCS

1. The density of the Mars atmosphere is 0.02 kgm^{-3}.
2. The gravity constant on Mars is 3.71 Ms^{-2}.
3. Both density and gravity are assumed to be constant below 2000 m.
4. The lander is modeled as a box with dimensions 1450 x 1450 x 500 mm.
5. Forces by wind perpendicular on the surfaces of the lander have a C_D of 1.
6. Moments due to wind disturbance are generated by the force times the distance between the center of pressure and the center of gravity.
7. Wind can be modeled by random noise with the magnitude comparable to Mars wind.
8. The thrusters have a minimum generated thrust of 5% of the maximum rated power level.
9. The center of gravity and inertia of the lander vary linear between full and empty mass.
10. The lander body is rigid.
11. The Mars surface is assumed flat.
12. The Mars reference frame is assumed inertial.
13. The origin of the Mars reference frame is at the location of the beacon.
14. When the lander is within 20 m around the beacon in x- and y-direction, it is assumed the lander is at target destination.

15. The distance the lander is removed from the target is an input from the beacon sensor, which is not included in the simulation model.

16. The desired drop location and final landing location are pre-programmed.

5.1.3 Assumptions structural

1. Weight of the Zebros acts in the middle of their geometry.

2. Bending stress on theLADS is distributed equally.

3. During the rocket propulsion fase the fuel in the tanks will be burned equally so that the center of gravity well not shift.

4. Torsion will only occur in the rocket propulsion fase while flying to the landing spot.

5. Eigenfrequencies of the structure of MACHETE is not equal to the one of the launcher.

6. The safety factor used during structural design is 10%.

7. Only 12.5% of the maximal torsion possible is considered in the calculations.

5.1.4 Assumptions touchdown system

1. The aerodynamic drag during final free fall is negligible.

2. Adiabatic flow occurs during venting [60].

3. The nitrogen behaves as an Ideal gas.

4. A constant deceleration occurs during impact.

5. Zebro activation can be done through sending a radio signal.

6. The airbag system must be able to account for the impact imposed on the payload without exceeding the maximum allowable gravitational deceleration of 30 g_M or 11.4 g_E. This has been set up as there is now information regarding the maximum allowable loads the Zebro can cope with. (see recommendations)

7. During the first strike on a flat surface, the airbag shall touch the ground with at least 30% of it's total contact area.

5.1.5 Assumptions EPS

1. The transfer-vehicle will be equipped with an energy source.

5.1.6 Assumptions CADH

1. The Mars Odyssey and Mars Reconnaissance Orbiter are in place to relay data to Earth.

2. The landing will take place during Mars-daylight.

5.2 Requirements

In order for the team to create the system the requirements that system has to fulfill are stated so the designs have a clear goal on what to reach.

5.2.1 Requirements parachute and propulsion

1. The parachute shall decelerate the system to an equilibrium velocity of 100 ms^{-1} at 2000 m mean Martian altitude.
2. The parachute shall be deloyed at 7500 m mean Martian altitude.
3. Each rocket engine on the CAESAR lander shall provide a maximum thrust of 1200 N and be throttleable down to 5% of RPL.
4. Each yaw control thruster on CAESAR lander shall provide a thrust of 10 N.
5. The fuel system of each CAESAR lander shall be able to 50 kg of propellant.

5.2.2 Requirements ADCS and Navigation system

ADCS requirements

1. The ADCS shall be operational in the Martian environment.
2. The ADCS shall provide attitude control of the entry vehicle, with respect to the yaw, pitch, and roll.
3. The ADCS shall be operational in the Martian environment.
4. The ADCS should be able to determine its velocity in the range of $10m/s$ and $16m/s$
5. The ADCS shall determine the roll of the lander, not exceeding more that 10° from the horizontal.
6. The ADCS shall determine the pitch of the lander, not exceeding more that 10° deviation from the vertical.
7. The ADCS shall orient the lander with the beacon once the lander and entry vehicle are no longer in contact.
8. The ADCS shall control the yaw of the lander to keep in constant contact with the beacon.
9. The ADCS shall control the altitude so is does not fall below below 28 meters

Navigation system

1. The navigation system should be able to detect obstacles larger than 0.5 meter in height while determining the landing spot.
2. The navigation system should be able to detect slopes exceeding 10° while determining the landing spot.
3. The navigation system should be able to avoid obstacles larger than 0.5 meters in height while determining the landing spot.
4. The navigation system should be able to avoid slopes exceeding 10° while determining the landing spot.
5. The navigation system should be able to autonomously detect the most optimal landing spot at the beacon.
6. The navigation system should be able to intercept the beacon signal.
7. The navigation system should be able to calculate the optimal glide slope to the beacon.
8. The navigation system should be able to determine the distance to beacon.
9. The navigation system should be able to operate under Martian conditions

10. The navigation system should be able to calculate alternative landing scenarios.
11. The navigation system should be able to navigate with loss of beacon signal.
12. The navigation system will function under the constraints imposed by the ADCS.
13. The navigation system will make sure no collision with in air obstacles will happen.

5.2.3 Requirements structural

1. The system should withstand loads associated with handling
2. The system should withstand loads in the range of $-1g_E$ to $-5g_E$ associated with the launch
3. The system should withstand loads in the range of $2g_E$ to $15g_E$ associated with re-entry
4. The system should withstand loads in the range of $0.378g_E$ to $11g_E$ associated with touchdown
5. The system should withstand temperatures in the range of $184K$ to $242K$
6. The system should withstand radiations occurring in space travel and on Mars
7. The Zebros should be able to leave the system after deployment

5.2.4 Requirements touchdown system

1. The airbag must be designed in such a way that it will not tip-over or dive-through at impact
2. The lander structure and airbag must be designed in such a way that all Zebro's can be deployed on the Martian surface without problems.
3. Maximum inclination at touchdown of the lander must not be more than 10 degrees at impact [60].
4. Maximum horizontal velocity must less than 16 m s^{-1} [60].
5. The airbag must be capable to protect the payload at impact for rocks up to 0.5 m [60].
6. The airbag must be capable of housing the lander structure as specified in Chap 8.

5.2.5 Requirements EPS

1. The systems should have a protection built-in against battery failure.
2. The systems should have a protection built-in against cell failure.

5.2.6 Requirements CADH

1. The system should log altitude, attitude, velocity, and position data during descent.
2. The system should send data at a rate of 512 kbs^{-1}.
3. The system should endure a total radiation of 117 rad.
4. The system should not fail due to bitflips during the mission.

5.3 Constraints

5.3.1 Project constraints

The following sections list the constraints on the project. The constraints are divided in constraints on the design and on the development.

Constraints on the design

1. The system size is constrained by the aeroshell and launcher, the largest mass and volume launched to Mars is the MSL aeroshell, rough dimensions given in figure 5.1
2. The maximum mass of the system including the aeroshell is 3300 kg
3. Off-the-shelf technologies must be used

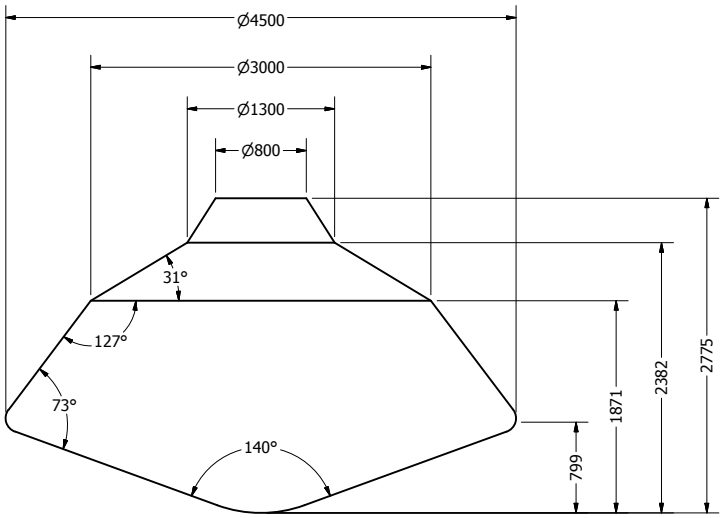

Figure 5.1: Schematic of the aeroshell of the MSL, dimensions in mm

Constraints on the development process

1. The mission should be sustainable
2. The design must be completed within 10 weeks by 10 students

5.4 Flight profile

The flight profile of the MACHETE mission exists out of 4 phases ranging from phase 0 to phase 3(see figure 5.2). Not indicated on the the figure are the launch and the transfer trajectory to Mars, these phases are not regarded as phases that needed to be designed. Nevertheless this does not mean these phases are not present in the total mission, and thus the flight profile will be given from the launch and trajectory to Mars to the last phase indicated on figure 5.2.

Launch The MACHETE vehicle will be launched into space using a large expendable launch vehicle which is suitable for injecting payloads into a hyperbolic trajectory to Mars. A vehicle like the ULA Atlas V 541 with Centaur upper stage is likely to be used. While this study will not deal with the launch vehicle itself, it is of importance to make sure that the MACHETE vehicle is able to handle the launch loads.

Mars transfer After launch, the vehicle will be in Mars transfer for a considerable amount of time. Depending on the launch window, the transfer time may be over a year. For this study it's of importance to make sure that the payload and landing vehicle systems are properly shielded from thermal and radiation loads. The actual design of the cruise stage is not covered by this study.

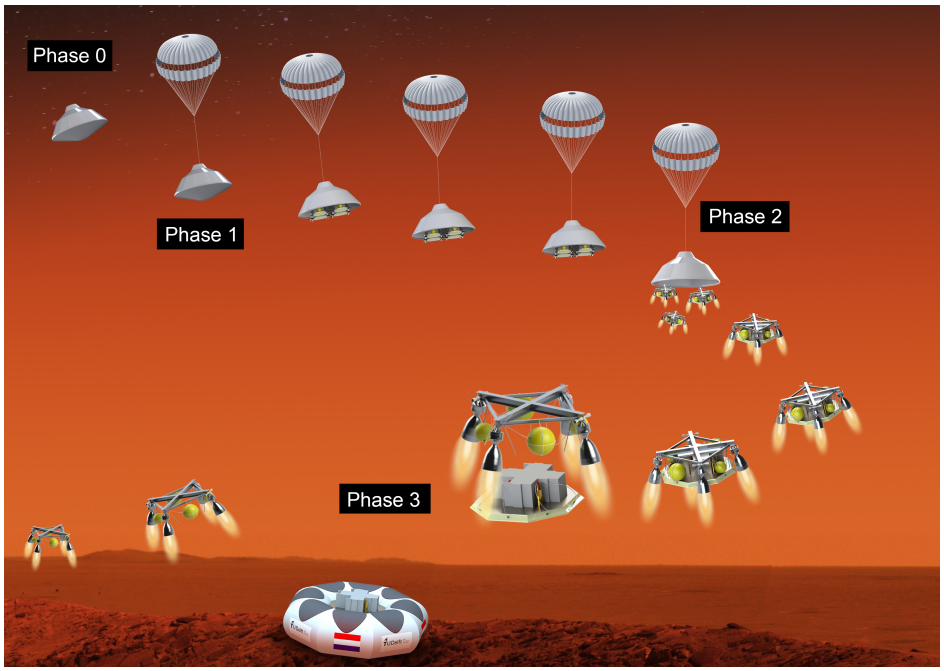

Figure 5.2: Graphical depiction of phases during post entry flight profile

Atmospheric entry / Phase 0 After arriving at Mars the vehicle will perform an atmospheric entry at a speed around 6 kms^{-1}. The heat shield will protect the MACHETE vehicle during its fiery deceleration in the upper Martian atmosphere. Past missions like MSL have used balance weights and/or thrusters to control the entry trajectory. While it is not part of this study to design the atmospheric entry system, it is assumed that some mass will be lost during entry.

Phase 1 After atmospheric entry the main parachute will need to be deployed. Exact deployment altitude and speed have been hard to predict during past missions due to the fact that they relied on atmospheric properties, which can vary significantly on Mars. At some point during phase 1 the heat shield will be dropped, significantly reducing the weight of the vehicle. The MACHETE starts scanning for beacon signal. Once the signal is found, the vehicle makes his approach towars the beacon.

Phase 2 After decelerating using parachute, the parachute and accompanying aeroshell are disposed off. The CAESAR will now transition to rocket powered flight in order to kill the remaining vertical velocity and to navigate toward the beacon. Disposing the main parachute and aeroshell will again significantly reduce system mass.

Phase 3 After arriving at the intended landing site and killing all vertical velocity (hovering) the payload will be deployed. After deployment the CAESAR will start it's fly away manoeuvre to to safely land away from the beacon.

Overview A summary overview of estimated masses and flight profile parameters is given in table 5.1. These values have mainly been taken from the MSL entry vehicle or are consensus values from previous Mars missions which relied on the Viking architecture. These values will be used in the preliminary design where more accurate estimates are unavailable. In case a clustered mission is designed, the total mass of all the clusters is taken as the full system mass.

Table 5.1: Summary overview of estimated vehicle masses and flight profile parameters per phase.

Phase	Mass kg	Speed ms^{-1}	Mach number	Altitude km
0	3150	5800	-	125
1	3000	360	1.5	7.5
2	283	110	0.45	2
3	233	0	-	0.3

5.5 Astrodynamics and landing site

A brief sketch on the astrodynamics has already been given in the midterm report [26]. Both the Mars Odyssey and Mars Reconnaissance Orbiter were considered suitable for transferring data back to earth, however timing is essential for contact. Since the focus of this project is in principle limited to the post Martian atmospheric entry phase, orbital and launch astrodynamics were not considered in the midterm. However, there are some considerations regarding astrodynamics. The date of launch affects the place where the MACHETE mission can land. When a certain land time and window has been created, a further elaboration can be made about possible landing sites.

5.5.1 Time window for landing

Every 2 years and 2 months, Earth and Mars are positioned in a suitable transfer position which requires the minimum amount of energy for transfer from Mars to Earth. Table 5.2 shows the possible launch windows in the future and it's estimated arrival date on Mars. Using this arrival date one is able to determine the season at arrival. Due to the more elliptic orbit of Mars, the spring season on the northern hemisphere is significantly longer then autumn. If it is assumed that the MACHETE mission will have a transfer time of about 250 days (Curiosity, MSL), the exact season on Mars, and thus the atmospheric Martian properties can be determined beforehand.

Table 5.2: Launch windows and its effect

Launch window	Arrival	Martian Season(Northern hemisphere)
April-May 2018	Dec-Jan 2018	Winter
July-Aug 2020	April-May 2021	Spring
Nov- Dec 2022	July-Aug 2023	Spring
Jan-Feb 2025	Oct-Nov 2025	Summer
Feb-Mar 2027	Nov- Dec 2027	Late summer- Autumn

All this information is useful for the mission as it provides us with information regarding temperature ranges, average wind speeds, dust storms, solar radiation and more. The fluctuations that have the largest impact on the MACHETE mission are listed below:

- During winter, pressure can drop 25% lower than during summer [33].
- A noticeably thinner atmosphere during winter due the absorption of CO_2 by the polar caps. [33]
- Larger chance of dust storms at the equator during Martian summer, affecting the LIDAR and other control systems [17]. These dust storms originate from the deepest impact crater of Mars, Hellas Basin (Southern Hemisphere, 9 km deep crater).

It seems that a summer landing is preferable above a winter landing. Most of the previous landed rovers landed in a Spring-Summer-Autumn season on the northern hemisphere of Mars(Fig. 5.3). During the northern summer temperatures in the northern, equatorial and southern hemisphere are accordingly around 260-275K, 260K, 220-150K [32].

5.5.2 Altitude

As the MACHETE mission requires time and distance to decelerate in the thin Martian atmosphere using its parachute, the thickness of the atmosphere should be sufficient. Furthermore enough navigational time is a must. It can been seen in Fig. 5.3 that almost the entire northern hemisphere of Mars has subzero mean Martian altitudes. Most of the historical missions have landed at this northern hemisphere exactly for this reason. It is only the NASA MSL Curiosity mission which so far has successfully achieved landing on a higher than zero mean Martian altitude. While from the performed sensitivity analysis is appears that there is ample of margin for higher altitude landings using the designed system, there surely are limits to the maximum landing altitude.

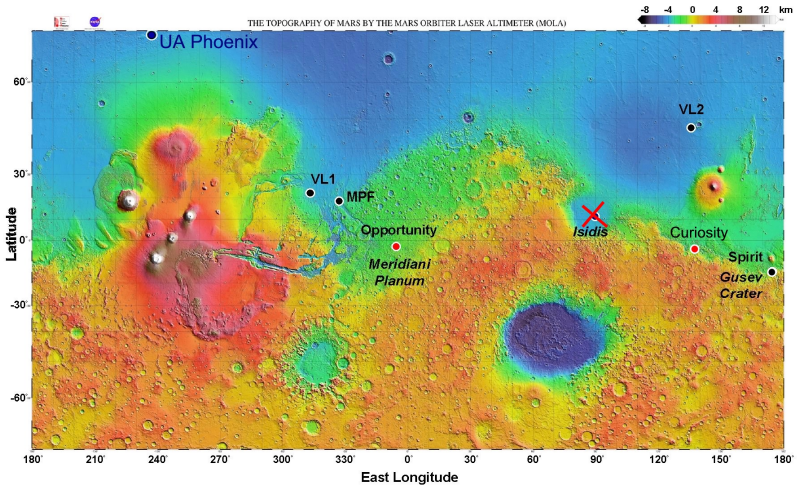

Figure 5.3: Mars landing sites on a topographic map of Mars, NASA

5.5.3 Terrain

Another important consideration is the nature of the terrain the mission will be designated to land on. Steep surface inclinations and rock cover may pose challenges to some extend. While the selected touchdown system is very capable in handling surface obstacles, there will be limits. The effects of the surface features on the mission are explored in detail in Sec. 9.1.2.

5.5.4 Landing location

The selection of the landing location is a combination of multiple factors. The customer will probably want to select a landing spot which is for example rich in caves to be explored. The desires of the customer will be combined with the above given parameters to select a suitable landing location.

Part II: Technical design

In the technical design part of the report the designs of the different subsystems are explained. There are five departments with systems that are elaborated on: the Attitude Determination and Control System (ADCS), the parachute and propulsion system, the structural system, the touchdown system, and the department that concerns itself with the Electrical Power Subsystem (EPS), the Command and Data Handling (CADH), the communications, and the thermal system. These departments all have their own chapter in which will be explained what the system consists of. In addition, at the end of each chapter there will be verification & validation, risk analysis, and sensitivity analysis which are explained in the following section.

Verification & validation

The verification & validation analysis is the process that allows designers to determine if the model implementation accurately represents the conceptual model and its solution. Verification answers the question: "Is this model build the right way?". Validation answers the question: "Is what we have build the right model?". Both verification and validation processes gather information that later will be used to determine the system's correctness of functionality and accuracy in following a specific scenario. Verification and validation form the link between the conceptual model, simulated model and the reality. The methods of verification and validation cannot prove that the model under investigation is accurate under all circumstances, but rather they provide evidence that the model is sufficiently accurate for its intended use.

Risk analysis

During the technical risk assessment, every step of the mission will be evaluated to understand its impact on the mission and its probability to fail. The consequences of these failures as well as the actions to minimize the risk are presented in a risk map. Furthermore the responsibilities for preventing these risks have been distributed. The severity, likelihood and importance of every risk are rated using a scale of 1 to 4 in which 1 indicates the points where the most attention is needed and 4 are the points that are insignificant.

Sensitivity analysis

Sensitivity analysis is the study of how the uncertainty in the output of a mathematical model or system, numerical or otherwise, can be apportioned to different sources of uncertainty in its inputs [61]. A sensitivity analyses is used to test the robustness of a system, meaning it is tested to what level of difference from the original scenario the model produces results that make sense or prove the system still works as intended. During a sensitivity test there is also a chance new errors are found due to unexpected relations found between the input en output in a new scenario, which could indicate a corrupt formula.

6 Attitude determination and control system

6.1 Introduction

In this chapter the complete Attitude Determination and Control System (ADCS) and navigation system is presented. Methodologies and concepts implemented in the creation of a functioning ADCS and navigation system are explained in the following sections of this chapter.

The ADCS is responsible for the stability and orientation of the system. The ADCS steers the system in desired orientation during the systems operational mission, despite any external perturbations that may act upon it. The ADCS requires the system to be able to receive information from its environment. This is done with the use of sensors. While the system control is done by actuators. The ADCS is strongly coupled to other subsystems, especially the propulsion system as also the navigation system [42].

While the ADCS is associated with the spatial orientation of the system, the navigation system is responsible to successfully guide the system and fulfil the mission profile. The navigation system at all times will be constrained by the ADCS. The navigation system can be consider a sub-system of the ADCS. The reason for this is that the system will have to have a predetermined dynamic behaviour to ensure the increased survivability of the payload.

The CAESAR is a fully automated system, that will be capable of payload deployment on target sites. How this fully automated system was created is described in this chapter.

6.2 Mission profile, navigation & ADCS

The mission of the MACHETE lander starts as it first enters the Martian atmosphere. There eight CAESAR's will be encapsulated in the Mars entry vehicle. This vehicle is an aeroshell that will protect the clusters from the aerodynamic loads and friction heat as the vehicle intercepts and crosses the Martian atmosphere at high speeds and decelerations. During this phase the ADCS will have to steer, by means of an actuators mechanism located in the supersonic parachute (AGAS) (refer to section 7.5), the entry vehicle into the landing ellipse while maintaining the vehicles angle of attack, bank angle, and side-slip angle [16] in the preprogrammed accepted value range.

Progressing on to the first phase of the mission, while the vehicle is in descent, the ADCS will accept data from the vehicles environment and when the correct altitude is reached the vehicle will deploy the supersonic navigational parachute while dislodging the heat shield from under the entry vehicle. While the entry vehicle is in descent the navigation system will calculate the glide slope needed for least mission fuel consumption, and steer the vehicle in that direction. Wind direction and wind speeds will continuously be monitored while deviations from the glide slope will be corrected [45].

The clusters in the second phase will start to prepare for de-attachment from the entry vehicle. It must be mentioned that it is assumed that on the ground, there exists a beacon. The beacon will help guide the CAESAR's to their destination. Several other methods have been considered to be used as means of target guidance. These systems will be analysed in proceeding sections, as well the reasons for disregarding them.

Before jettison of the supersonic parachute the ADCS will scan the landers horizon for the beacon signal intersection and signal lock will be obtained.

By the end of this phase the landing site will have been logged in the navigation system, and the trajectory of the lander with respect to the beacon will have been calculated. Through this stage, continuous calculation of the distance to the target will be done, the current speed of the ship, the altitude as also calculation of the fuel required to reach the target is estimated.

Since there are eight ships to be departed from the MACHETE vehicle, each ship will have different deployment coordinates. For all ships the maximum payload deployment hight will be done from an altitude of 30 m.

Once each target position is reached and payload deployed the the CAESAR will depart from the site, while collision amongst the rest of the ships will be avoided.

6.3 Parachute control

For the parachute control please refer to section 7.4.

6.4 Hazard avoidance

In order to detect hazards when the CAESAR navigates to the beacon the CAESAR is equipped with a flash LiDAR. Where LiDar is the abbreviate of 'Laser Imaging Detection And Ranging'. "The Flash LiDAR has been identified by NASA as a key technology for enabling autonomous safe landing of future robotic and crewed lunar landing vehicle [11]". The flash LiDAR system works with a single laser pulse and with a receiver that makes use of 'smart pixels' that are capable of recording the required sequential temporal information to create a 3D image of the surface. A flash LiDAR can be used for Hazard Detection and Avoidance (HDA),Hazard Relative Navigation (HRN),Terrain Relative Navigation (TRN), and for altimetry. A table with the flash LiDAR's operational range and precision/resolution can be found in figure 6.1.

In the scope of the current design the HDA and HRN functions are interesting sensor functions of the flash LiDAR to look in to. When the CAESAR is navigating down to the beacon signal, it should be able to recognize/detect hazards such as large rocks and steep slopes (mountains) in order to perform a safe landing. The HDA system of the flash LiDAR system is able to detect rocks beginning at a altitude of 30 cm and up, and is able to detect slopes of 5° or steeper from a height of 1000 km or less. The flash LiDAR system could also be used as a backup navigation system if the beacon may fail in navigating the CAESAR to the desired location, or when an emergency landing has to be performed. The flash LiDAR system is able to acquire terrain maps with its camera to perform terrain relative navigation. In this TRN phase the flash LiDAR system still provides altitude information while also generating consecutive 3D images which later on will be used for the HDA and HRN phase.

Sensor	Function	Operational Altitude Range	Precision/Resolution
Flash Lidar	HDA/HRN	1000 m – 100 m	5 cm/40 cm
	TRN	15 km – 5 km	20 cm/6 m
	Altimetry	20 km – 100 m	20 cm

Figure 6.1: Flash LiDAR precision/resolution for the different measurements functions [11]

6.5 Swarm flight

In the following section, the swarm behaviour of the total CAESAR's will by analysed. According to the mission profile each cluster will have to follow four consecutive stages to complete its mission. In all four stages communication of each cluster with its surrounding CAESAR's is of critical importance to avoid collision and thus partial or whole failure of the mission. In the following paragraphs strategies to avoid collision during the mission will be provided, through all four phases. The mentioned phases are the following:

- Detachment from the MACHETE vehicle, and free fall.
- Trajectory towards the target site.
- Deployment of the payload
- Post mission target site

6.5.1 Detachment from the MACHETE vehicle

The MACHETE is an entry vehicle that will transport the CAESAR's through the Martian atmosphere. Once the MACHETE has reached a predefined altitude it will release the CAESAR's. All eight clusters are located in the entry vehicle in two planes, as is seen from figure (6.2).

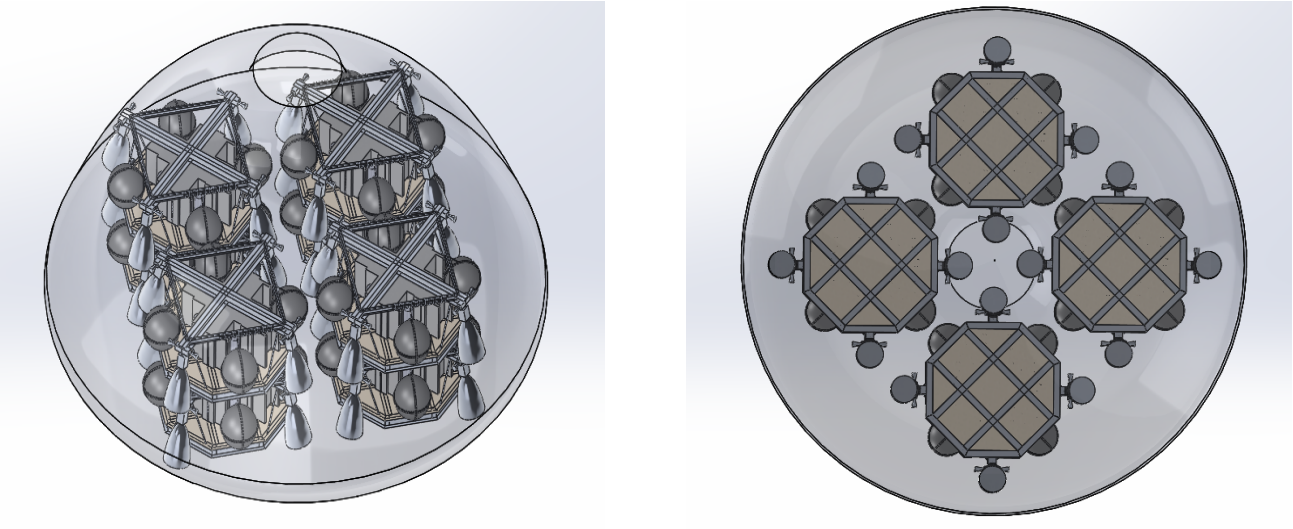

Figure 6.2: Side view, and bottom view of the payload layout within the MACHETE entry vehicle.

To avoid any sudden changes in the moment of the entry vehicle, it has been concluded that the CAESAR's will depart the vehicle in opposite pairs. It has been calculated that the entry vehicle will release the payload from an altitude of 2000 m and an initial vertical speed of -100 ms^{-1}.

A concern for further study is located in the distance of the two clusters within the MACHETE. The two opposite clusters are located 40 cm apart. While to ignite the thrusters of each CAESAR will take proximately 2sec. According to the initial conditions the clusters will have travelled 207.42 m before the ship is controllable. A collision avoidance mechanism is needed to be conceived in order to avoid such phenomena.

Several solutions to this matter have been proposed. Three solutions have survived the trade-off, but also have their drawbacks. One solution would be to deploy the CAESAR separately and within time integrals of 3 s. This solution is viable but will cause the entry vehicle to be unbalance. Secondly as a solution, would be to attach the two clusters with a rod that will prevent the CAESAR to collide but will be designed to fail once the thrusters ignite. This again is a viable solution but this mechanism would provide extra weight to the structure. Finally It is proposed that the clusters receive the order to ignite 1 s before their deployment thus attaining control much faster while activating a control avoidance software, that will manoeuvre accordingly when another cluster is in a specified region around it.

As mentioned all these solutions need to be investigated separately to find the most vital one. Though research for any further mechanism has not been done, though recommended. An assumption made to overpass this situation derives from the fact that the aerodynamic forces acting upon the two CAESAR are about the same, as will also be their motion and thus collision in such a small period of time is minimum. It should also be mentioned that the atmosphere of Mars is thin enough to cause little aerodynamic forces upon the CAESAR.

6.5.2 Trajectory to beacon

During the trajectory to the beacon collision needs to be avoided within the CAESAR swarm. Detection and collision avoidance software needs to be created that will detect for each CAESAR if any other ship is located within a defined radius around it. If collision is predicted both CAESAR's will move to correction manoeuvres.

It is also stated that collision avoidance during the transportation stage to the target position can be done by determining the different target position of each CAESAR. assuming that each deployment site for each CAESAR is 300 m apart, collision risks are reduced to minimum.

6.5.3 Payload deployment- Secondary target

After deployment of the payload the CAESAR will move toward their secondary target position. This position may be different for every ship or my be common for all ships, depending on their post mission functionality. For this reason , again, detection and collision avoidance software needs to be created that will detect for each CAESAR if any other ship is located within a defined radius around it.

6.6 Hardware Implementation

For the CAESAR to be capable to fully function it must consist of two parts. Where the software is now covered, hardware implementation is also needed. The following section will cover the hardware that will be implemented. The hardware will support the function of the software and both will function hand in hand to too create the ADCS. Each ship will be equipped with a set of hardware, as described bellow. For simplification the following section one CAESAR is considered. The following sections consist the description and function of the sensors, computational unit, actuators and the beacon.

6.6.1 Sensors

Sensors are crucial for the functionality of the system. They provide pathways that allow the system to measure its environment. Through the conversion of analogue measurements to digital signals, a sensor is capable to feed the process unit with information regarding spatial orientation, speed, heading, and their derivatives. This information will then be manipulated from the ADCS for decision making.

In the following subsection a complete profile of the sensors used in couple with the mission profile.

All phases

Sensors under this heading will be used in all phases of the mission.

- ***Inertial measurement unit (IMU):*** The inertial measurement unit is a sensor which exists out of a combination of multiple sensors. The IMU is able to measure velocity, orientation and accelerations, by making use of gyroscopes, accelerometers, and when needed also magnetometers are incorporated. It is one of the most important sensors in the vehicle for attitude determination and control.
- ***Beacon signal receiver*:** As mentioned, the CAESAR will be aided to its target site, by means of a beacon signal. A receiver for that beacon is needed to be displayed upon the CAESAR. Further information on the specifics of this system, please refer to Sect. 6.6.4.

Phase before detachment of the MACHETE

- ***Windpack dropsonde [5]:*** Is a small instrument that is attached to the parachute. This instrument measures wind data and the distance of the drop altitude to the ground surface. This information is transmitted to the entry vehicles navigation sub-system which calculates the path of descent.
- ***Thermometer:*** The thermometer is used to monitor system temperature, sensing of the system temperature is important since it determines if and when the cooling system of the lander should be activated which should protect the payload and electronics from thermal stresses that can occur in this phase of EDL.

Cluster deployment, target location and navigation

- ***Fuel sensor:*** The fuel sensor is used to determine fuel usage, and keep track of the remaining fuel. It is important to keep track of fuel usage and volume since the lander should be able to determine if a premature landing is needed when it is close to run out of fuel.
- ***LiDAR:*** Is a Laser Radar sensor that can provide a 3D image of the terrain below the lander, and identifies any hazards such as craters, slopes, or rocks during the final phase of payload deployment. Amongst the rest it can also sense a variation in altitude. See section 6.4 for more specific information on the LiDAR system.

6.6.2 Computational unit

All computations, logic flows, and controls of the lander will be handled in the CPU. The amount of computational power needed to control the lander is difficult to predict. However, previous missions like the Curiosity applied the PowerPC750 which runs at 525 millions of instructions per second (MIPS) at 233 MHz. Currently more powerful cores are available for example the ARM Cortex A series, which run from 1,000- to 10,000 MIPS. This proves that computational power will not be a problem, especially since more powerful cores will be developed in the upcoming years. Which type of CPU to apply and how to handle radiation levels will be discussed in the power, command and data handling chapter (chapter 10) of this report.

6.6.3 Actuators

For the actuator layout and control see section 6.7.5.

6.6.4 Beacon

Beacon functionality and placement

It is assumed that prior to the MACHETE mission, a mission to Mars was realised with the goal to place various beacons on the Martian surface close to the points of interest (caves and craters). These beacons will be able to guide the MACHETE to the desired landing location (a beacon location) by making use of radio waves. As mentioned in the mid-term report [26] a more in depth trade-off on the types of beacons will be given in the lower-level design of the ADCS.
To successfully guide the lander to the landing area the beacon must be able to operate under Martian conditions. Several atmospheric and weather aspects of Mars could influence the beacon radio signal. After a literature study it was concluded that only during the entry of the lander a serious risk of loss of signal is present due to the high entry speed relative to the local speed of sound creating plasma which distorts the signal. The attenuation of the radio signal due to clouds or Martian sand storms is small enough to be disregarded in the EDL scenario [35].

ILS and TLS Since the beacon must be able to guide a swarm of eight landers to the landing locations, the beacon must be able to handle and guide these eight landers at the same time.
The Instrument Landing System (ILS) can be a reasonable option for guiding multiple landers to the landing location, unfortunately a draw back of the ILS is the trouble it has on accurately navigating vehicles on a rough terrain like Mars.
The TLS system seems to be a feasible option to navigate a lander to the landing location due to its excellent qualities on guiding vehicles on the rough terrains the Transponder Landing System (TLS) is restricted to navigating one lander at a time making it infeasible for the MACHETE mission profile. Besides, a TLS system might be too big to transport to Mars, and it would thus be unreasonable to assume a system equal in size will be stationed on Mars prior to the MACHETE mission.

NDB The Non-Directional Beacon is a system that has been in use for both marine as well as aviation navigation. A major draw back of this system is it's sensitivity to atmospheric and terrain conditions, sometimes causing perturbations of more than 50 km due to reflection of the NDB radio signal. This distortion radius is too large which makes a NDB system infeasible for the MACHETE mission.

EPIRB At last the Emergency Position Indication Radio Beacon (EPIRB) system that is still currently in use for search and rescue mission could be a feasible option. Al tough initially a satellite connection is used to send the location of the beacon, it also sends it's location to nearby receivers when in a range of five to six kilometres from the beacon. The EPIRB is a readily available and a of the shelf product/technology, unclear however is how effectively this system can be used to actually successfully navigate the eight landers to the landing site. Due to its background in search and rescue it is also tested in harsh environments.

Phased array/beacon system In order to receive the radio signals, the landers need to be equipped with one or multiple antennas. By making use of a phased array antenna on each side of the lander, the signal will be easy to detect irrespective of the current orientation of the lander. The phased array antenna that receives the strongest and clearest signal will be on the side the lander has to manoeuvre to. The frequency of this signal should be around/above 450Mhz to prevent negative influence of the ionosphere of Mars on the signal. [35].While the lander on board also has an altitude scanner (LiDAR), and the radio signal has an angle of incidence on the phase array antenna the distance to the landing spot can be calculated. As a backup system in determining the altitude one could use a pressure gauge. When static ground pressure and the density are known the altitude can be derived from the pressure measured by the gauge. By making use of Doppler measurements also the speed of the lander can be calculated. When having the lander always adjust its attitude/altitude to keep the radio signal received on its antenna, navigation to the beacon will be possible.
Since navigating on Mars in these particular manners have never been done before, further research needs to be done to develop an optimal functioning system.

An overview of the possible beacons and their properties can be found in table(6.1).

Table 6.1: Different types of beacons and their characteristics

Beacon type	Frequency range	Transmission direction	Transmission range
Instrument Landing System (ILS)	108.1 - 335 MHz	Uni-directional	6km-11km
Transponder Landing System (TLS)	1030 - 1090 MHz	Omni-Directional	111km
Non-Directional (radio) Beacon	190 - 535 kHz	Follows earth curvature	NA.
Emergency Position Indication Radio Beacon (EPIRB)	406 MHz	Satellite/Omni-directional	5km-6km
Phased array antenna/beacon system	450 MHz	Omni-directional	NA

Beacon link budget

In the following section an estimation of the parameters required for the system to communicate with the beacon is given. This estimation will be done in the form of a link budget estimation. In the following figure (figure 6.3) a representation of the *beacon-ship* communication system is presented.

To size the communications system several parameters have been given with reasonable assumptions. The CAESAR will first attain connection with the beacon at a radius of about $r = 3000$ m in the Martian atmosphere. It is receiving telemetry data from the beacon by the means of an antenna with assumed 15 dBi gain; It is assumed that the beacon is transmitting a signal power of 9 dBm(8 mW) at a frequency of 433 MHz and with the use of an off-the-shelf antenna with a transmission gain of -5dBi. It is also assumed that the transmitter antenna is soldered together and thus there are no cable losses in that section.

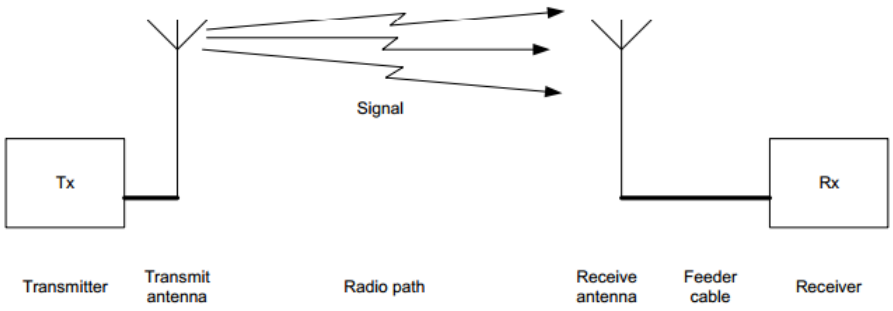

Figure 6.3: Communication representation of the beacon-CAESAR system.

The Minimum operational sensitivity, of the system is unknown and will be fine tuned based on the margin factor. A positive margin factor in the range of above ten is an acceptable value. It is estimated that the receiver is wired to the antenna using 2 m of cable with a loss of 0.1 dB/m at 433 MHz.

Table 6.2: Link budget of the mentioned antenna system

Parameter	Symbol	Value	Units	Units
Transmit power		9	dBm	Assumed transmitter specs.
Transmit cable loss		0	dB	Equation 2
Transmit antenna gain		-5	dBi	Assumed
Path Loss		-87.4	dB	Equation 1
Other path losses:		-3	dB	Atmospheric gases
Receive antenna pointing loss		0	dB	Assumed
Receive cable loss		-0.2	dB	2m @ 0.1 dB/m
Signal presented at receiver input		-86.60	dBm	Sum of all the above numbers
Required signal at the receiver		-93	dBm	From the receiver spec.
Margin		6.39		

The link budget has been calculated with the following equations, and tabulated in Table 6.2.

$$L_{fs} = 32.4 + 20\log_{10}(f) + 20\log_{10}(d) \tag{6.1}$$

$$L_{cable} = lx \tag{6.2}$$

Most of the information needed to assemble a link budget is provided in the table above. Path loss will be calculated while assuming that the transmitting antenna is isotropic, and thus radiates evenly in all directions. Since the transmitting antenna is considered isotropic it is assumed that there exist no pointing losses. Values for the transmitted antenna gain and any antenna pointing losses have been assumed. Path losses due to the Martian atmosphere composition are assumed negligible. The above values that have been obtained have been compared with figures obtained from amateur telemetry communication sets.

6.7 Simulation model

A simulation of the rocket powered stage was made with multiple purposes. First of all, it provides a platform to build and test the ADCS system. Second, it provides a more detailed performance prediction in terms of fuel consumption than earlier used analytical methods. Finally, the influence of certain design parameters can be analysed and required performance of for example the thruster system can be derived.
The simulation as integrated in SIMULINK® is shown in Fig. 6.4. The controller, actuator, and equations of

motion blocks form the closed loop system. The block labelled 'mass, inertia, c.g.' governs said parameters as the vehicle uses its fuel. With the 'dropped 0/1' signal, the controller can communicate that the payload is dropped and the system mass, inertia, and centre of gravity should be updated. The disturbances block includes the gravity force and the aerodynamic model. Each of these blocks will be individually discussed in subsequent sections.
Two reference frames are used throughout the model. One is the Mars fixed reference frame, and the other is the body fixed reference frame with the z-axis pointing upwards. To keep track of the reference frame used for each parameter, the notation _m and _b are used in Fig. 6.4. In the equations used in this chapter, all parameters are represented in the body frame unless a superscript m is used.

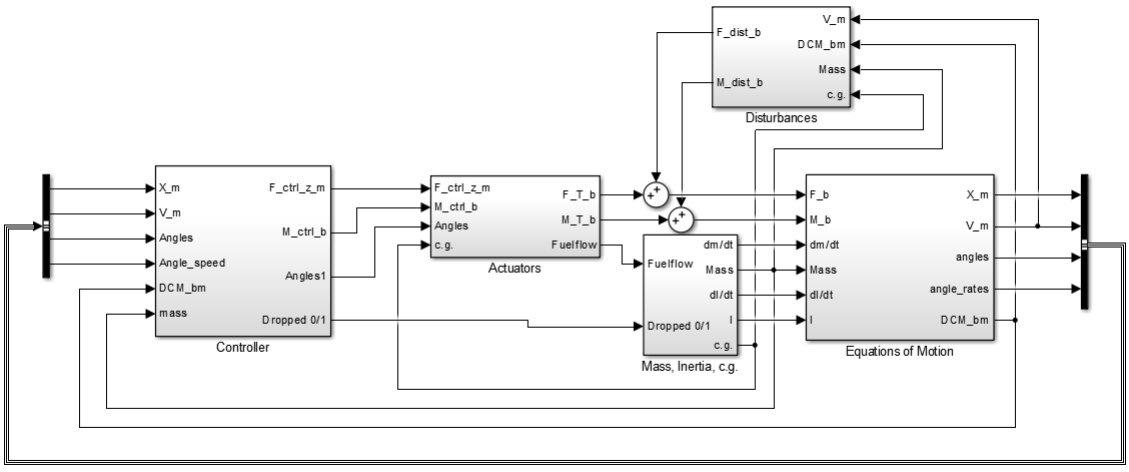

Figure 6.4: Rocket powered descent simulation as integrated in SIMULINK®.

The default ode45 solver of Simulink® is used for running the simulation, which uses a variable step size Dormand-Prince method with 4th and 5th order Runge-Kutta formulas. The relative error allowed between steps was set to 10^{-3}, with all other solver parameters kept on the default 'auto' setting.

6.7.1 Equations of motion

The equations of motion (EOM)are used to simulate the free-falling motion of the lander, and eventually take in to account the actuating forces and moments on the lander to control this free falling motion. It was chosen for the six degree of freedom (6DoF) quaternion EOM block from the aerospace toolbox in Simulink. With the six degrees standing for the x,y,and z direction and the rotations around these three axis. By making use of quaternions the problem of a eventual gimbal lock can be ruled out, al though the scenario of a gimbal lock in the landers attitude control is highly unlikely. Making use of quaternions also speeds up the computation time of the simulation due to the more clear mathematical processes of quaternion computations. The outputs of the EOM are used to translate vectors between frames, compute the forces and moments and the attitude in general. The 6DoF EOM block in Simulink assumes the (Martian) initial reference frame is a flat inertial reference frame, and the body frame has its origin in the center of gravity. Besides the lander is assumed to be rigid ,eliminating the need to consider the forces acting between individual elements of mass [44].

6.7.2 Simulation mass, center of gravity and inertia

This section deals with the mass, center of gravity, and the inertia changes during simulation.

Mass

The mass of the lander changes during simulation due to two aspects: First, the fuel used for propulsion depletes over time, decreasing the lander mass and causing lower thrust values to be required. Second, when

the target destination is reached, the LADS will be deployed. Causing a huge drop in total mass. The mass will be multiplied with the gravity constant on mars, transformed to the body axis system and fed into the simulation.

Center of gravity

During simulation, the center of gravity will gradually change due to fuel usage. The center of gravity will be determined using the Simulink® model. Asymmetric depletion of fuel is taken into account and four cases have been considered. The four cases are, in their respective order: Full tanks, two tanks depleted, all tanks depleted, and one tank full. The four cases are shown in Fig. 6.5. During simulation, a linear fit is used between the full and empty center of gravity.

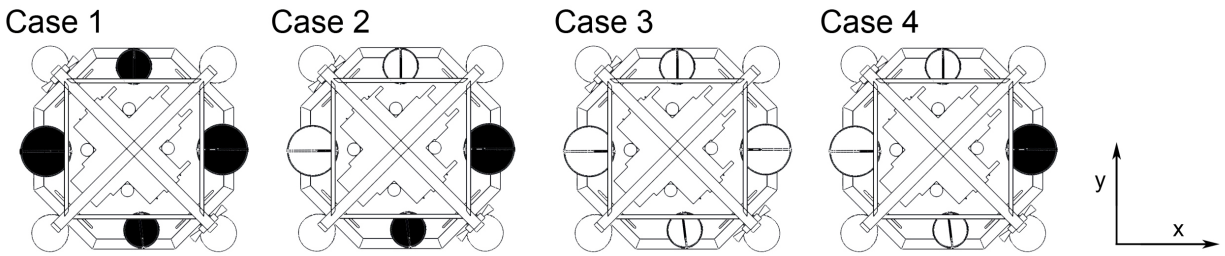

Figure 6.5: All four loading cases for which inertia has been determined. Full fueltanks are shown in black.

The determined locations of the center of gravity are shown in Eq. 6.3. The origin of the axis system is in the center of pressure. Note that the system is aerodynamically stable since the center of gravity is below the center of pressure. Small deviations in x and y direction between full and empty lander are accountable to small asymmetries.

$$c_{g,1} = \begin{bmatrix} 0 \\ 0 \\ -0.04434 \end{bmatrix} \quad c_{g,1} = \begin{bmatrix} 0.06929 \\ -0.01213 \\ -0.04832 \end{bmatrix} \quad c_{g,1} = \begin{bmatrix} -0.00747 \\ -0.00235 \\ -0.0536 \end{bmatrix} \quad c_{g,1} = \begin{bmatrix} 0.06956 \\ -0.00291 \\ -0.0481 \end{bmatrix} \tag{6.3}$$

Mass moment of inertia

Correct operation of the lander vehicle requires precise inertia measurements. However, since experimental measurements are not possible during this stage of design, inertia values are extracted from Solidworks® models. The inertia values taken from the Solidworks® models are not completely accurate, but give a good approximation of the final inertia values. The inertias are determined with the center of gravity at the origin. Since the lander consists of four fuel tanks the probability of asymmetric fuel depletion is considered. This creates four cases of fuel loading as mentioned before.
The Solidworks® models have a lower mass than the control system is designed for. This is accountable to small subsystems which have not been modelled in the 3d model. To correct this difference in mass, it is assumed that the difference in mass is uniformly distributed over the lander and that the inertia is scalable to the desired mass.
At the moment of deployment of the LADS, the inertia of the vehicle changes significantly. To account for this, the inertia of one LADS has been determined and will be subtracted from the total inertia at the time of the release.

6.7.3 Aerodynamics

This subsection describes the simplified aerodynamic model that is applied to the lander body. The CAESAR will experience forces and moments generated by the wind and movement through the atmosphere. These

forces and moments will act on the CAESAR and cause stability or instability. The aerodynamic model is simplified to give an early estimation of the effects on the mission.

Forces and moments

Calculation of the aerodynamic effects is done by decomposing the velocity vector in the three body axes, which gives the following velocity vector:

$$V = \begin{bmatrix} V_x \\ V_y \\ V_z \end{bmatrix} \tag{6.4}$$

Each velocity component perpendicular to the faces of the lander will generate a drag which is calculated using the drag equation shown in eq. 6.5.

$$F_{aero,x} = \frac{1}{2}\rho V_x^2 S_x C_D \tag{6.5}$$

During simulation, the sign of the drag forces will be lost due to the square function of the velocity. This is solved by taking the opposite sign of the original velocity and multiplying it with the calculated drag.
The aerodynamic forces act through the center of pressure (c_p) of the body. A moment is created by the forces when the c_p is offset from the center of gravity (c_g). Using the locations of c_p and c_g and the forces which have been calculated, the moment around each body axis can be calculated using the cross product of the position vector times the forces as follows (eq.6.6)

$$\vec{M}_{aero} = (\vec{c}_p - \vec{c}_g) \times \vec{F}_{aero} \tag{6.6}$$

The forces and moments will be used as an input to the equations of motion of the simulation.

Wind model

Observations done by the Mars Pathfinder (MPF) concluded that the average wind velocity on the Martian surface during daytime was between 0 ms^{-1} and 20 ms^{-1}. With an average speed of 7 ms^{-1} [70]. These wind speeds are modelled using a random noise generator which generates the windspeeds and subtracts them from the velocity in the Martian reference frame.

Lander body

For calculation of the aerodynamic effects on the lander body, a simplified model is used. The lander body is defined as a rectangular box with dimensions shown in Fig. 6.6. Since the lander is modelled as a box, for each side of the lander a C_D of 1 is assumed. The axis system is located at the center of the box.

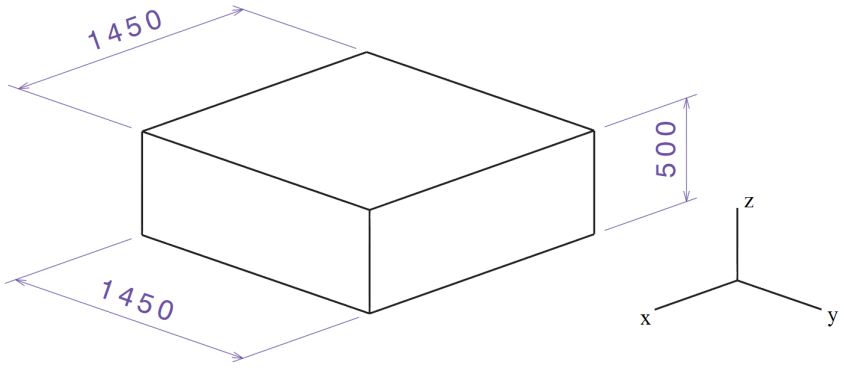

Figure 6.6: Layout of the model for the lander used in aerodynamics, the axis system is located at the center of the box. Dimensions in [mm].

6.7.4 Controller

For the control of the CAESAR, three PD (Proportional Derivative) controllers, each dedicated to one axis, are used to control its position in the Martian reference frame. The use of fixed thrusters pointing downwards dictate that in order for the CAESAR to move in any direction on the x, y plane, it must be tilted toward the direction of movement. The desired thrust vector, $\vec{F}^m_{ctrl}$, constructed by the position controllers therefore acts as an input for the attitude control. This controller then rotates the CAESAR's z-axis, $\hat{z}_b$, such that the thrust points in the desired direction.

This control principle also works for control while hovering at a fixed location. In this case the $\vec{F}^m_{ctrl}$ is pointed upwards and therefore the controller tries to position the vehicle horizontally in order to point $\hat{z}_b$ in the same direction. Any disturbance in the attitude will therefore be corrected. Furthermore, any disturbance in the horizontal position will give an horizontal component to $\vec{F}^m_{ctrl}$ in the opposite direction. Due to the resulting angular error the vehicle is tilted and in this sense corrects for the disturbance.
In the following sections the position and attitude control are individually discussed first. Afterwards a method for finding the initial control parameter values is given along with the results of tuning the parameters. Finally, the filtering method used for the derivative terms of the controllers is presented.

Position control

In this sections the responsible block of the navigation system that guides the ship to and away from the deployment site, will be presented. The goal of this block is to navigate the lander to the beacon. This is done by calculating the error of the current position of the lander and the desired location.
By using a Proportional Derivative (PD) controller, this position error is reduced until both current and desired location coincide. The PD controllers will provide the required thrust in each direction moving the lander to the target destination based on the position error. It should be stated that the PD controllers operate in accordance to the inertial frame of Mars. As the attitude control, thrust, and equations of motion are done in the body axis, the signal is converted to the body inertial frame to provide the correct magnitude and direction of thrust.
As the CAESAR approaches the target, the position error is compared against a position tolerance. This tolerance will make sure that when the error reaches a predefined value range (the tolerance) it will ground the error to zero, suggesting that the lander has reached its target position. The reason behind incorporating a radius around the target position, is firstly to be able to define the distance from the target where deployment of the payload will be done, and secondly to avoid the system to oscillate around the value zero. In this same manner the velocity is controlled. The tolerances mentioned above can be found in table 6.3.

Table 6.3: Tolerance for the x,y,z direction for range and velocity

Parameter	x	y	z	V_x	V_y	V_z
Tolerance	20 m	20 m	5 m	1 ms^{-1}	1 ms^{-1}	1 ms^{-1}

Both distance, and velocity deviation are compared to zero and later fed in to a boolean gate. This is an *AND* port that will accept true/false statements. The output of this gate will later determine the state of the CAESAR. The CAESAR is designed in a way that it will go through two states throughout its mission. The first state determines the autonomous navigation from the MACHETE to the deployment location, while the second state of the lander depicts the navigation from the deployment site to the post mission landing site.

Having a system that will function in two phases requires that this system will have a memory of its current state while according to its inputs will be able to switch to its second states. This type of finite state machine was conceived initially as the following Moore diagram (figure 6.7), and implemented as a Flip-Flop memory unit. According to the inputs two switches control the state the system operates in.

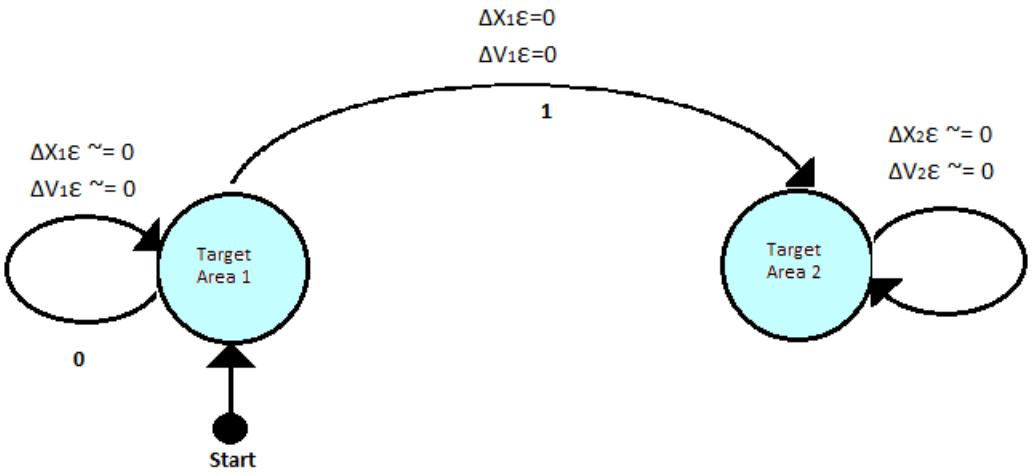

Figure 6.7: Finite state machine representation of the navigation system for the CAESAR vehicle

Attitude control

The attitude is controlled such that the direction of thrust, in line with $\hat{z}_b$, is parallel to the desired resultant force. Since the attitude control is done in the body axis, $\vec{F}^m_{ctrl}$ is converted to $\vec{F}_{ctrl}$. Since the pointing of $\hat{z}_b$ is independent from the yaw axis, a separate controller is used for the moment around the body's z-axis, $M_{ctrl,z}$. In the following sections the tilting controller is discussed first and the yaw axis controller is discussed afterwards.

For tilt control the angular error, e_{ctrl1}, between $\hat{z}_b$ and $\vec{F}_{ctrl}$ is used as an input for a PD controller. As shown in Eq. 6.7, the dot product is used for this calculation and gives a result between 0 and π. The use of the cross product was seen as unsuccessful, since the arcsin provides results between $-\pi/2$ and $\pi/2$. Because the direction of the control moment is already provided by the unit vector, this effectively only gives results between 0 and $\pi/2$.

The output of the PD is a moment magnitude that is multiplied with the unit vector $\hat{m}_{ctrl1}$. This vector is perpendicular to the plane formed by $\hat{z}_b$ and $\vec{F}_{ctrl}$, and it therefore makes sure that the shortened rotation angle is made. As shown in Eq. 6.8, $\hat{m}_{ctrl1}$ is constructed by normalising the cross product $\hat{z}_b \times \vec{F}_{ctrl}$. With the particular order in the cross product it is made sure that the positive moment resulting from the PD controller rotates the $\hat{z}_b$ towards $\vec{F}_{ctrl}$.

$$e_{ctrl1} = \arccos\left(\frac{\hat{z}_b \cdot \vec{F}_{ctrl}}{\|\hat{z}_b\|\|\vec{F}_{ctrl}\|}\right) \tag{6.7}$$

$$\hat{m}_{ctrl1} = \frac{\hat{z}_b \times \vec{F}_{ctrl}}{\|\hat{z}_b \times \vec{F}_{ctrl}\|} \tag{6.8}$$

As shown in Eq. 6.9, the yaw rate is used as the error for a proportional controller. Because the absolute yaw angle is not relevant for the navigation nor the release of the landing system, the objective of this controller is to keep the yaw rate zero. No derivative term is required in this controller since the moment and yaw rate form a first order system. The direction of the moment vector is derived from $\hat{z}_b$, as shown in Eq. 6.10, such that this controller only influences the yaw.

$$e_{ctrl2} = -\omega_z \tag{6.9}$$

$$\hat{m}_{ctrl2} = \hat{z}_b \tag{6.10}$$

With both the directions and magnitudes obtained as described in the previous paragraphs, the total moment requested by the control systems in the body frame, $\vec{M}_{ctrl}$, is found as given in Eq. 6.11.

$$\vec{M}_{ctrl} = M_{ctrl1} \cdot \hat{m}_{ctrl1} + M_{ctrl2} \cdot \hat{m}_{ctrl2} \tag{6.11}$$

Control parameters

For the initial tuning of the control parameters, the model is simplified such that analytical methods can be used for the first order estimation. As the simplifications made are substantial, the control parameters have been manually verified and tuned afterwards. The equations of motion are replaced by those of a point mass, with the resulting transfer function shown in Eq. 6.12. For the transfer function related to the moment control, the mass in this equation is simply replaced by the mass moment of inertia. Aerodynamic disturbances are neglected in this approximation.

$$H(s) = \frac{1}{m \cdot s^2} \tag{6.12}$$

During the first few simulations, it was seen that the simulation shows no steady state error when only proportional and derivative control action was applied. An integrator term to eliminate a steady state error is therefore not required. Moreover, due to the control action limits the actuators introduce in the system the integrator term was seen to cause integrator wind up.

In short the following occurs: The maximum thrust limit causes the position error to be sustained for longer then expected by the PD controller. The integrator term tries to counteract this sustained error by requesting more control action, however, as this extra control action is not supplied, the integrator control action accumulates over time. The result is that the integrator term causes the system to overshoot. An overshoot is not only inefficient in terms of fuel consumption, it also means that the system crashes if the altitude is overshot. For these reasons, the integrator term was set to zero on all controllers with the resulting transfer function shown in Eq. 6.13. The controllers will therefore be referred to as PD controllers.

$$C(s) = k_p + k_d \cdot s \tag{6.13}$$

With both transfer functions known, the closed loop system response can be constructed as shown in Eq. 6.14. The resulting transfer function can be classified as a second order system with a finite amount of zeros. As a first order approximation, the effect of the zero is ignored and the natural frequency and damping ratio of the system are respectively found by Eq. 6.15 and Eq. 6.16.

$$\frac{Y(s)}{X(s)} = \frac{C(s) \cdot H(s)}{1 + C(s) \cdot H(s)} = \frac{\frac{k_d}{m}\left(s + \frac{k_p}{k_d}\right)}{s^2 + \frac{k_d}{m} \cdot s + \frac{k_p}{m}} \tag{6.14}$$

$$\omega_n = \sqrt{\frac{k_p}{m}} \tag{6.15}$$

$$\zeta = \frac{k_d}{2\sqrt{k_p \cdot m}} \tag{6.16}$$

To arrive at the initial values for the control parameters, the settling time as approximated in the mid-term report [26] was used. By combining Eqs. 6.15 to 6.17, the control parameters are found for both the position and attitude controllers. A settling time of 40 s, a damping ratio of 1, and a mass of 280 kg were used for the position controllers. The tolerance was set to $2.5{\cdot}10^{-4}$, which is equivalent to a 0.5 m accuracy over a travel distance of 2 km. A settling time of 2 s, a damping ratio of 1, and a inertia of 35 kg·m^2 were used for the attitude controllers. Here, the tolerance was set to $5.6{\cdot}10^{-4}$, equivalent to 1 deg accuracy over a 180 deg rotation. The parameter values are shown in Table 6.4 together with their values after manual tuning.

$$T_s = -\frac{\ln(tolerance)}{\zeta \cdot \omega_n} \tag{6.17}$$

As mentioned in the section on attitude control, the yaw moment controller and yaw rate form a first order system. Analogous to the way a transfer function was found for the aforementioned controllers, the transfer function for the yaw rate control is shown in Eq. 6.18. The control parameter can then be found by setting a value for the time constant for the resulting exponential function. The time constant, calculated as in Eq. 6.19, represents the time required to reach 63.2% of a step input. The control parameter shown in Table 6.4 was then found by setting this time to constant 0.5, with an I_{zz} of 60 kg·m^2.

$$\frac{Y(s)}{X(s)} = \frac{\frac{k_p}{I_{zz}}}{s + \frac{k_p}{I_{zz}}} \tag{6.18}$$

$$\tau_{yaw} = \frac{I_{zz}}{k_p} \tag{6.19}$$

Table 6.4: Control Parameter values; initial approximation and manually tuned afterwards

	Position control						Attitude control		
	x		y		z		tilt		yaw rate
	k_p	k_d	k_p	k_d	k_p	k_d	k_p	k_d	k_p
Initial	12	116	112	116	12	116	236	180	120
Tuned	10	90	10	90	10	100	236	260	120

The initial guess for the control parameters work surprisingly well and result in a stable system. Manual tuning was used to see if the system performance could be further improved. The aggressiveness of the position controllers was slightly reduced. Although this elongates the mission duration and thus fuel use, it allows for a lower maximum thrust level as less control action is requested. A lower maximum thrust level has the benefits of a reduced engine mass and lower possible minimum thrust level. The significance of the minimum thrust level is described in section 6.7.5.

The derivative term for the controller in the z-direction was increased to increase the robustness of the system. Any overshoot in the z direction causes unwanted dust clouds and even a potential crash. The potential to avoid these hazards outweighs the longer descent time caused by the now overdamped system.

For the tilt controller, extra damping was introduced to reduce the oscillating behaviour that remained. The longer settling time for this motion did not negatively affect the way attitude control is used for horizontal manoeuvring. Finally, the yaw rate controller performed as predicted and did not require extra tuning.

Derivative Filtering

A reference input with sharp corners, e.g. a step input, results in a high derivative in the error. The derivative term in the PD controller will then react with an unreasonably high control action. The same problem arises in practice when typically high frequency noise is introduced by sensors. The mathematical origin of this problem can be seen in the bode plot of the PD controller, shown in Fig. 6.8a. It can be seen that the response magnitude goes to infinity as the frequency goes to infinity.

As a solution to this problem, a first order low-pass filter was introduced. The transfer function for such a filter is given in Eq. 6.20, where ω_f is the filter's cut-off frequency. The bode plot in Fig. 6.8 shows how frequencies above this cut-off frequency are attenuated. To make sure that the filter does not negatively affect the PD controller, the filter frequency should be selected outside the domain natural frequencies present in the system. As a rule of thumb, the cut-off frequency should be ten times higher than the highest natural response frequency in the system.

In Eq. 6.15 an approximation for the closed loop natural response frequency was already given. For the moment controllers, the mass in this equation should be replaced by the mass moment of inertia. The filter frequencies for all PD controllers can then be found using the tuned control parameters from Table 6.4, a

system mass of 280 kg for the position controllers, and an inertia of 35 kg·m^2 for the attitude controller. The used filter frequencies are shown in Table 6.5 and required no extra tuning after implementation.

Now, as shown in Fig. 6.8, the combination of the PD controller and filter has a constant response amplitude for frequencies above the filter's cut-off frequency.

$$F(s) = \frac{\omega_f}{\omega_f + s} \tag{6.20}$$

Table 6.5: First order filter cut-off frequencies used for the different PD controllers.

	Position control			Attitude control
	x	y	z	tilt
ω_f [rad·s^{-1}]	2	2	2	26

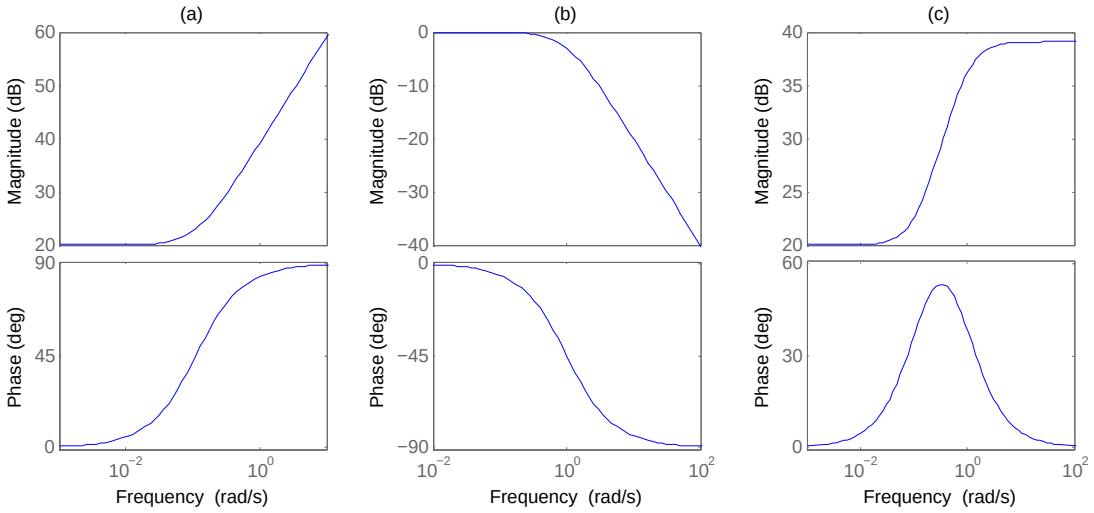

Figure 6.8: Bode plots for (a) PD controller with $k_p = 10$ and $k_d = 90$, (b) first order low-pass filter with ω_f 2 rad·s^{-1}, (c) the PD controller and the filter in series.

6.7.5 Actuators

The individual thrust levels of all main actuators can be calculated based on the desired control forces in the Martian frame, $\vec{F}^m_{ctrl}$, the orientation of the vehicle, the desired control moments in the body frame, $\vec{M}_{ctrl}$, and the thruster configuration. The method used to arrive at these individual thrust levels is presented in the following paragraphs. First the control force in the Mars frame is converted to a thrust force in the body frame. Second, a linear system is constructed based on the physical thruster layout to calculate the appropriate individual thrust levels. The maximum and minimum thrust levels are imposed on the solution afterwards. A similar procedure is followed for the thrusters dedicated to yaw control. Finally, the individual thrust levels are used to calculated all force and moment components that will act on the vehicle as a result of thrust.

Converting $\vec{F}^m_{ctrl}$ to the body frame

When converting $\vec{F}^m_{ctrl}$ to the body frame, simply using the transformation matrix from the Mars to the body axis T_{bm} was seen to be undesirable. In that case significant x and y components in the body axis resulted, which cannot be supplied due to the fixed and predominantly downward pointing of the thrusters.

Consequently, the vertical force in the Mars frame, $F^m_{ctrl,z}$,is lower than expected and the vehicle overshoots the altitude target.

To prevent this from happening, an equation is constructed that ensures that $F^{\mathrm{m}}_{\mathrm{ctrl,z}}$ is provided by the thrusters as accurate as possible. Deviations from the exact answer occur when side way thrust forces are created or when the maximum thrust limit is reached on at least one thruster.

The equation is derived from the transformation of the thrust in the body axis to the Martian inertial frame axis, as shown in Eq. 6.21. It is assumed that the main contribution to $F^m_{ctrl,z}$ will be the z component of the thrust. $F_{\mathrm{T,x}}$ and $F_{\mathrm{T,y}}$ are therefore set to zero in this equation. By close examination, it is seen that only element $T_{\mathrm{mb},33}$ is relevant if the horizontal forces in the Martian frame are allowed to take any value. The equation can then be solved for $F_{\mathrm{T,z}}$ with the result shown in Eq. 6.22.

As can be seen this equation is only depending on the roll and pitch angles, ϕ and θ. This is in line with the expectations as $F_{\mathrm{T,z}}$ should be independent from the yaw angle. Furthermore it is seen that the equation goes to infinity as either the roll or pitch goes to $\pi/2$. This is again in line with the expectations because when the vehicle is rotated $\pi/2$, $F_{\mathrm{T,z}}$ and $F^m_{\mathrm{ctrl,z}}$ become perpendicular and a singularity exists.

SIMULINK® experiences no problems in this case as the subsequent saturation block excepts Inf as an input and imposes the minimal and maximal total thrust on the $F_{T,z}$ signal. If such an implementation does not hold in practise, the roll and pitch angles could be checked with if statements and given a small offset in case of a $\pm\ \pi/2$ value.

$$\begin{bmatrix} \cdot \\ \cdot \\ F^m_{ctrl,z} \end{bmatrix} = \mathbb{T}_{mb} \begin{bmatrix} 0 \\ 0 \\ F_{T,z} \end{bmatrix} \tag{6.21}$$

$$F_{T,z} = \frac{F^m_{ctrl,z}}{\cos\phi \cdot \cos\theta} \tag{6.22}$$

Main thruster layout matrix

With the desired thrust force in the z direction derived in the previous section and the moments already given in the body axis by the attitude controllers, the individual thrust settings can be calculated. In the following paragraphs, a matrix multiplication will be found that solves this problem. First, the influence of each thruster on the resulting forces and moments is investigated. Afterwards, this information is used to solve the inverse problem.

Each thruster is positioned at the corner of a square. At this point, as illustrated in Fig. 6.9, the main thrusters are tilted slightly inwards over the angle ϕ_{T} towards the midpoint of the square. Because of the symmetry in this layout, the vector decomposition can now be done based solely on ϕ_T. Together with the thruster numbering shown in Fig. 6.10, the resulting thrust force can then be found based on the setting of each individual thruster by the matrix multiplication shown in Eq. 6.23. The yaw thrusters are not included in this equation since they will always be applied as a couple such that no resultant force is created.

$$\vec{F_T} = \begin{bmatrix} -\frac{1}{2}\sqrt{2}\sin\phi_T & -\frac{1}{2}\sqrt{2}\sin\phi_T & \frac{1}{2}\sqrt{2}\sin\phi_T & \frac{1}{2}\sqrt{2}\sin\phi_T \\ \frac{1}{2}\sqrt{2}\sin\phi_T & -\frac{1}{2}\sqrt{2}\sin\phi_T & -\frac{1}{2}\sqrt{2}\sin\phi_T & \frac{1}{2}\sqrt{2}\sin\phi_T \\ \cos\phi_T & \cos\phi_T & \cos\phi_T & \cos\phi_T \end{bmatrix} \begin{bmatrix} F_{T,1} \\ F_{T,2} \\ F_{T,3} \\ F_{T,4} \end{bmatrix} \tag{6.23}$$

In order to find a similar expression for the resultant thrust moment, the moment arm of each thruster needs to be found. This moment arm is constructed as in Eq. 6.24 by taking the difference between the thrusters position and the centre of gravity. Here, $\vec{d_i}$ is fixed by the thruster layout to $\begin{bmatrix} \pm 0.725 \\ \pm 0.725 \\ 0.169 \end{bmatrix}$, where the sign depends on the thruster number.

The thrust moment can now be found by taking the cross product of each thruster arm with the vector representation of its thrust. Summing this result for all eight thrusters gives the resultant thrust moment,

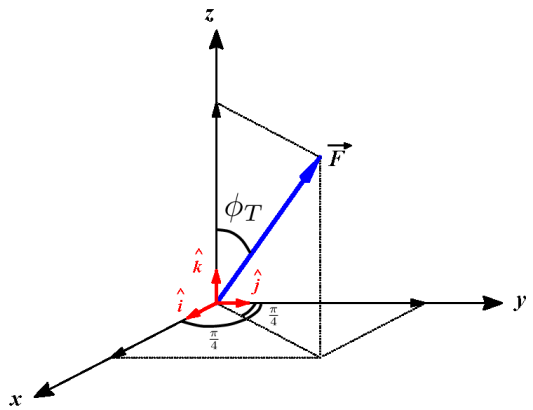

Figure 6.9: Thrust vector of the main thrusters in the body axis frame. An angle of ϕ_T is made with the z-axis such that the x and y components are equal in magnitude.

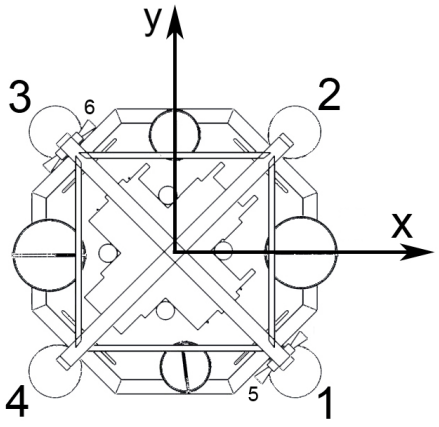

Figure 6.10: Numbering convention for the thruster. Thrusters 1-4 are the main thrusters, 5 and 6 are thruster pairs where a counter clockwise thrust is defined as positive.

$\vec{M}_T$, as shown in Eq. 6.25. The resulting 6x6 matrix is not shown as a whole, but relevant entries will be used and shown in Eqs. 6.26.

$$\vec{d}_i^* = \begin{bmatrix} x_i^* \\ y_i^* \\ z_i^* \end{bmatrix} = \vec{d}_i - \vec{x}_{c.g.} \tag{6.24}$$

$$\vec{M}_T = \sum_{i=1}^{4} \vec{d}_i^* \times \vec{F}_{T,i} \tag{6.25}$$

Now that the matrices relating the individual thrust forces to the resulting forces and moments are defined, these results can be combined to set up the required linear system of equations. The goal for the main thrusters is to achieve certain values for $F_{\mathrm{T,z}}$, $M_{\mathrm{T,x}}$, and $M_{T,y}$ set by the controller. The desired value for $F_{\mathrm{T,z}}$ was earlier defined, and $M_{\mathrm{T,x}}$ and $M_{\mathrm{T,y}}$ are desired to be equal to the x and y component of $\vec{M}_ctrl$.

By taking the rows for these parameters from Eq. 6.23 and 6.25, the first three rows of Eq. 6.26 are constructed. The contribution of the yaw thrusters to $M_{\mathrm{T,x}}$ and $M_{\mathrm{T,y}}$ is neglected as it is several orders of magnitude smaller than the contribution of the main thrusters. However, this system of three equations and four unknowns has infinitely many solutions. A fourth linear independent equation is therefore made such that a unique solution can be found.

The fourth equation is based on a symmetric application of thrust. With Fig. 6.10 in mind, it is seen that for both a moment around the x and y axis thruster 1 and 3 would have to apply opposite thrust forces. The same holds for thrusters 2 and 4. It can then be concluded that for every thruster to equally contribute to the moment generation, the sum of thruster 1 and 3 should be equal to the sum of 2 and 4. As this condition is linearly independent from the other rows, the matrix is now invertible.

Solving Eq. 6.26 for the individual thrust levels then yields Eq. 6.27, where $\mathrm{A}_{\mathrm{T}}^{-1}$ in the latter equation is the inverse of the matrix shown in the former equation.

$$\begin{bmatrix} F_{T,z} \\ M_{T,x} \\ M_{T,y} \\ 0 \end{bmatrix} = \begin{bmatrix} \cos\phi_T & \cos\phi_T & \cos\phi_T & \cos\phi_T \\ y_1^*\cos\phi_T - z_1^*\frac{1}{2}\sqrt{2}\sin\phi_T & y_2^*\cos\phi_T + z_2^*\frac{1}{2}\sqrt{2}\sin\phi_T & y_3^*\cos\phi_T + z_3^*\frac{1}{2}\sqrt{2}\sin\phi_T & y_4^*\cos\phi_T - z_4^*\frac{1}{2}\sqrt{2}\sin\phi_T \\ x_1^*\cos\phi_T - z_1^*\frac{1}{2}\sqrt{2}\sin\phi_T & x_2^*\cos\phi_T - z_2^*\frac{1}{2}\sqrt{2}\sin\phi_T & x_3^*\cos\phi_T + z_3^*\frac{1}{2}\sqrt{2}\sin\phi_T & x_4^*\cos\phi_T + z_4^*\frac{1}{2}\sqrt{2}\sin\phi_T \\ 1 & -1 & 1 & -1 \end{bmatrix} \begin{bmatrix} F_{T,1} \\ F_{T,2} \\ F_{T,3} \\ F_{T,4} \end{bmatrix} \tag{6.26}$$

$$\begin{bmatrix} F_{T,1} \\ F_{T,2} \\ F_{T,3} \\ F_{T,4} \end{bmatrix} = A_T^{-1} \begin{bmatrix} F_{T,z} \\ M_{T,x} \\ M_{T,y} \\ 0 \end{bmatrix} \tag{6.27}$$

With these results it can also be seen why it is impossible to also control the side way forces $F_{\mathrm{T,x}}$ and $F_{\mathrm{T,y}}$ in the body axis. By reviewing Eqs. 6.23 and 6.26, it can be shown that the rows for $F_{\mathrm{T,x}}$ and $F_{\mathrm{T,y}}$ are a linear combination of the rows for $F_{\mathrm{T,z}}$, $M_{\mathrm{T,x}}$, and $M_{\mathrm{T,y}}$. In conclusion, only three of these five parameters can be independently controlled by the current thruster configuration.

Minimum and maximum thrust level

Due to physical limitations of the thrusters a maximum and minimum thrust level exists for each thruster. Simply setting thrust values outside this bound to that bound will in many cases influence the moments. This would mean that attitude control, which is done by differences in thrust levels, is impossible in a phase of maximum deceleration. To avoid this situation, a method is constructed that keeps the thrust levels within bounds without influencing the resultant moment.

The logic imposing the maximum and minimum on the thrust levels is explained by means of pseudocode in Algorithm. 1. First, the thruster that lies most out of bound is found. Then, the required change to $F_{\mathrm{T,z}}$ to just bring this thrust level to the bound is calculated with the appropriate coefficient of the $\mathrm{A_T^{-1}}$ matrix. With the new value for $F_{\mathrm{T,z}}$, the new thrust levels are calculated with Eq. 6.27. These new levels are then again checked against either the minimum or maximum in the while loops. Effectively, $F_{T,z}$ is iteratively lowered or increased such that all thrust levels are forced within the bounds, while the resulting moments remain untouched.

while $min(F_{T,1-4}) < F_{T,min}$ **do**
  $i \leftarrow$ number of the thruster with $min(F_{T,1-4})$
  $\Delta F_{T,z} \leftarrow [F_{T,min} - F_{T,i}]/A_T^{-1}(i,1)$
  $F_{T,z} \leftarrow F_{T,z} + \Delta F_{T,z}$
  $F_{T,1-4} \leftarrow$ recalculate thrust levels
end
while $max(F_{T,1-4}) > F_{T,max}$ **do**
  $i \leftarrow$ number of the thruster with $max(F_{T,1-4})$
  $\Delta F_{T,z} \leftarrow [F_{T,i} - F_{T,max}]/A_T^{-1}(i,1)$
  $F_{T,z} \leftarrow F_{T,z} - \Delta F_{T,z}$
  $F_{T,1-4} \leftarrow$ recalculate thrust levels
end
all $F_{T,i}$ where $(F_{T,i} < F_{T,min}) \leftarrow F_{T,min}$

Algorithm 1: Psuedocode for imposing the minimum and maximum on the thrust levels

The final line is added in the exceptional case that one thruster is below the minimum and another is above the maximum at that exact same time. Due to the order in the code, the second while loop than undoes the first one and a thruster will still be below minimum. Because this case is so exceptional, it is decided that every thrust level still below the minimum will be set to the minimum.

Yaw thrusters

As the moment around the z axis is only influenced by the yaw thruster pairs, setting up the equation for this system turns out to be trivial. By requiring that both thruster pairs contribute equally to the moment generation, a pure couple is formed. The thrust levels then only depend on the distance between the two parallel thruster pairs, as shown in Eq. 6.28. Based on the sign of $F_{\mathrm{T,5}}$ and $F_{\mathrm{T,6}}$ it is determined which thruster of each pair is actuated. Here, $M_{\mathrm{T,z}}$ is desired to be equal to the z component of $\vec{M}_ctrl$.

$$\begin{bmatrix} F_{T,5} \\ F_{T,6} \end{bmatrix} = \begin{bmatrix} \frac{1}{0.725 \cdot \sqrt{2}} \\ \frac{1}{0.725 \cdot \sqrt{2}} \end{bmatrix} M_{T,z} \tag{6.28}$$

Resultant thrust forces and moments

With all the individual thrust levels determined, the resultant thrust forces and moments need to be recalculated. Recalculation is required as the imposing of the minimum and maximum thrust levels might have the result deviate from the values requested by the controllers. The calculation is conveniently done with the earlier defined Eqs. 6.23 and 6.25.

6.8 Verification

Verification is the process that determines if the ADCS model that is being implemented accurately represents the conceptual description of the initial model; as also the accommodating solution to it [67]. In other words the stage of verification answers to the question: "Are we building the ADCS right?"[72].
The above mentioned process consists of two main stages. Namely the code verification stage and the calculation verification stage, which are presented and analysed in the preceding sections.

6.8.1 Code verification

The purpose of code verification is to ensure that the Simulink® block set is working as intended. At this point the program is being checked and tested thoroughly for any errors within the coding itself, but also to verify the correctness of the results it provides to the user. After the passage of this stage, the code has no syntax errors, it is robust and can be trusted but also the program itself is easily modified and maintained. Thus verifying that the computer code and model are in complete agreement.

6.8.2 Calculation Verification

The purpose of this stage is to verify that the program is "calculating the right stuff" [72]. In other words the existence of this stage is two fold: firstly, to quantify the divergence of the simulation from the analytical solution and secondly to estimate the error created by the use of this numerical model[67]. For example if the solution of the computer code is within a predetermined margin of error than the program is verified for its numerical accuracy of the model.

6.8.3 Conclusions

During the verification of the Simulink® block set, the behaviour of the ADCS system did not always fulfil the required goals. The initial conditions of the CAESAR-lander have a large influence on whether the lander overshoots its target positions. The lander is designed for a release at an altitude of 2000 m and an initial speed of -100 ms^{-1} in "z"-direction. Variation of the initial conditions revealed that the lander operates as intended within a certain boundary. One can find the boundaries of the system in section 6.10.

The Simulink® block simulation was subjected to multiple tests to determine the error that causes this behaviour. It was determined that the code was correct, and the fault has been found to be located in the PD controller. With this in mind it has been concluded that the mathematical model that is used to express our conceptual model needs to be fine tuned for the system to be capable to work in all regions.
Several approaches have been proposed as a solution. Regulation of the PD controller is an option that can be done. Secondly, it is assumed that the location of the beacon is located at the beginning of the co-ordinate system. By virtually shifting up the location of the beacon ("z" - axis), even though the CAESAR will under shoot (as shown in figure 6.11) it will still remain within acceptable altitude limits.

Propellant mass estimations

The propellant mass estimation that is done during the simulation can be used to verify the model. The mid-term report [26] proposes an analytical method for fuel mass estimation. This method will be used to verify the final model. Also, as an intermediate step, a simplified version of the model will also be compared to the other results. The simplified model is the final model before all the rotations and horizontal movements are added.
The verification is done for the conditions where the Isp is 312 s, the start height is 2000 m, the velocity in z-direction is -100 ms^{-1}, the hovering time is 30 s, and the starting mass is 266.75 kg. Note: The starting mass used in this verification is lower than the final design mass, fuel consumptions might turn out to be lower than the final design. Using these values, two scenarios are calculated. The first scenario is a pure descent with no horizontal movements. The second scenario is a descent in which the lander has to translate 2200 meters in x-direction, this scenario will not be performed in the simplified model. The calculated masses are shown in table 6.6.

Table 6.6: Analytically and numerically calculated fuel masses for two scenarios.

Starting position	Calculation method		
	Analytical	Simplified model	Final model
[0 0 2000]	29.87 kg	32.96 kg	34.47 kg
[2200 0 2000]	38.23 kg	N/A	45.75 kg

The mass estimations show us that the simulations require more fuel mass once the simulations become more detailed. These differences in fuel mass are predictable and make sense. Therefore, it is assumed that the results are verified.

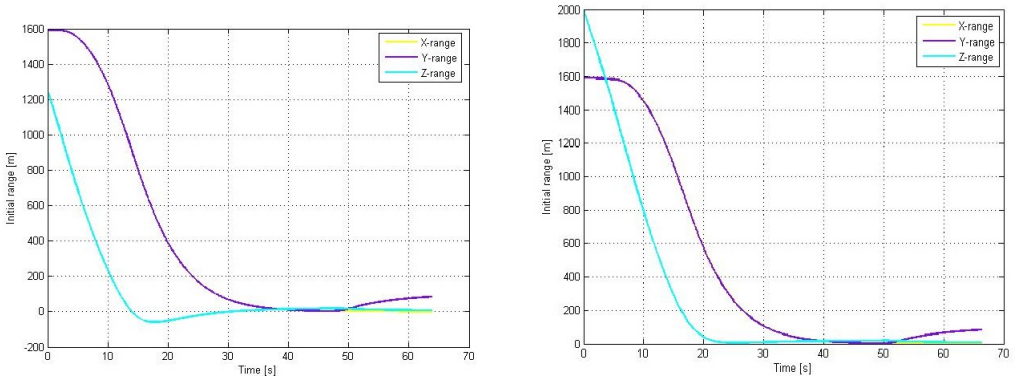

(a) For values in the non acceptable area the CAESAR undershoots once reached target area.

(b) For values in the acceptable area the CAESAR levels once reached target area.

Figure 6.11: Location graph of the CAESAR's in the acceptable area. The three colours of the graph depict the three axis systems (x,y,z - yellow,purple,blue).

6.9 Validation

This chapter will mainly discuss recommendations on the validation process. Due to the boundaries on the project it is impossible to conduct real life experiments on the powered descend/navigation stage.

6.9.1 Validation of internal behaviour

The validation of the internal behaviour should be conducted by testing the communication between electronics. Responses might have a delay on hardware/software level and the PD-controllers might react different

to certain inputs. Validation of the system board should be done on single unit level to full scale system tests.

6.9.2 Validation of hardware subsystems

Validation on hardware level includes testing of subsystem performance and comparison with assumed performance in the model. The first subsystem that requires validation is the thruster subsystem. The simulation assumes thrusters which function as required. In reality thrusters might deliver a slightly lower thrust output. Also, thrusters might have a slightly slower response time than required by the control system. Finally, a certain fuel consumption is assumed associated with the required thrust level. The actual propulsion system might have a slightly lower I_sp value or other fuel losses due to inefficient operation. In summary, the thruster system should be validated on the points shown below:

Thruster validation subjects

- Thruster throttling response time.
- Actual achieved thrust values.
- Fuel flow against thrust values.
- Thrust line of action.

Other subsystems which require validation include the sensors which deliver data for the position and velocity of the lander. The output of a sensor could be non-linear or it might consist of errors which should be accounted for. All sensors used should be properly validated.

6.9.3 Validation of disturbances

The current model features a wind disturbance modelled by a random noise generator. The wind magnitude applied to the model is comparable to the wind on Mars to ensure that the lander is capable to withstand and perform normal operation in Mars' atmosphere.

6.9.4 Validation of full scale lander

The final step of the Validation process consists of full scale model tests. The inertia and center of gravity of the lander are taken from a 3d model generated in Solidworks®. This model lacks the small details such as production errors or small changes applied in the production process. Therefore, the full scale lander should be tested for changes in inertia and center of gravity.

Finally when possible, the full lander will be tested in a complete system test. The simulation model incorporates wind and gravity on Mars, but small adjustments could be made to ensure functionality on Earth. If the lander produces the same performance on Earth as predicted, the simulation model will be validated and expected to be accurate on Mars.

6.10 Sensitivity analysis

In the following sensitivity analysis a set of 9 parameters will be varied. These parameters will be varied till a total fuel consumption of 50 kg is reached which is the total amount of fuel on-board of each CAESAR, or till the CAESAR crashes.

6.10.1 Influence of range on fuel consumption

To identify the influence of the x,y,z range components the range of each component is varied individually with steps of 250 meters while keeping the other two components constant. For the altitude range (z-component) the x and y value are set on 1591 meter (now called the average initial range), which are the x and y component of the standard initial range of 2250 meters when CAESAR is located at an angle of 45° from the beacon. When decreasing the range of the x and y component only fuel usage will decrease with no limit to the range. However when decreasing the range of the z-component there is a range limit of 1200 meters, when decreasing the z-component further the CAESAR will overshoot zero which means it will crash in to the ground. This overshoot will happen due to a low altitude to slow down the CAESAR. The other component ranges are limited by the fuel consumption maximum of 50 kg. The results can be found in figure 6.12. The first plot of figure 6.12 are the x,y,z range values plotted against the total fuel consumption.

6.10.2 Influence of initial velocity on fuel consumption

For this test the average initial range is used with an altitude of 2000 m to explore the sensitivity of the initial velocity on the CAESAR mission profile. At a velocity of more than or equal to 50 ms^{-1} in y-direction and more than or equal to -125 ms^{-1} in z-direction the z-location component will overshoot zero and thus the CAESAR will crash in to the ground. CAESAR is restricted in the x-component by the fuel consumption that exceeds the maximum of 50 kg. The initial velocity in the z-direction show parabolic behaviour with the fuel consumption due to the fact the engine also has an idle mode, resulting in the longer it takes for the CAESAR to reach the ground the more fuel this idle mode will burn. The results can be found in figure 6.12. The second plot of figure 6.12 are the x,y,z velocity values plotted against the total fuel consumption.

6.10.3 Influence of initial angle on fuel consumption

Also for the sensitivity analysis of the initial angle of the CAESAR the average initial range with an altitude of 2000 m is used. With only a initial velocity component in the z direction of -110 ms^{-1} is present (free fall velocity). The roll angle (x-axis) is limited to a maximum roll angle of 0.7 radians, any roll angle larger than this value will result in too much fuel consumption. The pitch angle (y-axis) is both limited to a negative angle of -0.875 radians and a positive pitch angle of 0.7 radians, any angle respectively below or above these values will also result in too much fuel consumption. The yaw angle (z-axis) is the only angle that will not limit the CAESAR in navigating to the beacon. The results for all three angles can be found in figure 6.12. The third plot of figure 6.12 are the x,y,z initial angle values plotted against the total fuel consumption.

6.10.4 Influence of initial mass on fuel consumption

The influence of the initial mass is as expected. The higher the initial mass the higher the fuel consumption. The lower the initial mass the lower the fuel consumption.

6.10.5 Influence of wind on fuel consumption

Due to the thin atmosphere the influence of the wind is very small on the total fuel consumption since the aerodynamic forces will be small. Even with a gain of 15 (which means 15 times the normal expected wind speed that is modelled in the simulation model) the fuel consumption changes with just 440 grams.

6.10.6 Operation on other planetary bodies

The simulation is used to imitate conditions on other planetary bodies to see how the lander will behave. Only the Earth and Moon have been considered. For Moon conditions, a possible change to the design has been proposed to ensure functionality.

The conditions on Earth have been imitated by changing the gravity to 9.81 ms^{-1} and the conditions on the Moon have a gravity constant of 1.625 ms^{-1} and a wind velocity of 0 ms^{-1}.

No surprises have been encountered when looking at the results. The lander crashed without a doubt on the surface of the Earth, the thrusters of the lander do not have sufficient power to sustain a constant altitude. On the Moon, the lander took off after the airbag system was deployed. The drop in mass caused the minimum thrust value to be higher than the gravity force. A simple change in thruster size proved not to solve the problem easily. Decreasing the thrust caused the lander to overshoot its target altitude, crashing the lander. To ensure functionality on the Moon, the controllers should be tuned accordingly.

6.10.7 Influence of hover time on fuel consumption

Increasing the hover time also increases the fuel mass. The main contributor to fuel usage is the counteraction of the gravity force. As expected, the fuel usage increases almost linearly with the increase of hover time. When hover time increases beyond 30 seconds, the fuel usage slowly decreases due to decreasing lander mass. The lander consumes approximately 0.128 kg of fuel per second of hover time.

6.10.8 Influence of asymmetric fuel tank depletion on fuel consumption

The fuel used in the rocket system will be drawn from two fuel tanks, due to minor difference in the tubing or valves, asymmetric depletion might occur. This asymmetry causes the center of gravity to shift in horizontal direction. The sensitivity analysis showed that minor differences had no influence on the performance, however, when the shift in center of gravity increased beyond 7 cm in x- or y-direction, which is the maximum shift possible due to complete asymmetry in fuel. A slight overshoot occurred in the altitude controller which caused the lander to hit the surface of Mars. The reason of this overshoot is the fact that due to the shift in the cg, the thruster arm changes. Due to the change in thruster arm-length the moment incurred by the thrusters changes, due to the change the thrusters need a difference in thrust to maintain the required moment. During the maximum thrust phase, this change in thrust can only be achieved by decreasing thrust on one side of the lander. Which lowers the total thrust output of the lander, causing it to overshoot its altitude target and crash.

Three solutions are proposed to this problem. First, this problem occurs because the thrusters hit their respective maximum thrust level. Increasing the maximum thrust level solves this problem but increases inefficiency and fuel weight. The second solution is a regulator which monitors the fuel consumption in each tank and regulate the fuel flow to prevent large differences in consumption. Finally a link between the fuel tanks can be made which operates through the law of communicating vessels.

6.10.9 Influence of thruster angle on fuel consumption

The thruster angle of the lander is variable but will be chosen in the design phase and then be fixed. A thruster angle of zero degrees is the most efficient angle setting since it consumes the least amount of fuel. But taking in to account that the payload will be dropped and the hot propulsion gasses should not be damaging the payload a minimal thruster setting of 15 degrees is needed. The thruster setting can be varied to just above 25 degrees, past this angle the lander will crash.

6.11 Risk analysis

Now the ADCS design is worked out on a higher level, more risks could be identified. To successfully take in to account the risks, and to explore the eventual risks a risk analysis needs to be performed. The risks found will be presented in two tables, and will be evaluated on their likelihood to happen, the severity of the risk when it occurs, and the importance to prevent the risk. In Table 6.8 the risks are tabulated and an indicator from 1 (high likelihood) to 4 (low likelihood) will be given to the above mentioned aspects.

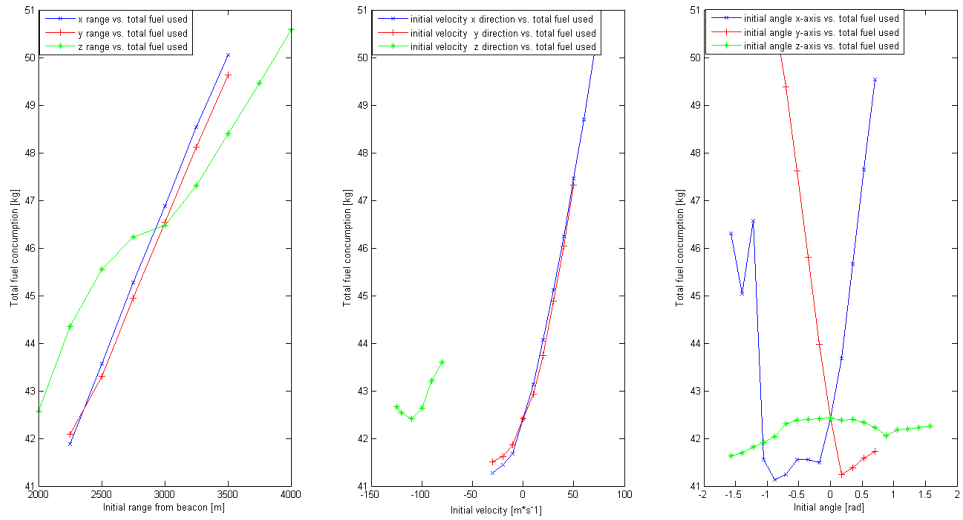

Figure 6.12: Plots of the influence of the initial conditions on the total fuel consumption

Table 6.7: Table showing the relative importance of all different risks involved in the ADCS and simulation. Closer to the top right is more important. See Table 6.8 for the risk explanations.

Severity	Likelihood			
	Impossible	Improbable	Probable	Frequent
Catastrophic		1		
Critical		2,4,5,6,8,10	9	
Marginal		3,7		
Negligible				

6.12 Conclusion

In the previous section, a complete walk through of the ADCS and Navigation system was presented. Initially the mission profile and the role of the ADCS and Navigation system to this was presented. Hardware systems that will be needed to be implemented to the system have been presented. Sensors that will allow the system to measure its environment have been studied while a complete profile description of the actuators needed is presented.
To check the Simulink® model created on its correctness it needs verification. The verification is done by comparing the model outputs to analytical solutions of the same scenario, and check if the output is within a predetermined error range. It was found that the initial conditions of the CAESAR have a large influence on whether the lander overshoots its target position. The simulation proved the designed control mechanism works for navigating the CAESAR towards the beacon while maintaining attitude by making use of PD controllers and respecting the maximum fuel capacity of 50 kg. Hazard avoidance during navigation to the beacon location will be done by making use of a flash LiDAR system.
Where a sensitivity analysis is done on the model to explore the boundaries of the model, the model itself delivers several plots of the thrust, position, and fuel usage as well an animation of the mission profile to actually check if the model delivers the desired output. Validating the model is something for in the near future, since testing in Mars like conditions on earth involve difficulties as high atmospheric testing and large costs will be involved. As final conclusion it can be stated that the simulation designed in the chapter proves the ADCS and navigations system is able to deliver a payload at a beacon location, while maintaining and controlling its attitude and altitude.

6.13 Recommendations

As far reccomendations go for the ADCS/navigations and simulation system. One should perform further research in the development of a Martian telemetry beacon system. The complete system should be build and be tested in a Mars like environment, to validate the systems ADCS/navigation behaviour.

Table 6.8: The risk analysis table shows all identified risks with 1 (high) to 4 (low) weighting factor, severity and importance indicators.

ID	Risk	Effect	Likelihood	Severity	Importance	Action to minimize risk
1	Failure of ADCS software	CAESAR cannot navigate/keep attitude	3	1	2	Extensively stress test the software until no errors occur
2	PD controllers not tuned correctly	CAESAR will not navigate/keep attitude correctly	3	2	2	Auto tuning PDs
3	Simulation not representing real case scenario	Simulation not correctly predicting the behaviour of the CAESAR	3	3	3	Perform tests in Mars like condition and validate the system with it
4	Wrong sensors used	The lander becomes uncontrollable	3	2	1	Testing of model in Mars like conditions/simulations
5	Wrong actuators used	The lander will crash	3	2	2	Testing of model in Mars like conditions/simulations
6	Beacon failure	No signal for navigation is present	3	2	1	Have a backup beacon/safe mode on the CAESAR that autonomously guides the CAESAR to the surface
7	Bit flip in system	The system functionality is disrupted	3	3	3	Radiation hardening/Fast rebootable system
8	ADCS to power demanding	The power supply can't handle the power demand of the ADCS and the lander becomes partly/completely uncontrollable	3	2	1	Double check maximum power consumption of all elements and adjust power supply when needed.
9	Fuel consumption too high	Lander does not have enough fuel to navigate	2	2	1	Excessive testing of the simulation and real model
10	Extreme initial landing conditions and landing ellipse	ADCS is not able to correct attitude and position of the lander	3	2	2	Double check entry calculations
11	Large shift in horzontal C_g	The lander will crash	4	2	2	C_g tests on Earth & Fuel flow regulator

7 Parachute and propulsion

The MACHETE and CAESAR vehicle architecture relies on a parachute and rocket engines to decelerate the vehicle after entering the Martian atmosphere. The midterm report [26] saw a general downselection of rocket engine propellant combinations and a selection of a parachute, with the option of making it guided. This chapter delves into the details of the guided parachute in order to determine the gains it provides.

From the simulations performed using the ADCS system controller final requirements on rocket engine and attitude control thruster thrust levels followed. A final choice on the propellant combination will be made. This chapter will also see the final sizing of the rocket engines, as well as investigation into some aspects like rocket engine throttling.

Finally some verification and validation methods will be presented to verify and validate the design methods presented in this chapter and the corresponding chapters in previous reports.

7.1 Propellant trade-off

In the midterm report a detailed rocket engine design option tree was presented on which a partial trade-off was performed. The trade-off however left the exact choice of propellant open. The remaining propellant options are discussed after which a final trade-off is made. The considered propellant combinations are common mono propellants and storable bi-propellants.

Hydrazine Hydrazine mono-propellant engines have the advantage that they are very simple. Because they are catalytically ignited they are also very reliable. The major disadvantages however are the toxicity of the propellant which imposes serious spacecraft handling difficulties and the relatively low specific impulse. Hydrazine propulsion systems are very well proven but do require pressurization.

NOFBX Nitrous oxide fuel blends, known under the Firestar trademark 'NOFBX', are a novel type of mono-propellant. Hydrocarbons are blended in the nitrous oxide in order to achieve high specific impulse, while keeping the advantages of a mono-propellant feed system. The engines can be ignited catalytically by decomposing the nitrous oxide and the feed system can be self pressurizing due to the high vapor pressure of nitrous oxide. Demonstrator versions of these engines have been operated, but not yet flown in space. While the propellant can be considered green, there are concerns with it being explosive as pointed out by A. Karabeyoglu [39].

Hydrogen peroxide High concentration hydrogen peroxide used as propellant is usually known as High Test Peroxide (HTP) and was primarily used shortly after the second world war. Nowadays HTP is only used for satellite attitude control. While HTP is fairly benign compared to hydrazine, it does require some care with handling and delivers a low specific impulse of 161 seconds. Hydrogen peroxide is catalytically decomposed in the rocket engines, simplifying the engine design. HTP systems require pressurization, increasing system complexity.

Nitrous oxide Nitrous oxide has been used in the past in cold gas thruster systems for attitude control. Catalytically decomposing the nitrous oxide can significantly raise the delivered specific impulse to 192 seconds. Nitrous oxide is self pressurizing, non-toxic and is fairly safe to handle. Some safety considerations however need to be taken as shown by A. Karabeyoglu [39] and the 2007 accident at Scaled Composites [66]. No records of hot nitrous oxide thrusters being flown in space have been found, but their theoretical advantages are backed up by V. Zakirov at Surry Space Centre [73].

Nitrogen tetroxide and MMH Nitrogen tetroxide (N_2O_4) combined with monomethylhydrazine is one combination of a broad family of hydrazine related bi-propellants. All of these propellants share the properties of delivering a fairly high specific impulse of up to 340 seconds. Both nitrogen tetroxide and hydrazine variants

are however highly toxic and require special care in selecting wetted materials. In addition the system needs to be pressurized and has a higher complexity than mono-propellant systems.

Propane and nitrous oxide By burning nitrous oxide with a hydrocarbon, the oxygen released by decomposing nitrous oxide is burned, greatly increasing the specific impulse over pure nitrous oxide thrusters. The Qualis Corporation developed and tested a demonstrator engine which burns nitrous oxide with propane (NOP), delivering a specific impulse of about 312 seconds [34]. The propane is ignited by catalytically decomposing the nitrous oxide. The system can be made self pressurizing using the high vapor pressure of the nitrous oxide, which will also can used to pressurize the propane fuel. While nitrous oxide does require some handling considerations, neither of the two propellant components is considered particularly dangerous or toxic.

Ethane and nitrous oxide An engine running on ethane and nitrous oxide has the added benefit over a propane based system that the vapor pressure of ethane is about equal to nitrous oxide. This further simplifies the pressurization of the feed system, by allowing both the oxidizer and fuel system to self pressurize independently. Specific impulse is about equal to propane based systems around 312 seconds. Experimental engines have been built and tested by Delft Aerospace Rocket Engineering at the Delft University of Technology [15]. The engine can be ignited using a classical igniter or by catalytically decomposing nitrous oxide.

Nitrogen tetroxide and kerosene Nitrogen tetroxide and kerosine (RP-1) bipropellant engines were widely used during the start of the cold war delivering a specific impulse of about 323 seconds, but is now less common in use. The engine requires an igniter and the system is pressure fed, resulting in a fairly more complex feed system than various mono-propellant systems. Nitrogen tetroxide is highly toxic.

Hydrogen peroxide and kerosene The British briefly used hydrogen peroxide and kerosene (RP-1) bipropellant engines in early rockets including the Bristol Siddeley Gamma family. While not being a true hypergolic propellant combination, hot hydrogen peroxide will readily react with kerosene. Hydrogen peroxide can be catalytically decomposed. This propellant mixture delivers a specific impulse of about 319 seconds, but the feed system does require pressurization. While both propellant components are non toxic, hydrogen peroxide is unstable and does need some handling care.

7.1.1 Trade-off method and criteria

Each propellant combination is scored on delivered specific impulse, where below 200 seconds is considered low and scored negative, between 200 and 300 seconds average and over 300 seconds high granting a positive score. The required ignition method is scored positive where catalytic or hypergolic ignition, and a normal igniter is scored as average. The rationale is that having a classical igniter invariably increases system complexity and reduced reliability to some degree relative to autoigniting systems. A pressurized system is scored as average, where a self pressurizing system is scored as positive. A pump fed system would score negative, as this requires most mass and increases system complexity the most.

Propellants are scored on safety and toxicity as well. Safety refers mainly to the degree in which propellants require special technical care during handling, storage and use. NOFBX being explosive scores negative, while peroxide systems require special care to avoid contaminations and being corrosive scores average. Propellants like nitrous oxide, which require fairly little care, score positive. Toxicity is scored positive for being non-toxic, average for being slightly toxic, and negative for being highly toxic.

Finally, overall system complexity and the degree to which a propellant combination is proven are scored. Low complexity scores positive while average complexity scores neutral. A large turbo pump fed system would score negative. A proven propellant combination scores positive, a demonstrated combination scores average and a theoretical combination scores negative.

Propellant combinations are given a final score by summing up the scores for the individual criteria. A negative score equals -1, average 0 and positive +1. All criteria are assigned equal weight. The results are summarized in Table 7.1.

Table 7.1: Propellant trade-off table

Propellant	Isp_{vac}	Ignition	Pressurization	Safety	Sustainability	Complexity	Readiness	Score
Monopropellants:								
Hydrazine	220	Catalytic	Pressure fed	Handling issues	Toxic	Low	Highly proven	2
NOFBX	320	Igniter	Self pressurizing	Explosive	Green	Low	Demonstrator	3
Hydrogen peroxide	161	Catalytic	Pressure fed	Handling issues	Green	Low	Highly proven	3
Nitrous oxide	192	Catalytic	Self pressurizing	Fairly safe	Green	Low	Demonstrator	4
Hydrazine bipropellants:								
Nitrogen tetroxide & MMH	340	Hypergolic	Pressure fed	Handling issues	Toxic	Moderate	Highly proven	2
Non-cryogenic bipropellants:								
Ethane & nitrous oxide	312	Catalytic	Self pressurizing	Fairly safe	Green	Moderate	Demonstrator	5
Propane & nitrous oxide	312	Catalytic	Self pressurizing	Fairly safe	Green	Moderate	Demonstrator	5
Kerosene & nitrogen tetroxide	323	Igniter	Pressure fed	Fairly safe	Toxic	Moderate	Proven	2
Kerosene & hydrogen peroxide	319	Catalytic	Pressure fed	Handling issues	Green	Moderate	Proven	4

7.1.2 Trade-off result

From the trade-off as presented in Table 7.1 it is concluded that a bi-propellant engine operating on a combination of nitrous oxide and either propane or ethane is most promising. Because ethane has the added benefit of being self pressurizing by itself, ethane is favored over propane which requires pressurization using nitrous oxide.

A serious consideration however is the fact that nitrous oxide ethane engines have only been demonstrated on the ground. It is thus expected that this propellant combination is not fully characterised yet. Especially combined with a deep throttling engine it is expected that significant development effort will be required to build a flight proven system. This will invariably result in a an increase in development time and cost.

In case development time and cost end up to high, a performance-wise alternative would be to make use of nitrogen tetroxide and MMH or a kerosine based system. These propellant combinations provide slightly better or comparable performance and are well proven. This however does come at the cost of being either highly toxic and/or requiring great care with handling. While being viable alternatives performance wise, these propellants do not fit the sustainability goals of this design assignment.

7.1.3 Main propulsion engine throttling

In order to be able to decelerate after release from the aeroshell, the lander vehicle needs to be able to generate considerable thrust using its main thrusters. Those same thrusters are to be used to hover the vehicle during deployment of the payload, requiring the engines to be throttled to a significantly lower amount of thrust. While it is fairly common for liquid rocket engines to be throttleable to a lower than maximum rated power level (RPL), being able to throttle to very low fractions of the RPL thrust is much less common.

Throttling below 25% of the RPL is commonly referred to as "deep throttling" and poses various technical challenges. Erin M. Betts performed a historical study on liquid rocket engine throttling capabilities [14]. In this study 3 successfully used liquid rocket engines are described which are capable of deep throttling to 10% or less of RPL.

Lunar Module Descent Engine Oldest of the two described engines is the Lunar Module Descent Engine (LMDE). The LMDE was used on all the Apollo missions which landed or intended to land on the surface of the moon. The engine ran on a mixture of nitrogen tetroxide and hydrazine and was capable of throttling down to 10% of RPL.

RL-10 and derived engines The RL-10 engine and its derivatives have been used on various vehicles for over 50 years and runs on mixture of liquid hydrogen and liquid oxygen. A recent derivative of the RL-10 named Common Extensible Cryogenic Engine (CECE) demonstrated stable throttling to 8% of RPL, while generating a nominal thrust of 57 kN [53].

Aeroject MR-80B The Aeroject MR-80B is a hydrazine fueled engine developed by Aeroject for powering the MSL Sky Crane and is capable of being throttled between 31 and 3603 N thrust. A detailed description of its properties and the design process are given in 'Monopropellant Hydrazine 700 lbf Throttling Terminal Descent Engine for Mars Science Laboratory' [18]. The MR-80B engine is a derivative of the MR-80 which was used to land the Viking probes.

Based on the three discussed engines it is assumed that, while developing a deep throttleable main propulsion engine for the studied mission may not be without its challenges, there should be no theoretical nor technical issues preventing its development. In addition, it is assumed that a throttle level of at least 10% of RPL will be achievable without overly complicating the engine design. Allowing for throttle levels far below 10% is possible as shown by the Aeroject MR-80B, but throttling to such power levels is likely to carry serious penalties in efficiency and may result in trouble with combustion instability.

7.2 Attitude control

Two viable options for attitude control remained in the trade-off in the midterm report; a separate thruster system, or main engine gimballing. Due to time constraints in the project it was not possible to conduct a full trade-off between both control methods. Instead it was chosen to employ differential throttling for pitch and roll attitude control of the CAESAR vehicle while using a separate dedicated set of four attitude control thrusters for the yaw control.

The rationale for this decision is that while engine gimballing may eliminate the need for dedicated yaw control thrusters, it is perfectly possible to control pitch and roll using differentially throttled main engines. Employing gimballing thus only saves the need for four comparatively small control thrusters. In addition it is deemed unfeasible to properly develop a controller for gimballed engines during this project due to time constraints. Engine gimballing results in a quite a complicated dynamic system, increasing the required effort to develop a controller.

7.2.1 Thruster sizing

From the ADCS simulation results it is found that it is desirable to have each of the yaw thrusters deliver up to 10N of thrust. Because the main propulsion system is chosen to use a propellant combination of nitrous

oxide and methane, one is left with the option of either using bipropellant thrusters running on the same propellant combination, or to use monopropellant thrusters running solely on nitrous oxide. As presented in the propellant trade-off, a hot gas thruster which decomposes nitrous oxide can attain a specific impulse of up to 192 seconds. A bipropellant thruster will yield higher efficiency at the cost of a higher system complexity and mass. Since the systems are about equal on every other aspect, both will ignite catalytically, and both have been demonstrated on the ground, a trade-off is made on system mass alone.

Using the rocket engine estimation methods presented by Zandbergen [74] the engine mass, length and diameter are estimated for both the monopropellant and bipropellant engine. The results are presented in Table 7.2.

Table 7.2: Attitude control thruster sizing results.

Propellant	Mass [kg]	Diameter [m]	Length [m]
Bipropellant	0.45	0.31	0.17
Monopropellant	0.34	0.16	0.045

Based on the obtained results it is decided to opt for the mono-propellant thrusters as they are lighter, smaller and the resulting system complexity will be lower. The lower specific impulse is deemed less relevant as the required control momentum is small.

7.3 Parachute trade-off

In the midterm report [26] several parachute design options were presented. So far only the Disk Gap Band (DGB) parachute has been flown on actual missions in the Martian atmosphere. The set of presented parachute concepts contains quite a few parachute types which are closely related to the DGB parachute. Experiment performance comparison between these related parachutes was recently performed by K. Gonyea in the 2013 Aerodynamic Stability and Performance of Next-Generation Parachutes for Mars Descent study [30]. Knacke provides information on some more exotic parachute concepts [40] and McKinney performed an experimental study on guided ringsail parachutes in Martian atmospheric conditions [46].

Systems comprised of multiple parachutes are not considered in further detail due to the deficiencies listed in the midterm report, with the primary one being their lower total drag. While multiple parachutes could potentially have the added benefit of higher reliability, it was decided that the disadvantages outweight the potential gains.

Despite there being a significant amount of studies being done to potential candidate systems for deceleration in Martian atmosphere, information is limited. This is most likely due to the fact that only the DGB parachute ever saw service in Martian missions. Nevertheless, it is attempted to make a trade-off based on available information. The parachute performance is judged based on drag performance and stability, using the DGB parachute as a baseline. The degree to which a technology is proven is taken into account as well. A parachute type qualifies as experimental if is has been tested in Martian like atmospheric conditions. The label highly experimental indicates a parachute type is only theoretically suitable for the job and has only be tested in lower Earth atmosphere. The results are summarized in Table 7.3.

7.3.1 Tradeoff result

Based on the listed parachute options in table 7.3, the disksail parachute type has the preference. Disksail parachutes are essentially modified ringsail parachutes, with improved stability. The maneuverable ringsail parachute tested by McKinney [46] has the added benefit of being controllable. Since this parachute has even been tested in Martian like atmospheric conditions, this parachute type is deemed an excellent candidate for a Mars mission like the one being discussed in this report. With the maneuverable ringsail offering performance close to the DGB parachute, this parachute is selected.

Because it was found that disksail parachutes have improved stability over ringsail parachutes, it may be interesting to investigate the possibility of modifying the maneuverable ringsail into a disksail parachute. Due to time constraints, this possibility will not be further explored in this report.

Table 7.3: Mars atmospheric parachute trade-off table

Concept	Maneuverable	Performance relative to DGB	Proven
Maneuverable ringsail	Maneuverable	Slightly lower	Experimentally
Conical Ribbon	Non-maneuverable	Lower	Experimentally
Disk Gap Band (DBG)	Non-maneuverable	N/A	Proven
Ringsail	Non-maneuverable	Slightly lower	Experimentally
Disksail	Non-maneuverable	Slightly higher	Experimentally
Starsail	Non-maneuverable	Slightly lower	Experimentally
Vortex Ring	Non-maneuverable	Higher	Highly experimental
Ballute	Non-maneuverable	Unknown	Highly experimental

7.4 Guided parachute

The guided parachute system under investigation, is based on the US Army Affordable Guided Airdrop System (AGAS). The AGAS system works using a circular parachute of the ringsail type. A horizontal glide is induced by grouping the reefing lines in four sets where each set contains exactly one quarter of the reefing lines. Each of these sets is connected to a separate winch. A sketch of the division of the reefing lines is given in Fig 7.1.

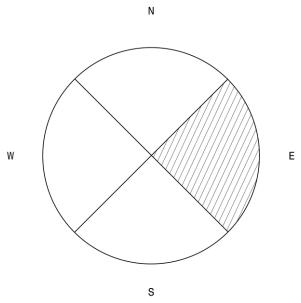

Figure 7.1: Guided parachute canopy top view

By winding each of the winches, the length of the reefing can be controlled. The amount of parachute line that is winched is referred to as the actuation length. By pulling the reefing line connected to the top quadrant, the parachute is made to glide to the north.

Based on the work of McKinney [46], the required actuation lengths of the risers which are connected to the reefing are determined. These lengths are given as a fraction of the canopy reference diameter D_0 related to the glide ratio in Table 7.4.

Table 7.4: Actuation lengths relative to desired glide ratios for manoeuvrable parachute

Actuation length	Glide ratio
$0.02D_0$	0.20 - 0.25
$0.03D_0$	0.40 - 0.45

The Earth bound version of the AGAS system can attain glide ratios up to about 0.7. During testing, McKinney found that attempting to induce glide ratio's of about 0.7 in Martian atmosphere-like conditions has the potential to induce undesirable effects like spin [46]. Restricting the induced glide ratio to lower numbers like 0.45 did result in these effects not appearing. While it may very well be possible to make the parachute design more stable to allow glide ratios of 0.7 without inducing undesirable effects, this will require further investigation and possibly real world testing. Due to time constraints no further detail design of the

parachute will be performed in this study. It is therefore assumed for this study that a stable gliding flight can be achieved with a maximum glide ratio of 0.5.

7.4.1 Parachute deployment

Part of the parachute system is the parachute deployment mechanism. In order to ensure proper parachute deployment, the deployment system should:

- Minimize the parachute snatch force by keeping the canopy closed until line stretch occurs.
- Keep tension on all parachute parts during deployment in order to prevent canopy flutter which can cause a range of problems.
- Minimize opening time and opening force scatter.

According to Knacke [40], a forced-ejection parachute deployment method is generally required when deploying a parachute from a spinning and/or tumbling vehicle or when deploying the parachute in a large wake. Because the entry vehicle may very well be spinning and tumbling after entry and surely will generate a large wake, a force-ejection method is considered required.

In the past, a mortar has been used to deploy parachutes from entry capsules. This method was also used on the various past Mars missions like the Mars Science Laboratory and Mars Exploration Rover missions. Alternative methods include deploying only a drogue parachute using a small mortar, which is commonly referred to as drogue gun deployment. Extracting the parachute using a rocket is another method.

Due to time constraints no detailed trade-off on the parachute deployment method will be made. The mortar based method has successfully been employed the in past on various occasions and has generally favorable characteristics according to Knacke [40]. Therefore a mortar based deployment method is used in the presented design.

7.4.2 Power estimation

In order to estimate the required power of the guided parachute, it is assumed that the force in each of the risers F_w in N is equal to one fourth of the total parachute force F_D in N:

$$F_w = \frac{F_D}{4} \tag{7.1}$$

According to McKinney the winches are fairly fast and will attain maximum actuation length after 2 seconds when starting from the minimum actuation length. It is assumed that the final system will attain similar performance. Assuming the maximum actuation length of $0.03D_0$, one can calculate the required winch power P_w in Watt as follows:

$$P_w = \frac{0.03F_D D_0}{4t_w} \tag{7.2}$$

Where t_w is the time required to attain maximum actuation starting from the minimum actuation in s. In case of moving the parachute into a combined direction (for example north-west), two out of four winches need to be operated. The efficiency by which the electric motor and winch η_w is estimated at 85%. The total peak power required can then be formulated as:

$$P_{w,peak} = \frac{2P_w}{\eta_w} = \frac{0.03F_D D_0}{2t_w \eta_w} \tag{7.3}$$

Because the required power found is extremely high; in the order of tens of kilowatts during the first section of the parachute descent. This is mainly caused by the high forces during parachute deceleration. A method to partially circumvent these high power requirements would be to pre-winding a section of reefing lines which can be unwinded as desired during the descent. Instead of pulling a single set of reefing lines, one could opt to veer the other three sets of reefing lines when commanding a glide direction. In this manner one could partially circumvent the large power requirements for at least part of the descent and only powered winch operation would be required during the portion of the flight where the parachute is near or at equilibrium velocity.

7.4.3 Mass estimation

For the steerable parachute mass estimation it is assumed that the parachute itself requires very little modification from the standard Viking type parachute which was used on previous NASA Mars missions. The mass estimation methods presented in the Baseline report [25] will thus be used to estimate the mass of the parachute itself.

Top brush-less electric motors attain a power to weight ratio of well over 5 kW kg^{-1} [22]. Based on these findings it is assumed that it should be well within technical constraints to construct a space proof electric motor having a power to weight ratio of 5 kW kg^{-1}.

It is assumed that the winch assembly includes the electric motor, a reduction gearbox, a spool and mounting brackets. The mass for the full winch assembly including motor is estimated to be roughly equal to 4 times the electric motor mass. This assumption currently cannot be backed up by any references at this point, further studies will thus need to look into more detailed winch design.

7.4.4 Attainable glide ratio

In order to be able to determine the maximum distance that can be traversed using an AGAS based guided parachute system, it is of importance to obtain an estimate of the response time. McKinney found a response time of about 4.5 seconds for a 10 meter diameter parachute and proposed an analytically determined response time of 16 seconds for a 45 meter diameter parachute [46]. The exact analytical method is not given.

7.4.5 Results

By employing the in the baseline report [25] described parachute sizing method, combined with the Viking reference parachute design and the presented mass and power estimation method, the following results given in Table 7.5.

Table 7.5: Parchute design results

Property	Symbol	Value
Parachute reference diameter	D_0 [m]	20.4
Parachute reference area	S_0 [m^2]	327
Parachute mass	- [kg]	32.1
Parachute winches mass	- [kg]	1.6
Parachute deployment system mass	- [kg]	48.1
Parachute winch power	$P_{w,peak}$ [W]	$2.0 \cdot 10^4$

7.5 Guided parachute range

With the guided ringsail parachute selected for use on the MACHETE vehicle, the question arises of how much distance can actually be covered using such a parachute. A simple solution to this answer would be to simply multiple the attainable glide ratio with the deployment altitude to obtain a glide distance. After entry the flight path angle is however still close to horizontal and as discussed earlier in this chapter, the response time of the guided parachute is significant. Considering these factors, it is unlikely that the simple solution is accurate.

In order to obtain a more accurate range estimation of the guided parachute, a simulation of the parachute flight is made. Building a simulation will also yield an estimate of the parachute flight time. For this simulation, the following assumptions were made:

- The generated 'thrust' acts perpendicular to the lift vector.
- Thrust can be generated at any angle in the Y_B - Z_B plane.
- The lift vector is aligned with the velocity vector.

- The MACHETE vehicle and parachute are radially symmetric along the X-axis in the body frame.
- The body frame is aligned with the aerodynamic reference frame, with the parachute canopy normal to the negative velocity vector.
- Maximum glide control is commanded at all times.
- A flat Martian surface is assumed.
- Influences due to the rotation of Mars are neglected.
- Thrust and lift coefficients do not change with the Mach number.
- Gravity is assumed to be constant.
- The parachute is instantly fully deployed.
- System mass is constant.

The vehicle carried normal Earth reference frame is naturally fixed to Mars in the case of flight in the Martian atmosphere. For the sake of nomenclature, the term Earth reference frame will be used for the rest of the report.

7.5.1 Reference frames and transformations

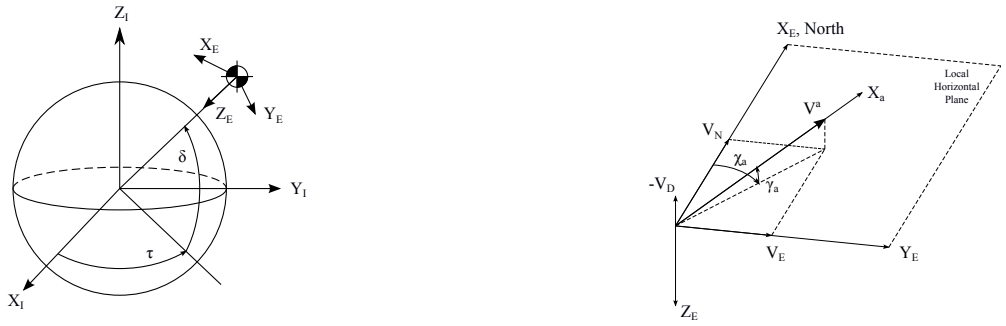

(a) Vehicle carried Earth fixed reference frame relative to the inertial Earth reference frame

(b) Aerodynamic reference frame relative to the Vehicle carried Earth fixed reference

Figure 7.2: Reference frames and relative transformation rotation angles

In order to be able to transform vectors between the Earth and aerodynamic reference frame, the aerodynamic angles χ_a for heading and γ_a for pitch need to be obtained from the velocity vector. The aerodynamic bank angle μ_a is not of interest due to the assumption that the vehicle is radially symmetric around the X_b axis and is thus assumed to be zero at all times. A sketch of the used reference frames and their relations is presented in Fig 7.2. The Delft Technical University Flight Dynamics lecture notes provide the following relations for these aerodynamic angles [64]:

$$\chi_a = \arctan\left(\frac{V_E}{V_N}\right) \tag{7.4}$$

$$\gamma_a = -\arcsin\left(\frac{V_D}{|V|}\right) \tag{7.5}$$

Where V_N, V_E, and V_D are the respective components in X_E, Y_E, and Z_E direction of the velocity vector. For transformations aerodynamic reference frame to the Earth reference frame, the following sequence of rotations is applied:

$$
\begin{aligned}
\mathbb{T}_{Ea} &= \mathbb{T}_z(-\chi_a)\mathbb{T}_y(-\gamma_a)\mathbb{T}_x(\mu_a) \\
&= \mathbb{T}_z(-\chi_a)\mathbb{T}_y(-\gamma_a) \\
&= \begin{bmatrix} \cos(-\chi_a) & \sin(-\chi_a) & 0 \\ -\sin(-\chi_a) & \cos(-\chi_a) & 0 \\ 0 & 0 & 1 \end{bmatrix} \begin{bmatrix} \cos(-\gamma_a) & 0 & -\sin(-\gamma_a) \\ 0 & 1 & 0 \\ \sin(-\gamma_a) & 0 & \cos(-\gamma_a) \end{bmatrix}
\end{aligned} \tag{7.6}
$$

Reversing these rotations in a transformation from the Earth reference frame to the aerodynamic reference frame yields:

$$
\begin{aligned}
\mathbb{T}_{aE} &= \mathbb{T}_x(-\mu_a)\mathbb{T}_y(\gamma_a)\mathbb{T}_z(\chi_a) \\
&= \mathbb{T}_y(\gamma_a)\mathbb{T}_z(\chi_a) \\
&= \begin{bmatrix} \cos(\gamma_a) & 0 & -\sin(\gamma_a) \\ 0 & 1 & 0 \\ \sin(\gamma_a) & 0 & \cos(\gamma_a) \end{bmatrix} \begin{bmatrix} \cos(\chi_a) & \sin(\chi_a) & 0 \\ -\sin(\chi_a) & \cos(\chi_a) & 0 \\ 0 & 0 & 1 \end{bmatrix}
\end{aligned} \tag{7.7}
$$

7.5.2 Glide ratio

Because no exact analytical method to determine the response time as a function of parachute diameter is given by McKinney [46], it is assumed that the response time is linearly dependent on the parachute diameter. The response time τ_{par} in s for a parachute with a reference diameter D_0 in m can then be expresses as:

$$
\tau_{par} = 4.5 + \frac{11.5}{35} D_0 \tag{7.8}
$$

In addition it is assumed that during this response transient, the effective glide ratio of the parachute varies linearly from zero at the start to the maximum commanded value at the end of the response time. This results in the following expression for the glide ratio E_{gr}:

$$
E_{gr} = \begin{cases} \frac{E_{gr,max}}{\tau_{par}} t & \text{if } t < \tau_{par} \\ E_{gr,max} & \text{if } t \geq \tau_{par} \end{cases} \tag{7.9}
$$

7.5.3 Forces

During flight, the following forces act on the vehicle: lift, drag and gravity. The lift force is assumed to be aligned with the velocity vector at any moment, but acting in opposite direction. Since the X_a axis is aligned with the flight direction, the means that the lift force is acting in negative X direction in the aerodynamic frame. For the force magnitude, the standard lift equation is used. Transforming the lift vector to the Earth reference frame results in the following expression:

$$
\begin{aligned}
L^a &= \begin{bmatrix} -1 \\ 0 \\ 0 \end{bmatrix} \frac{1}{2} \rho V^2 S C_L \\
L^E &= \mathbb{T}_{Ea} L^a
\end{aligned} \tag{7.10}
$$

As stated, the thrust vector is assumed to be acting perpendicular to the lift vector and thus perpendicular to the velocity vector as well. In order to provide control, the thrust vector can be rotated around the X_a axis. Effectively this is accomplished by pulling different sets of reefing lines. The thrust angle is indicated by α_d. The default drag direction is given to in the positive Z_a direction. First rotating the thrust using the control angle and then transforming the thrust to the Earth reference frame gives:

$$F_{st}^{a} = \mathbb{T}_x(\alpha_d) \left(\begin{bmatrix} 0 \\ 0 \\ 1 \end{bmatrix} \frac{1}{2} \rho V^2 S C_{st} \right)$$
$$F_{st}^{E} = \mathbb{T}_{Ea} T^{a} \tag{7.11}$$

The weight of the MACHETE is conveniently defined in the Earth reference frame, with the force acting downward in positive Z_E direction:

$$W^{E} = \begin{bmatrix} 0 \\ 0 \\ 1 \end{bmatrix} m \cdot g_M \tag{7.12}$$

7.5.4 Control

As mentioned the direction of the induced drag force which will make the parachute glide in a certain direction is controlled by the angle α_t. Given a target heading angle χ_t which is given as a rotation about the Z_E axis, the parachute control angle α_t is given as:

$$\alpha_t = \pi + \chi_t - \chi_a \tag{7.13}$$

Effectively this manner of control attempts to direct the horizontal component of the thrust vector in the desired heading, increasing velocity in that direction. During the portion of the flight which is largely horizontal due to the low flight path angle after atmospheric entry, this may result in the thrust acting for a large portion in the vertical direction effectively retarding or accelerating descent toward the surface.

7.5.5 Simulation approach

The position state vector will be kept in the Earth reference frame from the initial position of the vehicle at the start of the simulation. The position at any time of the simulation is thus the position relative to the initial position of the vehicle.

The acceleration of the MACHETE vehicle is calculated by summing the forces acting on the vehicle and calculating the resulting acceleration using Newton's second law.

By time stepping the simulation with steps of 0.01 seconds until the MACHETE vehicle reaches the CAESAR release altitude of 2000 meters, the vehicle velocity and position are updated

7.5.6 Results

The results on parachute range from the simulation using different time steps are presented in Table 7.6. The attainable range is given per heading angle, where a heading of 0 degrees is a target heading in X_E direction, which is equal to the initial horizontal flight direction. A visualisation of the flight profiles is given in Fig. 7.3.

7.5.7 Considerations

While the obtained results are very likely more accurate than the simple calculation of just taking the initial altitude and multiplying it with the glide ratio, there are quite a few assumptions made which certainly decreased the accuracy of this simulation. The two most significant are listed below.

Transonic flight At parachute deployment, the MACHETE vehicle is traveling at about Mach 1.5. During deceleration, the vehicle passes through the transonic regime. During the transition the parachute thrust and drag coefficients of the parachute are bound to vary widely. In addition the drag coefficient during subsonic and supersonic flight are likely to differ. These effects have not been considered in the simulation and will have to be investigated in further work.

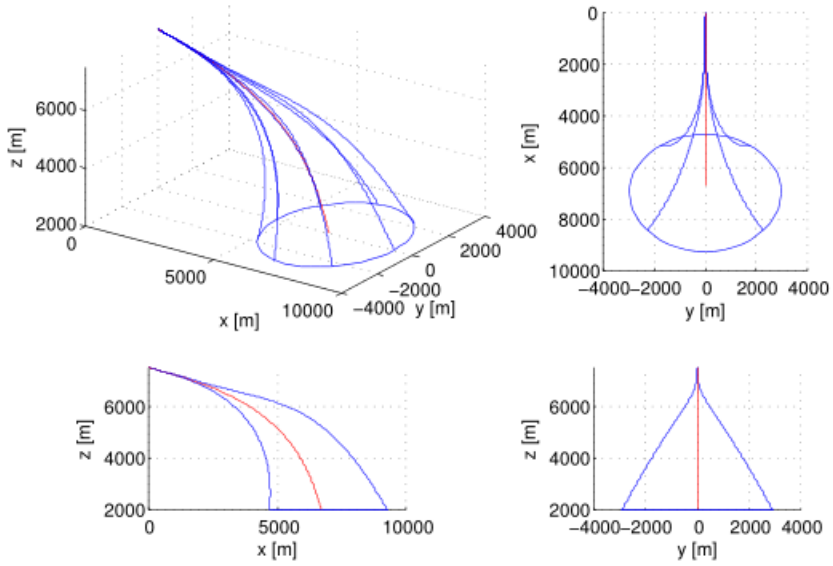

Figure 7.3: Estimated maximum glide range of guided parachute plot

Supersonic flight Supersonic parachute flight itself also has its issues. It is known that during supersonic flight, parachutes often experience an effect known as parachute area oscillation. During parachute area oscillation the parachute repeatedly experiences partial deflation and inflation [59]. This will have effects on the controllability of the parachute during supersonic flight.

Parachute deployment Parachute deployment was assumed to be instant. In reality parachute deployment will take a significant amount of time and during deployment the parachute may only be controllable to a certain degree, if at all.

Constant mass It is assumed that the system has constant mass. In reality the heat shield will be jettisoned at some point during the parachute flight, considerably lowering the mass. At the end of the flight the propulsive landers are released as well, further reducing system mass.

7.6 Guided parachute sensitivity analysis

With an estimation of the performance of the guided parachute, the question of sensitivity arises. It is known from both studies and empirical data from previous Mars missions that it is problematic to deploy the parachute at an exact altitude; the 3σ altitude range can be in the order of multiple kilometers. What is the effect of an parachute deployment considerably different from the design altitude? During further detail design it is almost certain that changes to the selected parameters will be made. In this section it is attempted to answer the question of what the effect of such changes on parachute performance is.

7.6.1 Analysed parameters

Due to time constraints only a limited number of parameters is selected for analysis and only the effect of single parameter variation is considered. The varied parameters are shortly discussed. It was chosen to only characterize the effect on minimum attainable glide distance, as this is the driving factor for the propulsive lander design.

From the range simulation it was determined that attempting to fly a heading of 180 degrees relative to the post entry flight direction in the horizontal plane resulted in the shortest glide distance. This is thus the

Table 7.6: Estimated maximum glide range, flight time, and final velocity of guided parachute per target heading relative to entry direction including simple glide distance estimation and uncontrolled parachute descent.

Heading [deg]	Range [m] $\Delta t = 1$ s	Range [m] $\Delta t = 0.1$ s	Range [m] $\Delta t = 0.01$ s	Time [s] $\Delta t = 0.01$	Velocity [ms^{-1}] $\Delta t = 0.01$
Uncontrolled	0	0	0	62.6	101.8
0	2467	2556	2567	89.0	94.4
45	2734	2841	2851	84.1	94.4
90	2824	2992	2929	70.4	96.0
135	2296	2362	2365	55.5	103.2
180	1970	2022	2026	49.8	108.3
225	2296	2362	2365	55.5	103.2
270	2824	2922	2929	70.4	96.0
315	2734	2841	2851	84.1	94.4
Simple	2750				

heading used in this sensitivity analysis. All parameters used are equal to the parameters used in the final design iteration, except for the parameter being varied.

System mass Currently the system mass is driven by the maximum launch capability to Mars. Improvements in launch vehicle technology will likely change the maximum allowable mass. Conversely mass is one of the notorious system properties to experience runaway growth during detailed design. This makes mass an interesting parameter to vary. Mass is varied from 2250 to 3750 kg.

Drag coefficient The drag coefficient is one of the primary performance parameters of a parachute. Since the parachute drag coefficient heavily depends on the parachute design, the final drag coefficient is likely to be different from the selected number. Previous Mars missions have seen slight changes to the Viking parachute for tailored drag performance. The drag coefficient is varied from 0.49 to 0.94.

Deployment altitude As already mentioned, it's hard to deploy the parachute exactly at the design altitude. Investigating the effect of an off-design altitude deployment is thus of great interest. The deployment altitude is varied from 5625 to 9375 m.

Deployment velocity With a differing parachute deployment altitude likely comes a differing deployment speed. The effect of an off nominal deployment speed thus needs to be investigated. The deployment speed is varied from 270 to 450 ms^{-1}.

Glide ratio Being one of the primary performance characteristics of the guided parachute, the effect of changes in the glide ratio are of great interest. As mentioned there is still some doubt about the maximum attainable glide ratio of the guided parachute. Improved stability may allow significantly higher glide ratios to be commanded. The glide ratio is varied from 0.375 to 0.625.

7.6.2 Results

The results from the various analysed parameters are displayed in Fig 7.4. It is of interest that the deployment velocity, drag coefficient and system mass do not really appear to have a significant influence on the attainable glide distance. The glide ratio and deployment altitude however have a nearly linear relation with the attainable glide distance, where a higher glide ratio or higher deployment altitude result in a higher glide distance.

Further studies may focus on the effect of combined parameter variation and the effect on glide performance in all distances. In addition it may be important to look at the effect of parameter variation

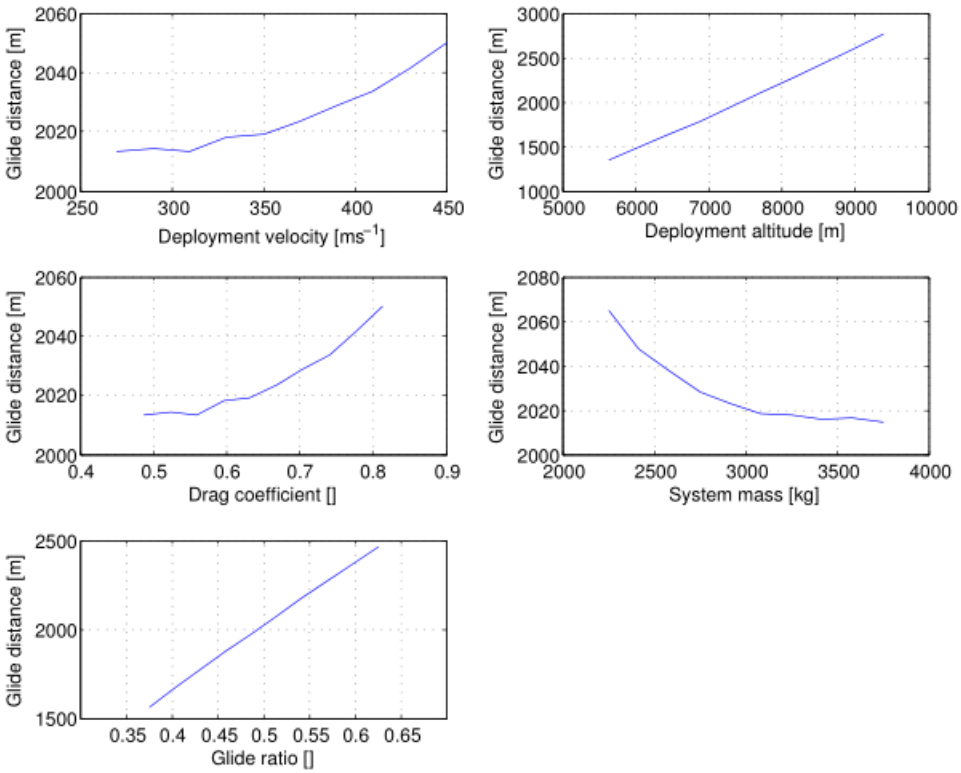

Figure 7.4: Estimated maximum glide range of guided parachute plot

on the location of the landing ellipse, instead of just the attainable glide distance. This should give more information on the required propellant or general performance reserves.

7.7 Verification & Validation

In this section various verification and validation methods are presented for the propulsion systems and parachute. In addition some of the presented validation methods are performed to test the used theory against reality.

7.7.1 Power estimation

The methods used to estimate the power of the ADCS thruster valves as presented in the midterm report [26] can easily be validated by applying the method to existing thruster values. By taking specified properties of the valves as input for the estimation method and comparing the output with the specified maximum power rating will tell if the estimation method is accurate.

The power estimation method was verified using a solenoid thruster valve produced by MOOG, which is a US based company involved in the production of propulsion systems. In Table 7.7 the specified and estimated parameters of the MOOG 'Solenoid Actuated Thruster Valve' as presented on the MOOG website [47] are given.

While the estimation method does not include energy losses due to coil inefficiencies, the estimated power requirements are off with two orders of magnitude. In addition it was found that for various MOOG valves, power requirements do not necessarily appear to increase as valve size increases. This leads to the conclusion that the valve power estimation method is likely to be wrong and that it may be more correct to estimate the required power by taking an average value based on existing propellant valves.

Table 7.7: Estimated and given power rating for the MOOG 'Solenoid Actuated Thruster Valve'

Property	Value
Thrust	445 N
Pressure	22.1 bar
Response time	0.020 s
Mass flow	0.206 kgs^{-1}
Plunger travel	0.00160 m
Estimated power	0.47 W
Rated maximum power consumption P	22 W

7.7.2 Rocket engine mass estimation

The monopropellant thruster mass estimation method given by Zandbergen [74] is fitted to engines up to about 500 N of thrust. Because the main engines for the non clustered lander are of considerably higher thrust, it is of interest to check if this mass estimation method also yields acceptable results for these larger monopropellant engines.

In order to validate this mass estimation method, a selected number of engines specified in table 17-13 in SMAD [42] and a couple of engines produced by Aerojet are used. Engines are selected if their exact specifications are available (as opposed to mass or thrust ranges). For these engine the masses are estimated and compared with the actual engine masses. Of special interest are engines with thrust levels of 500 N and higher.

Table 7.8: Comparison of estimated and actual mass of several hydrazine monopropellant rocket engines

Developer	Number	Thrust N	Mass kg	Estimated mass kg
Olin/RRC		25	1.55	0.405
Aeroject	MR-104	44	1.86	0.492
Walter Kidde, Olin/RRC		600	11.3	3.05
Aerojet	MR-80	3100	8.51	14.6

Based on the results given in Table 7.8, it can be concluded that the mass estimation method from Zandbergen [74] will result in a mass estimation which is likely to be within a few multiples of the actual engine weight. While this may be sufficient for an initial mass estimation, any further design steps will require more detailed mass estimations. An alternative method may be to estimate the rocket engine mass by estimating the masses of the various individual components in the engines. This however will require more detailed specifications for the rocket engines like specific impulse and area ratios.

7.7.3 Parachute mass estimation

The parachute mass estimation method presented in the baseline report [25] can be validated by comparing the estimated masses with the masses of parachutes of actual Mars missions. A difficulty with this approach is obtaining the required data for performing the validation. It has proven to be difficult to obtain all required parameters for missions other than the MSL mission in the time spent on parachute design in this study. The results are presented in Table 7.9.

Table 7.9: Parachute parameters for MSL mission

Mission	Drag coefficient	Terminal velocity ms^{-1}	Terminal altitude m	Payload kg	Mass kg	Estimated mass kg
MSL	0.67	100	1800	3000	54	30

Due to the lack of data points it's hard to draw a firm conclusion from the in table 7.9 presented results.

Table 7.10: This table shows the relative importance of all different risks for the touchdown system. Closer to the top right is more important. See Table 7.11 for the detailed risk explanations.

Severity	Likelihood			
	Impossible	Improbable	Probable	Frequent
Catastrophic		3, 7, 8, 9 , 12	13	2, 6
Critical		11	3	1
Marginal		15	5, 10, 13	
Negligible				

Nevertheless it appears that the parachute mass estimation method does yield the parachute mass within at least the correct order of magnitude. Further validation needs to be done in a follow up study.

7.7.4 Parachute range estimation

A notorious point of error are the employed transformation matrices when using multiple reference frames. The transformation matrices can be validated by using the property $\mathbb{T}_{12} = \mathbb{T}_{21}^{T} = \mathbb{T}_{21}^{-1}$. Checking if these equalities hold for the employed matrices can point out errors in the transformation matrices if they are present.

The predicted glide distance using the simulation should in no case exceed the glide distance as calculated by simply multiplying the initial altitude with the glide ratio by a large margin. Because the simulation assumes a initially slowly increasing glide ratio, finding a much larger glide distance than with a simple calculation would be a strong indicator something is wrong.

The simulation is found to be convergent. Precision appears to increase with about an order of magnitude when decreasing the time step with an order of magnitude. This effect is clearly seen when comparing the change in results between a time step of 1 s and 0.1 s and the change in results between a time step of 0.1 s and 0.01 s.

Validating the results will need to be done using actual parachute tests in Martian atmospheric conditions. Such tests are possible in high Earth atmosphere, as proven by McKinney [46] and various test for previous Mars missions. The results from McKinney are unfortunately not usable for validating the simulation results. Reason for this is that McKinney did not perform parachute deployment at realistic post entry velocities. McKinney solely focused on testing the gliding control of the parachute under Martian conditions, while deployment was not considered.

7.8 Risk analysis

In this section the risks associated with operating the deceleration and propulsion subsystems are discussed. This analysis should both inform the reader of the general risks, as well as be a guide to which areas require most detail during further mission design and studies. Risks are grouped according to their probability and severity in Table 7.10, while they are elaborated on in Table 7.11.

7.9 Conclusion

With the selection of a propellant combination of nitrous oxide and ethane providing both high performance and being eco friendly, and selection of the final attitude control actuation system, the high level design of the propulsion system is closed. It was verified that there should be no major technical hurdles in designing an engine which is capable of throttling to the required low power levels. Due to the combination of a fairly novel propellant combination and deep engine throttling it is however expected that a significant development effort will be required for the engines.

It is decided to opt for a guided parachute in order to not only decelerate the MACHETE, but also to reduce the distance to be covered by the rocket powered CAESAR landers. An AGAS based parachute system with a ringsail parachute was selected because it has been proven in Martian-like atmospheric conditions.

In order to determine the distance which can be traversed using the guided parachute, a simulation was performed from which it was determined that in the worst case scenario about 2 km can be traversed. In addition a sensitivity analysis was performed to determine the effect of further changes to the mission design.

Finally attention was spent on validating estimation and design methods presented in the baseline [25], midterm [26] and this report. It was determined that some estimation methods needed revision, while it was shown that some others produced reasonably accurate results. In addition suggestions for further verification and validation were given. Combined with the presented design results these should lay a solid foundation for further detail design of the deceleration and propulsion system.

Table 7.11: The risk analysis table shows all identified risks with 1 (high) to 4 (low) likelihood and severity indicators.

ID	Risk	Effect	Likelihood	Severity	Action to minimize risk
1	Rocket engine hard start	Possible structural damage to rocket engine	1	2	Adequate igniter design and adequate engine start. procedure design. Avoid restarts.
2	Valve failure	Engine failure or loss of thrust	1	1	Proper valve selection and valve testing. Compensating controllers. Valve heating
3	Engine debris ingestion	Engine failure	3	1	Strict assembly procedures.
4	Combustion instability	Vibrations and possible structural damage to rocket engine	3	2	Rigorous engine testing through throttle range.
5	Insufficient self pressurization	Loss of thrust	3	2	Sufficient propellant heating, select warm landing zone.
6	Inadequate propellant characterisation	Combustion instabilities, off design performance	1	1	Perform propellant characterisations.
7	Nitrous oxide decomposition	Propellant system overpressurization, explosion risk	3	1	Test propellant system design for possible decomposition triggers, avoid nitrous oxide contamination.
8	Engine igniter failure	No rocket engine start	3	1	Igniter testing, redundant igniter.
9	Parachute inflation failure	Limited to no deceleration	3	1	Extensive wind tunnel and high altitude testing. Proper parachute rigging procedures.
10	Supersonic parachute area oscillations	Vibrations, increased load, changed drag performance	1	3	High altitude supersonic testing. Design for loads.
11	Parachute winch failure	Partial or full loss of parachute control	3	2	Adequate winch selection and testing.
12	Parachute deployment failure	No parachute deployed, loss of mission	3	1	Mortar ground and high altitude testing.
13	Parachute entanglement	Loss of parachute	2	1	High altitude parachute testing. Proper parachute rigging procedures.
14	Off design altitude parachute deployment	Limited effect, possibly higher loads, in extreme cases insufficient deceleration	2	3	Design parachute deployment trigger accordingly, design for loads.
15	Off design post entry flight path angle	Increased loads	3	3	Design for loads.

8 Structural design

For the final design of the structural components of the mission this chapter will explain the process to obtain the precise geometry and sizes of all the components. The main design driver is mass reduction. First the assumptions used for this design will be listed. Then the layout of the structure will be presented. Afterwards a word will be given about the material selection process. This will be followed by the actual sizing of every component of the structure. The next two sections will present the verification and validation of the design. Finally the performed risk and sensitivity analysis will be presented.

8.1 Lay-out of the system

In this section the evolution of the lay-out of MACHETE will be discussed. First the modifications performed after the midterm design[26] will be listed. Then the final lay-out of the vehicle will be presented.

8.1.1 Modifications

After the midterm design [26] it was decided to design MACHETE using eight detachable modules that would separately perform the actual landing and put the Zebro's on the Martian surface. More details became available from the propulsion department and from the deployment department. Following from this several modifications were performed in order to save mass. These changes are listed here:

- The rocket engines were smaller than in the midterm design. After deciding to design a clustered system more time could be spent on making a proper size estimation.
- Four tanks are needed instead of five. The tanks are placed at the same height as the payload. This was decided in order to save space inside the aeroshell and to simplify the placement of the CAESARs in the aeroshell.
- The bottomplate must have an octagonal shape. This is required in order to fit in the airbag design[26].
- The eight CAESAR's are placed in two layers inside the aeroshell. Every layer contains four CAESAR's. This was done in order to allow a proper separation from the aeroshell and to simplify the structure.
- The honeycomb structure used for the bottomplate is no longer used. Instead of this the weight of the Zebro's will be carried by a plate that will transfer the loads to I-beams which are placed underneath the Zebro's. This was done in order to reduce the mass of the bottomplate.
- The number of Zebro's has been decreased to 28 per cluster. This results into the rearrangement of the Zebro's on the bottomplate.
- Aluminium 7075.T6 is used as final choice for the material. More details are given in Sect. 8.2.

8.1.2 Final lay-out

Now the final lay-out will be discussed. The structure consists of three parts. The first part is the LADS which will perform the touchdown with the Zebro's. Then there is the empty CAESAR. It is the part from the CAESAR which will decelerate the LADS using rocket engines after separation with the aeroshell. Finally there is the structure holding the CAESAR inside the aeroshell. After that the whole structure of MACHETE is defined, the next step will be to define the dimensions of every component. This will be done in Sect. 8.3.

Loads acting on the structure

The loading on the LADS is mainly caused by the Zebro's. As they are stacked on four piles of seven Zebro's, it can be assumed the acting forces are situated at the centre of every stack. Next to this the tanks also rest on the LADS allowing them to transfer their weights directly on the LADS during the highest deceleration instead of loading the beams supporting the rocket engines. Note that since the tanks are not attached to the LADS, their weights will be taken by the beams supporting the rocket engines during the launch.

For the second structure the main loadings will be from the rocket engines, the tanks, and the LADS. It must able to withstand the loads from the entry phase, transfer the lift generated by rocket engines to the other components of the CAESAR, and carry the rocket engines and the tanks away after separation from the LADS.

The structure holding the CAESAR's inside the aeroshell is attached to it. Its function is to transfer the loads from the CAESAR's to the aeroshell during the launch and the entry phase. It must be able to safely deploy the CAESAR's once the aeroshell is open. During launch it must be able to withstand compression loads and vibrations.

Appearance of the structure

Now the loadings acting on the structure are known, the different components of the structure can be defined. As mentioned earlier it was decided for the LADS to use a plate supported by beams instead of a honeycomb structure. The resulting plate is illustrated in Fig. 8.1. As it can be seen the plate has an octagonal shape with every side supported by a beam. Next to this there are also beams placed through the plate in order to support the Zebro's. The plate is present in order to transfer all the loads from the Zebro's to the beam.

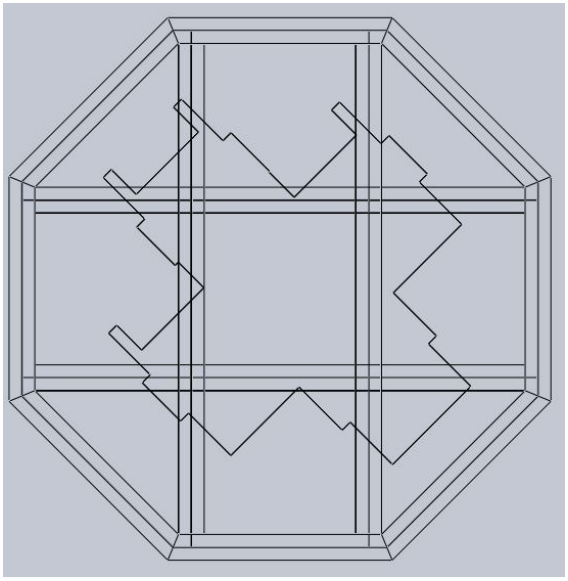

Figure 8.1: Configuration of bottom plate

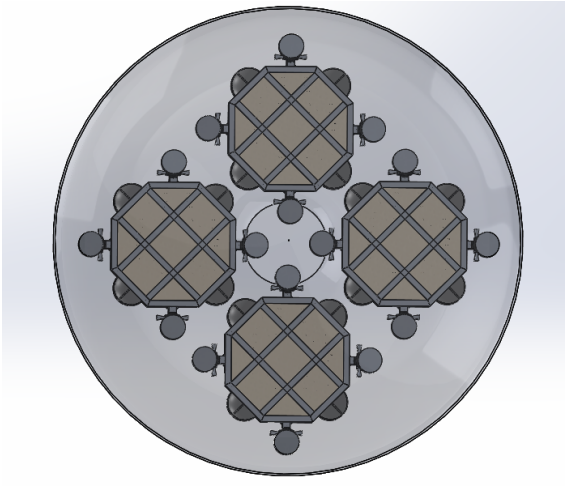

Figure 8.2: Placement of the CAESAR inside the aeroshell per layer

The CAESAR illustrated in Fig. 8.3 must be an autonomous flying vehicle consisting of the thrusters, the tanks, and other navigation system. Therefore the rocket engines must be attached together resulting into bending loads towards the center. This is why it was decided to work with beams with an I-profile attaching the rocket engines at the center of the structure. The loads from the tanks are carried by beams placed at an angle of 45° of the top central beams. Since the tanks are placed such that they can rest on a side beam of the LADS, they cannot be placed right under the beams. In order to fix that, every tank is attached by two vertical circular beams that will carry the tank when the LADS fulfil this function (e.g. during launch

and after dropping the LADS). Since the circular beams are not attached at the vertical neutral axis of the tank this results in a moment. In order to make up for this, there is another circular beam attaching the vertical neutral axis of the tank to the beam supporting the tank. Finally there are beams needed in order to attach the present structure to the LADS. These will be circular beams capable of taking loads in every direction. This is required since CAESAR must fly around to its destination. For preventing failure, these beams are designed to give structural redundancy.

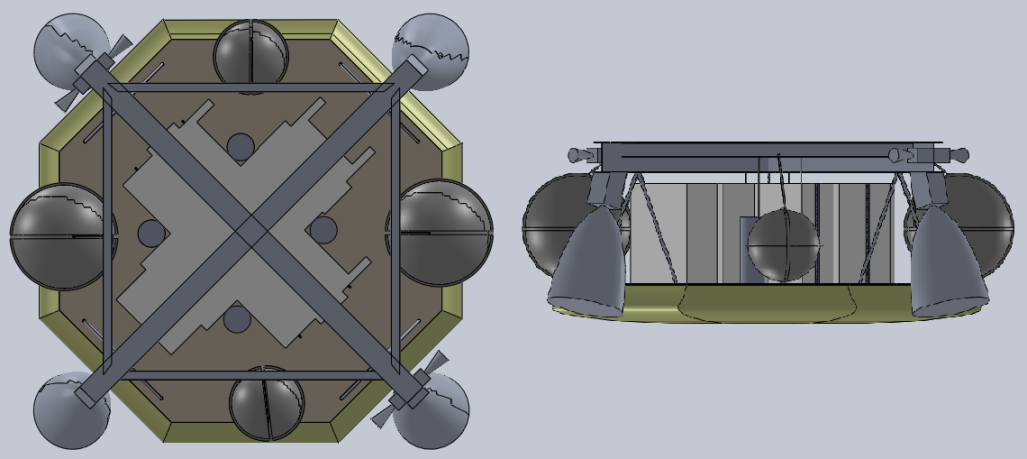

Figure 8.3: Lay-out one CAESAR vehicle

The placement of the CAESAR's inside the aeroshell is presented in Fig. 8.2. In order to withstand the loads occuring during launch I-beams are used. This is due to their ability in having a high moment of inertia which is essential against buckling. The loads coming from one CAESAR is distributed to four beams placed around the module. As two beams are placed between two CAESAR's they are supporting both of the two modules. Furthermore there are horizontal beams placed on the side of the LADS in order to prevent moments and vibrations.

8.2 Material selection

The selection of the right material is primordial for defining the mass of the MACHETE. Therefore an in-depth investigation of the commonly used materials must be conducted. A preliminary selection of the material has been done in the midterm report[26]. First the mechanical properties will be discussed. Then a word about the behaviour of metal at low temperatures, will be given. Finally the trade-off for selecting the material will be done. The materials selected during the midterm report are listed here:

- Aluminium alloy
- Ferrous alloy
- Heat resistant alloy
- Magnesium
- Titanium
- Composite

8.2.1 Mechanical properties

The mechanical properties of the materials are shown in Table 8.1. This table gives information about the density, the Young's modulus, the yield strength, the thermal expansion, and the material efficiency criterion for the case of a deflecting beam. Next to this, several properties not being shown in this table are:

- Composite fibres are uni-directional. So their properties is only valid in one direction. Even though multi-directional composites exist, investigating them and designing them in order to meet the requirements coming from the structural load would cost too much time.
- Ferrous alloy is magnetic. Therefore it is not recommended to use it as it might cause perturbation into some of the used sensors.

Table 8.1: Properties of selected used materials

Material	Material Code	ρ_{mat} (kg $\cdot$ m^{-3})	E (GPa)	σ_y (MPa)	α ($\mu \cdot$ K^{-1})	$E \cdot \rho_{mat}^{-1}$ (N $\cdot$ 10^9 kg^{-1})
Aluminium alloy	6061.T6	2700	68	276	23.6	0.0252
	7075.T6	2800	71	503	23.4	0.0254
Ferrous alloy	AM 350	7700	200	1034	11.9	0.0260
Heat resistant alloy	A-286	7940	201	640	16.2	0.0253
	Inconel	8220	203	853	12.2	0.0247
Magnesium alloy	A2 31B	1700	45	220	26	0.0265
Titanium alloy	T16A1-4V	4400	110	1035	9	0.0551
Composite	Kevlar 49 0°	1380	76	1379	-4	0.0040
	Graphite epoxy	1620	282	586	-11.7; 29.7	0.0250

8.2.2 Behaviour at low temperature

The material must be able to perform at low temperatures. As mentioned in the midterm report[26], the atmospheric temperature on Mars is around 184 K. This is much lower than the ambient temperature on Earth. The consequences of this temperature difference are explained in this subsection.

When exposed to low temperatures, metals can be divided into two categories depending on their ductility and toughness[38]. The first category is the one containing the materials that remain ductile. This group is relatively small as the only relevant metal choice is aluminium. The second category is the metals that lose their ductility over a certain range. The group represents most of the metals used in aerospace industry. In general these materials have limited ductility at room temperature. Figure 8.4 shows how ductility is typically affected by low temperature. Note that several factors influence the temperature where this transition occurs. These factors are the loading types, the rate of application of the loading, the geometry of the structure, and the presence of notches. It is more interesting for the design to use materials able to retain their ductility as the structure is expected to react according to the calculations.

8.2.3 Final choice

The driving requirement for selecting the material was to get the lightest structure. At this stage the structure is already defined and all there is to do is to select a material and to define the dimensions such that the resulting stress is smaller than the yield stress. A less important requirement is that the structure still fits in the aeroshell. From these two requirements aluminium appeared as a result of the lightest structure. Furthermore the Al 7075.T6 alloy was selected due to its good yield strength vs. density ratio.

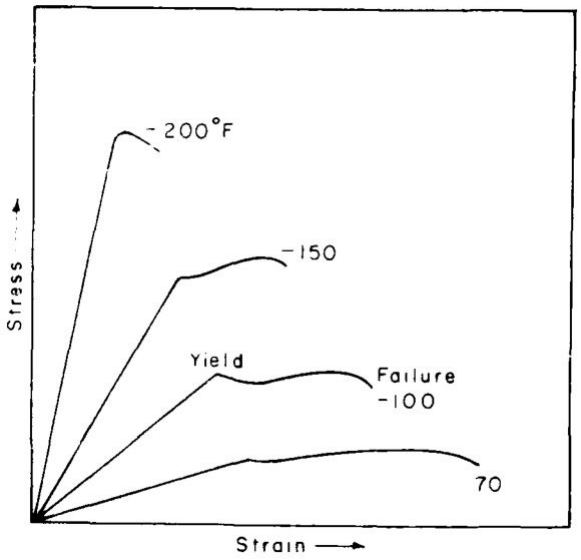

Figure 8.4: Typical mechanical property evolution of the most metals for lower temperatures[38]

8.3 Sizing the structures

The project has several different driving factors that predetermine how much space is available for a structure to hold all the parts together. These are the airbag system, the entry vehicle, and the dimensions of the payload. The other driving matter to design the structure are the forces applied on the system during the entire mission. The limit forces the structures are designed for are the launch on Earth and the entry on Mars. For more information on the loadings see the midterm report [26].

8.3.1 Moment of inertia

The first thing that is done, is calculating the moment of inertia of different shapes of the structure. The shape most often occurring in the design of MACHETE is the I-beam of which the cross sectional shape is shown in Fig 8.5. The definitions of the dimensions are also given in this figure. The equation for the area moment of inertia is then:

$$I_{a,xx} = 2 \cdot (\frac{b \cdot t_2^3}{12} + b \cdot t_2 \cdot (dy + 1/2 \cdot t_2)^2) + \frac{t_1 \cdot h^3}{12} \tag{8.1}$$

$$I_{a,yy} = 2 \cdot (\frac{t_2 \cdot b^3}{12}) + \frac{h \cdot t_1^3}{12} \tag{8.2}$$

The equation for the used hollow tubes is:

$$I_z = \frac{\pi \cdot t_{wall} \cdot d^3}{8} \tag{8.3}$$

8.3.2 Buckling

Another aspect that the program takes into account is the possibility of buckling. Buckling is the manner of failure where a beam deforms as shown in Fig. 8.6. This phenomenon is caused by compressive forces that act on top and on the bottom of the beam.

Equation 8.4 is used to calculate the load when a beam is just about to buckle with n the mode in which the buckling occurs (in this case it is assumed this value is always 1, for more information see the midterm

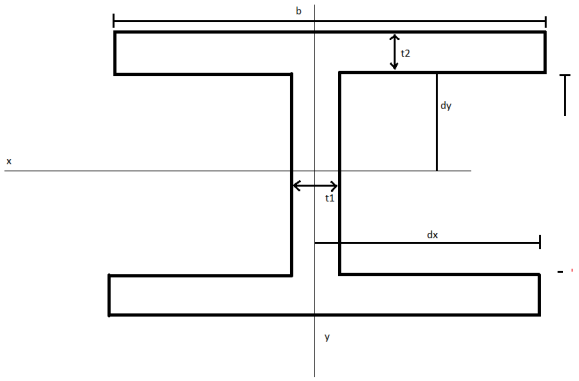

Figure 8.5: Definitions in the calculations of the moment of inertia of an I-beam

Figure 8.6: Normal beam (left) and the beam when buckled (right)

report[26]). F is the force applied, E is the Young's module of the material, I is the moment of inertia, and l is the length of the beam where the compression acts upon.

$$F = \frac{n^2\pi^2 \cdot E \cdot I}{l^2} \tag{8.4}$$

The length l is determined by the layout inside the aeroshell for the large middle beam. The material properties and the manner in which the beam bends n is also also predetermined. So the thing that can be altered is the moment of inertia I. Solving the equation for the maximum forces gives a moment of inertia which would buckle critically at that point. So the beams dimensions should be designed that they are nearly failing when the maximum possible load occurs. A safety factor of 10% is taken in order to prevent failure. This number arises from a convention used in space engineering where normally a safety factor from 10%-35% is used. The fact that the 15 g_E is not likely to be encountered but a lower value of 11 g_E is expected allows for the lowest safety factor.

Using the layout of the structure it shows that only a portion of the beam is under compression, and therefore has the hazard of buckling. Fig. 8.7 shows where the beam is under compression and tension. So the length should be taken in the area where there is actual compression.

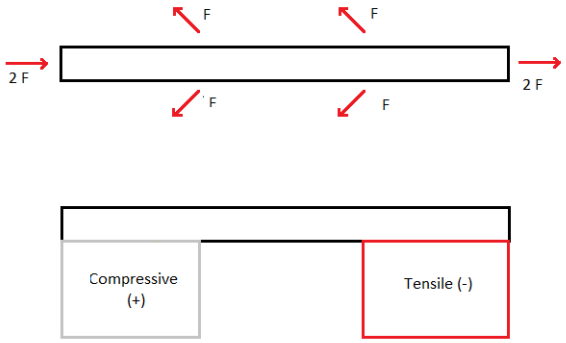

Figure 8.7: Beam under the applied forces found in the aeroshell configuration

From the applied force with the safety factor and all other quantities known a suitable moment of inertia is obtained.

8.3.3 Bending

Bending loads are also a manner in which a structure can fail. Bending is caused by a normal force on a beam causing it to deflect sideways like in Fig. 8.8.

Figure 8.8: Beam bending caused by an applied normal force.

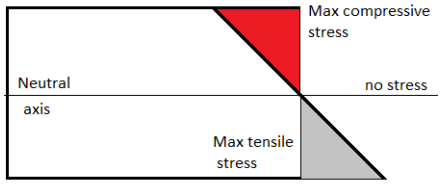

Figure 8.9: Compressive and tensile forces distribution within a bending beam, this beam bends upwards.

This deflection can lead to failure when the compression or tension within the beam becomes too great for the material. The distribution of the tensile and compressive forces is shown in Fig. 8.9. The maximum compressive forces are taken as the forces that have to be countered.

To calculate the maximum compressive forces Eq. 8.5 is used. With σ the stress, M the moment, y_n the distance from the neutral axis, and $I_{a,xx}$ the moment of inertia in the direction of the deflection.

$$\sigma = \frac{M \cdot y_n}{I_{a,xx}} \tag{8.5}$$

The goal here is that the σ does not exceed the yield strength of the material, which would lead to failure. When a component has been checked for buckling and the $I_{a,xx}$ and $I_{a,yy}$ are known it is checked whether the beam can handle the bending load. When buckling is not a possibility the moment of inertia is iterated up or down until the final value is achieved that is required to sustain the bending loads.

8.3.4 Torsion

Torsion must also be considered since during navigation asymmetric loads might be occurring from the rocket engines. One typical example of torsion acting on a beam segment is shown in Fig. 8.10.

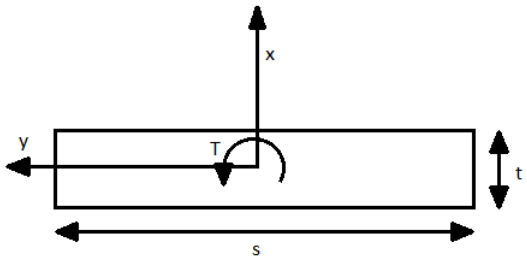

Figure 8.10: Torsion acting on one beam segment

The first thing required to calculate torsion T is the torsion constant J for every beam segment using Eq. 8.6 where the dimensions for one beam segment are given in Fig. 8.10.

$$J = \frac{1}{3}\sum_{i=1}^{N} s_i t_i^3 \tag{8.6}$$

The shear stress resulting from the acting torsion is then calculated with Eq. 8.7. The purpose is then to dimension the beam such that the shear stress resulting from torsion does not exceed the maximum shear stress bearable by the material.

$$\tau = \frac{T \cdot t_{wall}}{J} \tag{8.7}$$

8.3.5 Material failure

The material itself also can fail without special deformations of the components used. For small components this is more often the case since these will need bigger compressive loadings to actually deform. But when pure tension is applied to a component this also occurs. So the material will encounter failure purely due to the loads applied to an area of material. Equation 8.17 shows the simple relation to the loads and this type of failure with σ the stress, F the applied load, and A the area in the plane perpendicular to the applied force. When pure tension is the case or an object has a small length this equation is applied to see if it will fail.

$$\sigma = \frac{F}{A} \tag{8.8}$$

If the area is too small to carry the loadings the area will be adapted in such a way the $I_{a,xx}$ and $I_{a,yy}$ also have the biggest increase in order to have a larger safety margin in other possible manners of failure.

8.3.6 Resulting dimensions of the structure

Now that all the equations needed for sizing the structure are known, the dimensions of the structure will be presented. The loads that each of these beams are designed to withstand is presented in Sect. 8.1. Next to the dimensions the total mass of every components will be given.

Dimensions of the LADS without the airbags

The dimension of the LADS excluding the airbag is given in Table 8.2. It consists of a plate, eight I-beams along the sides of the plates, and four I-beams supporting the center of the plate. The dimension of the bottom plate is not given since it is a requirement coming from the airbag. It is an octagonal shape with a side of 497 mm.

Table 8.2: Dimensions of the components of one LADS without airbags

Dimensions	Base (mm)	Height (mm)	Thickness (mm)		Mass (kg)
			Vertical segment	Horizontal segment	
I-Beams	57	69	2	1	4.9
Plate	N/A	N/A	1	N/A	3.3
Total mass					8.2

Empty CAESAR

The empty CAESAR consists of two I-beams forming the skeleton of the structure, four I-beams holding the tanks, twelve small O-beams attaching the tanks to the previous beams, and eight O-beams attaching the bottom plate to the central beams. The dimensions of the beams is shown in Tab. 8.3. For the O-beams only the diameter and the thickness is needed therefore certain columns in the table where left blank.

Aeroshell

Table 8.4 shows the dimensions of the structure inside the aeroshell holding the CAESAR's. It consists of four beams holding two CAESAR's, eight I-beams holding only one CAESAR, and sixteen O-beams holding the CAESAR horizontally.

Table 8.3: Dimensions of the components of one empty CAESAR

Dimensions	Base (mm)	Height (mm)	Thickness (mm)		Mass (kg)
			Vertical segment	Horizontal segment	
Central I-beams	72	85	2	2	3.7
I-beams holding the tanks	26	36	1	2	1.4
O-beams holding the thanks	5	N/A	1	N/A	0.16
O-beams between central beams and LADS	27	N/A	1.7	N/A	1.3
Total mass					6.56

Table 8.4: Dimensions of the components inside the aeroshell

Dimensions	Base (mm)	Height (mm)	Thickness (mm)		Mass (kg)
			Vertical segment	Horizontal segment	
I-Beams holding two CAESAR's	73	73	1	2.6	11.1
I-Beams holding one CAESAR	36	36	1	2.6	7.2
Horizontal O-beams	9.5	N/A	1	N/A	0.8
Total mass					19.1

8.4 Verification

In order to verify the programs used to calculate the dimensions of the structures and therefore the loadings it can handle all of the equations used will be tested by a manually calculated example. The middle large beam as seen in fig. 8.11 will be the example used to verify the calculations presented in section 8.3.

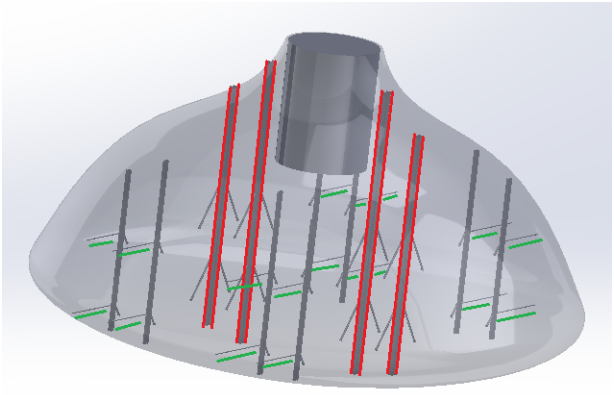

Figure 8.11: The vertical beams inside the MACHETE, the middle beams that hold two CAESAR's are in red. The tension rods used to keep the outer vertical beam from bending are in green.

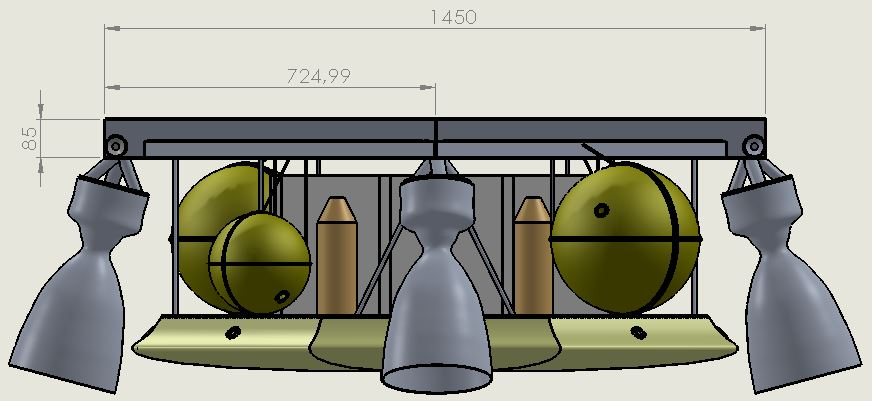

Figure 8.12: Dimensions of the CEASAR used for verification

8.4.1 Moment of inertia

The optimised dimensions for the middle beam given by the program are $t_1 = 1$ mm, $t_2 = 2.5$ mm, $h = 3.6$ cm, and $b = 3.6$ cm which give an $I_{a,xx}$ of $7.07 \cdot 10^{-8}$ m^4 and an $I_{a,yy}$ of $1.94 \cdot 10^{-8}$ m^4. Using equations 8.1 and 8.2 these values are:

$$I_{a,xx} = 2 \cdot \left(\frac{0.036 \cdot 0.0025^3}{12} + 0.036 \cdot 0.0025 \cdot \left(\frac{0.036 + 0.0025}{2} \right)^2 \right) + \frac{0.001 \cdot 0.036^3}{12} = 7.0683 \cdot 10^{-8} \text{m}^4 \quad (8.9)$$

$$I_{a,yy} = 2 \cdot \left(\frac{0.0025 \cdot 0.036^3}{12} \right) + \frac{0.036 \cdot 0.001^3}{12} = 1.9443 \cdot 10^{-8} \text{m}^4 \quad (8.10)$$

Comparing them to the values given by the program shows they are exactly the same.

8.4.2 Buckling

To verify the calculations, the final result of the optimisation is taken and then checked whether it can handle the loadings that are expected to be applied to the structure. The long middle beam is again used for this verification. All dimensions for the moment of inertia are the same as in section 8.4.1. The length is measured to be 0.7 m.

$$F = \frac{1^2 \cdot \pi^2 \cdot 71 \cdot 10^9 \cdot 3.39 \cdot 10^{-8}}{0.7^2} = 4.84 \text{kN} \quad (8.11)$$

The value provided by the program is 4.85 kN so it is off by 0.25% which is probably due to rounding errors. So it is concluded that the buckling calculations are accurate.

8.4.3 Bending

For bending the top beam of the CAESAR vehicle is used, where the rocket engines apply a maximum force of 1.2 kN each providing a maximum moment of 0.87 kN·m at 0.725 m distance. The designed distance to the top of the beam is 42.5 mm. The dimensions of the CAESAR are coming from the 3D-model illustrated in Fig. 8.12. The moment of inertia of this beam is:

$$I = 2 \cdot 75 \cdot 2 \cdot (\frac{85}{2})^2 + \frac{1 \cdot 85^3}{12} = 5.93 \cdot 10^5 \text{mm}^4 \quad (8.12)$$

Then the bending stress is:

$$\sigma = \frac{87000 \cdot 0.725}{5.93 \cdot 10^5} = 106 \text{MPa} \quad (8.13)$$

This is far less then the yield stress. This is because it is also designed to withstand the 15 g_E force from the entry phase. It can then be concluded that it can withstand all the loads.

8.4.4 Torsion

Torsion will most likely occur during navigation. There is a possibility of a torsion of 0.87 kN·m. This is however not realistic because the flying structure is not attached to the ground and therefore will rather rotate. An instant torsion force consisting of 12.5% of the maximal torsion will be considered. Also the rocket engines have an inclination of 15° towards the vertical axis. So a factor equal to cos 15° must be included. The torsion constant J is:

$$J = \frac{1}{3} \cdot 85 \cdot 2^3 + 2 \cdot \frac{1}{3} \cdot 72 \cdot 2^3 = 611\text{mm}^4 \tag{8.14}$$

Then the shear stress is:

$$\tau = \frac{0.85 \cdot 0.125 \cos 15° \cdot 10^3 \cdot 2}{611} = 344\text{MPa} \tag{8.15}$$

The maximum shear stress bearable by Aluminium is 330 MPa. The calculated value is superior to the one of the material. This might be because the torsion value is only an estimation of what can happen. A more precise estimation from the ADCS department is needed for a next iteration.

8.4.5 Normal forces

The final method of failure is when the compressive or tensile forces are simply too great for the material to carry the forces. The tension rods shown in Fig. 8.11 to keep the outer vertical beams from bending inwards are the example. The surface for this beam is calculated using Eq. 8.16 with A the area, R_o the outer radius, and R_i the inner radius of the rod. the values provided by the program for these values are also given.

$$A = \pi \cdot ({R_o}^2 - {R_i}^2) = \pi \cdot (0.0079^2 - 0.0069^2) = 4.6 \cdot 10^{-5}\text{m}^2 \tag{8.16}$$

The force applied to this tension rod is 20 kN so the tensile pressure is as Eq. 8.17 shows low enough for the material to hold.

$$\sigma = \frac{20000}{4.6 \cdot 10^{-5}} = 435\text{MPa} \tag{8.17}$$

8.5 Validation

The validation of the structure is not performed at this stage of the project. A plan however is described in the following section. This plan involves all issues that are likely to arise when the structure is actually built. This plan is written with the assumption that a real life model is built and available for full scale testing.

8.5.1 Vibrations

The validation should begin with applying the vibrational loadings that are likely to occur at launch to the MACHETE vehicle. This validates that the structures that will be validated for other loads afterwards are really not affected by the vibrations. For example the Hydra shaker [6] at ESTEC could be used.

8.5.2 Entry

The most critical phase in the mission for the structure is the entry, at this point in time the possible deceleration reaches 15 g_E. This force should be validated applying 15 times as much mass as the actual payload and subsystems and working from the big system to smaller components.

8.5.3 Launch

The MACHETE is designed in order to withstand the enormous deceleration at Mars entry, the orientation at launch is however directed 180 degrees to the other side. This changes tensile to compressive and the other way around for a lot of structural components. This should be tested the same way as for the entry, but then turning the system around and applying 5 times the normal mass.

8.5.4 Flight

The last test for the structure is for the in flight situation where the rocket engines apply loads on the vehicle. This can be done first by just using forces on the structure but afterwards is is advised to make a scaled model and fly with it to test the structure. The scale model is needed for the different gravity field on Earth.

8.6 Risk and sensitivity analysis

This section will present the risk analysis and the sensitivity analysis of the structural design. These two analyses are made in order to get an estimation of the risks that might cause the system to fail and how fast these situations might occur.

8.6.1 Risk analysis

As the structure has been defined, it is now possible to perform a risk analysis on the structure. The purpose of this analysis is to assess the factors that can to make the structure of MACHETE fail resulting into the failure of the mission. The analysis takes into account every aspect of the trip from the launch from Earth to the EDLD phase where MACHETE comes in action. The risk analysis is presented in Table 8.5. This analysis table shows the identified risks using a scale of 1 (high) to 4 (low) for the likelihood, severity, and importance indicators.

Table 8.5: Structure risk analysis table

ID	Risk	Effect	Likelihood	Severity	Importance	Action to minimize risk
1	Structure take too much fatigue loading	Structure fails at an early state of the mission	3	2	2	Eigenfrequencies of structure must not coincide with these of the launcher
2	The release structure of the bottom layer do not activate	Separation can not be performed	3	1	1	Use proven technology
3	The release structure of the upper layer do not activate	Separation can not be performed	3	2	1	Use proven technology
4	Wrong estimation of temperature	Structure deforms due to temperature difference	4	3	3	Use material with low thermal expansion coefficient
5	Asymmetric loading from the rocket engines	Structure fails under torsion	2	1	2	Design for the highest torsion possible
6	External forces or objects damage the structure	There is no guaranty anymore about the structure integrity	2	2	3	Use safety factor

8.6.2 Sensitivity analysis

For the sensitivity analysis the three main components of the structure are subject to the most extreme loads occurring during the mission while varying the mass of the payload. The most extreme loads are 15 g_E during the entry, and the maximum thrust forces from the rocket engines. The purpose is to see how

the stress in the structure will react with different masses. Three tests will be performed. The first one will simulate the stress produced by the weight of the Zebro's on the bottom plate. The second test will calculate the bending stress coming from the rocket engines through the central beams of the empty CAESAR. The last test will assess the tension and compression on the beams holding the CAESAR's inside the aeroshell.

Stress from the Zebro's on the LADS

During the trip to Mars the payload, 28 Zebro's per cluster, will be attached to the platform of the LADS. It must be able to transfer the weight coming from the Zebro's to the rest of the structure. In this test the behaviour of the structure is assessed by adding and removing Zebro's while being loaded at 15 g_E. As a result the maximal stress occurring on various beam section through the beam is plotted. This plot in Fig. 8.14 shows that the stress is constant between two piles of Zebro's and also that slope between the extremity of the beam and the location of the Zebro's (approx. 380 mm and 920 mm) increases linearly with the mass.

Bending stress through the central beams of the empty CAESAR

The primary function of the empty CAESAR is to carry the loads generated by the rocket engines and to transfer it to the LADS after separation with the aeroshell. In this test the mass carried by the central beams is being varied in a range 20%. Figure 8.13 shows that the stress does not change from the beginning of the beam until approx. 125 mm then the stress varies linearly with the mass.
Fig. 8.15 illustrates the amount of lift generated in function of the mass of CAESAR. From this plot it can be seen that the lift decreases linearly as the mass increases.

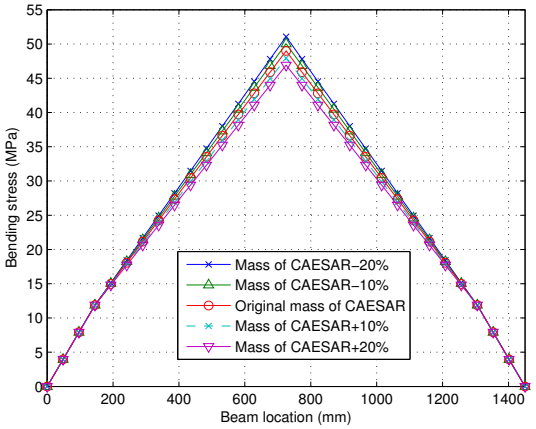

Figure 8.13: Bending stress through the central beams of the empty CAESAR

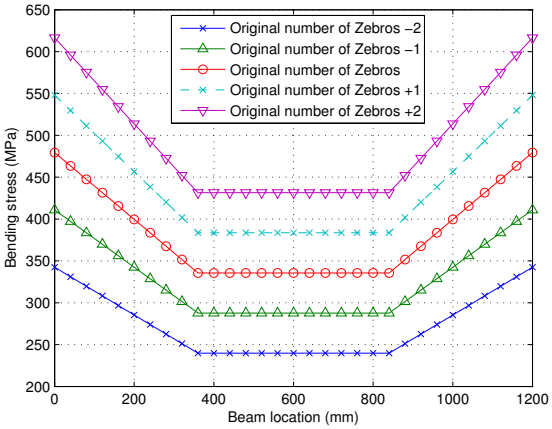

Figure 8.14: Stress acting through one beam of the LADS

Tension and compression on the beams in the aeroshell

The structure inside the aeroshell must hold the CAESAR's during the trip to Mars. Therefore the main loads occurring are tension and compression. For this purpose this sensitivity analysis assess the behaviour of the beam with varying the CAESAR's mass in a range of 20%. As it can be seen in Fig. 8.16 the stress varies linearly with the mass.

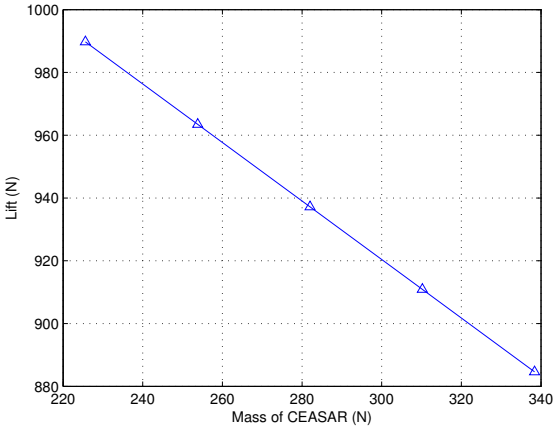

Figure 8.15: Total lift versus the force produced by one rocket

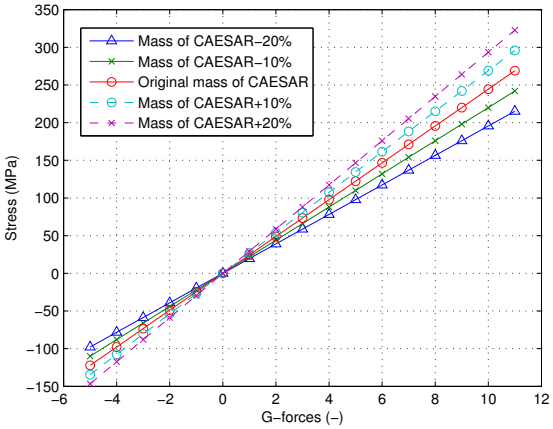

Figure 8.16: Tension and compression on one beam carrying two CAESAR's

8.7 Conclusion

The Zebro's are stacked as four piles of seven Zebro's and held together using a magnesium shell. This package rests on an octagonal shaped plate under which the airbag is attached. This structure forms the LADS. Its structural mass is 8.2 kg. Using circular beams the LADS is attached to two perpendicular I-beams placed above the Zebro container. The rocket engines are also attached to these beams.The fueltanks rest on the octagonal bottomplate but they are not attached to it allowing them to fly away from the bottom construction, they are however attached to the structure that also holds the rocket engines. This structure together with the LADS form the CAESAR. Its mass is equal to 6.6 kg. The 8 CAESAR's are placed in 2 layers inside the aeroshell. They are held by a structure consisting of beams attached to the aeroshell. These beams are placed vertically, clamping the CAESAR's allowing them to fall out during deployment. The mass of this structure is 19 kg.

8.8 Recommendations

Several points in the design still need attention, these are listed here:

- Further design is required in order to take in account the materialization for other systems such as power or electronics. Even though the loads where the structure is designed includes these systems. The structure fastening these systems is not defined. The only system which was taken into account is the propulsion system because its mass and its size were too significant to neglect.
- More precise tools can be used in order to detect local loads occurring in the structure in order to avoid over designing it. Using beams with variable dimensions should be considered. This can help optimizing the structure.
- Local stresses at the release mechanism should be investigated. As should the performance of this mechanism, especially for the separation with the aeroshell, can determine the success or failure of the mission, more attention must be paid to the design of the release structures.

9 Touchdown & deployment system

In this chapter the design of the touchdown system will be discussed. It starts by introducing the function and selecting the conceptual design for the touchdown system in Sect.9.1, then it will describe the mission profile in detail and research detailed requirements in Sect.9.2 and in Sect.9.3 the final design of the system is given. Section 9.4 will deal with verifying the feasability of the system as well as validation of the design after which in Sect. 9.5 the results of a risk and sensitivity analysis can be found. Finally conclusions and recommendations are given in Sect.9.6.

9.1 Introduction

In this chapter the design of the touchdown system will be discussed. It describes the function and conceptual design of the system and gives an analysis of the Martian surface.

9.1.1 System description

The touchdown & deployment system is the final stage of the mission. After the separate clusters have navigated to their desired landing area the payload will be dropped. The structure around the payload that has ensure intact touchdown of the Zebro's is the touchdown system. In the midterm report[26] the conceptual design of the touchdown system was given. In this chapter the design will be further detailed, but first a summary of the design process so far is given.

The mission profile for the touchdown system consists of the following phases: drop, venting and post-landing. These different phases will be explained in more detail in Sect.9.2.

Touchdown system selection

The following will give an introduction to the vented airbag concept and recap the conclusions drawn in previous reports[26][9].

The reason for using an airbag system as opposed to other options is that it has a very low mass combined with good reliability [26]. During the design it was discovered that the mass of the airbag system could be significantly lower than estimated when making the trade-off by the use of vented instead of unvented airbags.

A vented airbag can be seen in Fig.9.1. The main reason for the vented airbag system being so much lighter relative to an unvented system is the mass saved in fabric and structure. See Fig.9.2 as a reference. The predetermined landing orientation means that airbags are only required on one side as well as only one direction of loading has to be taken into account, significantly lowering requirements for the structure. The primary differences between the two airbag systems are summarized in Table 9.1.

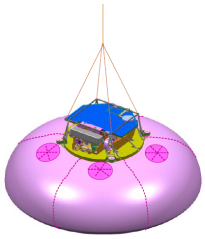

Figure 9.1: Concept vented airbag system, as used for Exomars. [60]

Figure 9.2: Unvented airbag system, as used for the MER [54]

Table 9.1: The differences of vented and unvented airbag systems

Vented	Unvented
Single impact	Multiple impacts
Lower probability of hazardous rock impact	Higher risk of hazardous rock impact
Precise landing	Landing accuracy in the order of 300 m
Unidirectional landing stresses	All direction stress analyses needed
Deterministic landing reduces testing required	Needs to be tested for impact in any direction
Lighter design as only 1 side needs airbags	More airbags needed, heavier system
Risk of roll-over failure	Roll-over capable
Full scale test have been done on Earth	Proven on several Mars missions

System division

The vented airbag system can be divided in three main groups: the primary structure, inflation system, and control system. The primary structure consists of the the actual airbag with the connection to the payload mounting plate, from which the the structural design can be found in Chap.8. The inflation system consists of a gas generation system and the plumbing to connect the gas generators to the airbag. The control system is tasked with initiating both airbag inflation and venting. In order to achieve this, the system needs to recieve a signal upon release from the CAESAR lander and a signal when touchdown occurs. In Sect.9.2 the different phases and functions of these systems are examined in more detail and in Sect.9.3 the design of these systems is given.

9.1.2 Mars surface analysis

In this section a brief investigation of the Martian surface is given because no exact landing site(s) have been designated at the moment of design of this mission. It is of interest to explore the Martian surface and the effects of it's feautures on the requirements for the touchdown system. To ensure flexibility of the mission a large range in possible landing locations is required. The focus of this surface analysis is thus on the presence of rocks and slopes.

Slope presence on Mars

The presence of slopes is interesting for the touchdown system, because using the vented airbags introduces the risk of tip-over(roll-over). This failure mode is the must common upon vented airbags. It occurs when the airbag falls on an inclined surface or landing with enough horizontal velocity, tipping the airbag over on it's top, crashing the payload to the ground without protection. The second failure mode is called dive-through and occurs when the payload fall through the airbag, hitting the surface significantly hard. Both failure modes probability increase with the presence of steep slopes. Figure 9.3 illustrates both failure modes.
Figure 9.4 shows the slope distribution on Mars on an order of kilometers scale[58]. From this picture it can be concluded that the requirement of a 10 degree angle between the touchdown system and the surface allows landing almost anywhere on Mars. However, locally slopes can be higher. It is assumed that in this case there will always be a suitable landing spot nearby and the hazard detection system from the ADCS should be able to detect and avoid these local variations in inclination.

Rock distribution on Martian surface

Rocks are of interest to the touchdown system for two reasons: tip-over and airbag puncturing. For tip-over the main concern is large rocks, while for airbag puncturing the main concerns are half buried triangular or pyramidal shaped rocks.

The risk of airbag puncturing can be mostly neglected. Unvented airbag systems have undergone full-scale drop tests on surfaces with up to 60% rock coverage, and have shown very high survivability, as shown by Golombek [29]. As the main failure mode for these tests was airbag puncturing it is safe to say that this risk does not limit the choice of landing area very much, especially considering that vented airbags with

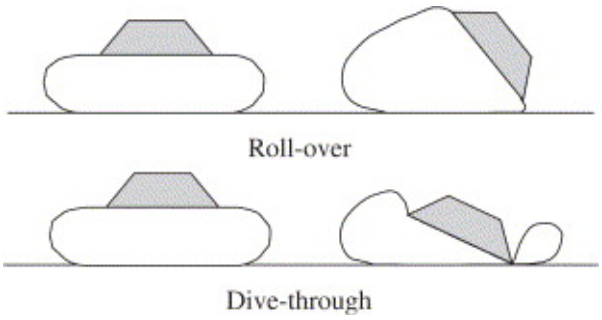

Figure 9.3: Both failure modes with vented airbags

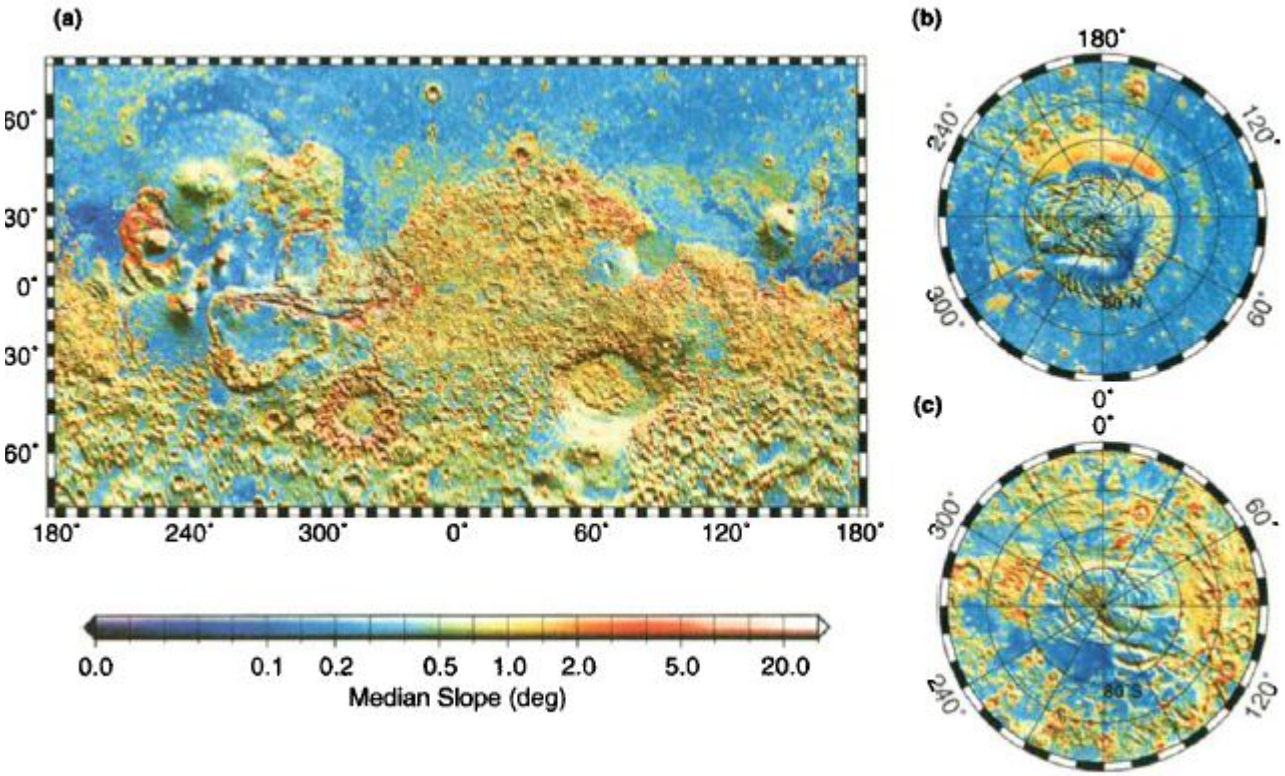

Figure 9.4: Large scale slope distribution on Mars. See [58] for a color map.

compartmentalized venting can puncture without catastrophic consequence, it just means that they will have a slightly larger vent area.

The hazard of large rocks(>0.5m) depends largely on the area selected for landing, the density of the rock coverage varies largely per area, see Fig. 9.5. Abundance of rocks higher than 0.5 m in previous Mars landing areas differs from 2 - 22% [29]. Simulations done on the landing of unvented airbags in these areas concluded that the chance of hitting a rock this size varies from respectively 0.02-39.9%. However this took into account 2 bounces with an airbag area of 8.95 m^2, while the vented airbag does not bounce and has an area of 6.97 m^2. It is thus expected that the large rock impact probability for the design is significantly lower. Further studies will have to perform simulations to obtain the actual probabilities. It can be concluded that for landing in low rock abundance zones a hazard detection system is not required, but since this mission should be flexible in its landing areas a hazard detection system still remains an option.

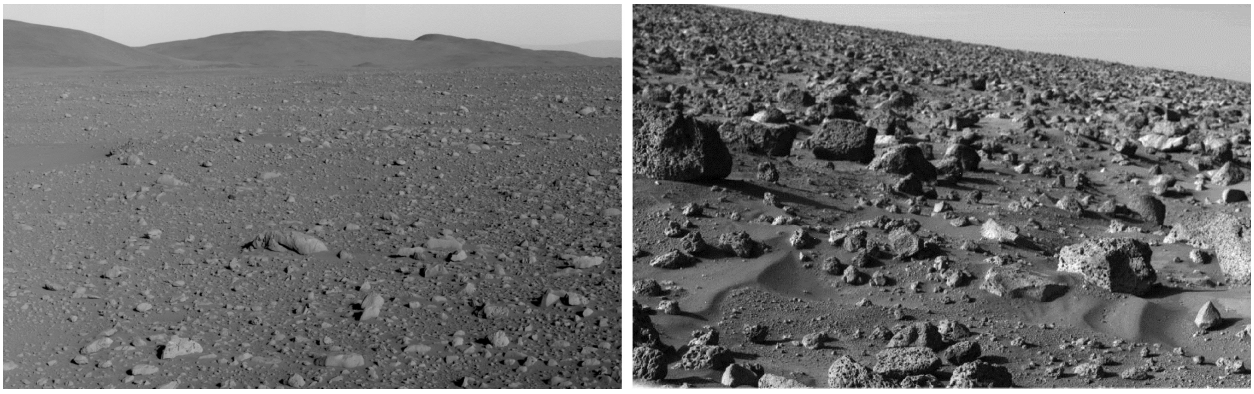

Figure 9.5: Local variations in rock density, photo from the MER-A (left) and Viking (right) missions courtesy of NASA/JPL-Caltech respectively PIA05875 and PIA00364

9.2 Mission profile

This section presents an overview of the mission profile for the touchdown system, as well as identification of additional requirements following from each phase.

9.2.1 Drop phase

After separation from the CAESAR, the LADS will begin its free fall, inflate the airbag and come to a safe stop on the Martian surface. The following figure illustrates the free fall phase of the airbag. This model neglects any perturbations possibly caused by aerodynamic drag. The CGG tanks have an inflation time of 3 seconds. This means that if the total drop time is about 4 seconds, free fall from 30 m, under a constant Martian gravitational acceleration of 3.72 ms^{-2}, the limit time to start inflating is after 1 second of free fall. After 1 second of free fall, the lander will have fallen 1.86 m.

The CAESAR will remain hovering at the release position for several seconds before it flies away. This is done to provide clearance for the airbag as it is inflated during free fall. The nozzles from the CAESAR are inclined at an angle of 15 degrees to provide additional clearance for the airbag inflation. Fig. 9.6 shows the critical inflation point and its interaction with the under-expanded exit flow of the engines.

The model has been created using the official dimension from the lander, airbag, nozzles and CAESAR structure. As no information was available of the exact expansion ratio and the exhaust flow behavior the following assumptions where made.

- Under-expanded flow.
- Straight nozzle flow with a small divergence of 2 degrees.
- Straight free fall: no wind perturbations.

The airbag interaction shown in situation 1 is however unlikely to happen as the airbag is stored underneath the lander platform and is not expanded to its full shape immediately after inflation starts. Situation two on Fig. 9.6 however shows that after 0.48 seconds of inflation, there is no interaction anymore with the under-expanded flow, even if the airbag has reached its full shape. Honeywell has shown that the airbag fabric Spectra 75 can cope with temperatures up to 145 degrees. This is however unfavorable as the tensile strength properties drastically drop at higher temperatures: only 55% remaining at 100 degrees[37] .
This is something which will require further investigation using FEM-software(e.g. LS-DYNA) in a follow up study. In case the FEM analysis results in severe interaction with the airbag at the critical inflation point ,which might cause damage to the airbag material, the following solution is proposed. In stead of letting the CAESAR hover at the release altitude, give it an impulse directly after release, from which it flies straight up to provide enough clearance.

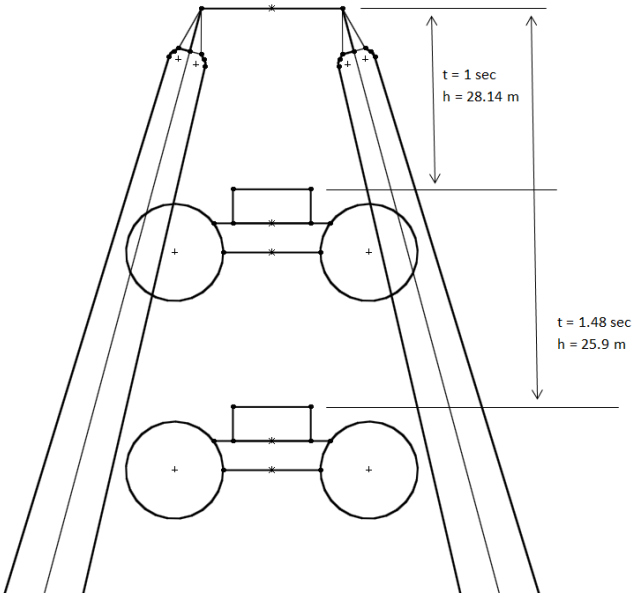

Figure 9.6: Illustration of drop phase clearance from rocket exhaust jets, situation 1(top) and situation 2(bottom)

9.2.2 Venting

As mentioned in the baseline report, the venting itself still needs some investigation. The team had waited for this design decision as it wanted to determine this by means of a FEM, using LS-DYNA. This unfortunately did not work out. An analytical approach was thus used to illustrate and investigate the actual venting phase of the airbag.

Venting an airbag uses the following equation from the Wang-Nefske airbag model [12]:

$$\dot{m} = k \cdot A_{vent} \cdot \frac{P}{\sqrt{RT_{atm}}} \cdot Q^{1/\gamma} \cdot \sqrt{\frac{2\gamma}{(\gamma-1)} \cdot [1 - Q^{\frac{(\gamma-1)}{\gamma}}]} \tag{9.1}$$

Where

- k = discharge coefficient = 0.6 [28]
- A_{vent} = Vent Area [m^2] (TBD)
- R_u = Universal Gas constant = 8.314 J Kmol^{-1}
- P = Airbag pressure = 11.7 kPa
- P_{atm}= Atmospheric pressure = 440 Pa
- T_{atm} = Mars atmospheric temperature = 184 K
- γ = Ratio of specific heats = 1.4

Concerning the pressure ratio Q, the following relations hold:

- $Q = \frac{P_{atm}}{P}$ if $Q > Q_{crit}$
- $Q = Q_{crit} = \frac{2}{\gamma+1}^{\gamma/(\gamma-1)}$ if $Q < Q_{crit}$

The following assumptions have been made:

1. The finite opening time of the vent and any changes in its shape during impact are neglected. The vent area remains constant during venting.
2. $Q < Q_{crit}$ during almost the entire venting procedure, due to the low Martian atmospheric pressure, thus a constant Q is assumed.($Q_{crit} = 0.5281$). This results in the assumption of choked sonic flow conditions.
3. Adiabatic flow, this is valid because of the short impact time and limited heat exchange.
4. As no FEM software was available in time to run simulations, a linear volume decrease was assumed during venting.

Iteration

An analytical model was set up using the following method. As can been seen from Eq. 9.1, the mass-flow is only time dependent on the pressure at a particular moment. The specific pressure is then time dependent on the actual volume and the actual gas mass in the specific airbag volume, assuming no temperature change during impact. The ideal gas law is used to determine the specific pressure at a certain moment.

The iteration starts at the following initial conditions taken from the fully inflated airbag just before impact.

- $P(1)$ =11700 Pa : Initial inflation pressure where the airbag is designed for.
- $v(1) = 5.13$ m^3 : Total airbag volume.
- $m(1) = 1.05$ kg : Total gas mass in the airbag under the above mentioned circumstances and using the ideal gas Law (Pv=nR$_u$T)

Given a certain time step of 1 ms (= dt) the mass flow at each time step is calculated using the following three relations

$$m(t) = m(t-1) - dt * \dot{m}(t-1) \tag{9.2}$$

This specific gas mass is then used in the following equation in order to calculate the specific pressure.

$$P(t) = \frac{m(t) \cdot R_u \cdot T_{atm}}{M \cdot v(t)} = \frac{[g] \cdot [J/Kmol] \cdot [K]}{[g/mol] \cdot [m^3]} = [Pa] \tag{9.3}$$

Where the specific volume is linearized from v(1) to 0 over the time step dt. The specific mass-flow can then be calculated using Eq. 9.1. After this step, the procedure starts again at Eq. 9.2.

Venting area

The specific mass flow however is still dependent of one unknown, the venting area. This area is limited by boundaries as seen in Fig. 9.7 illustrating a single section of the octagonal airbag. To reduce the chance of rupture during the opening of the vents, a circular shape has been chosen for the vent itself. Furthermore the vent should not be placed beneath the center line of the airbag as this would limit the venting during impact as the airbag shape deforms. Together with the choice to leave some extra space left from the walls, a maximum venting area of about 0.43 m^2 was found per section, which gives a total venting area of 3.43 m^2.

Now that the specific mass-flow has been calculated per time step, a relation between time and deflation can be plotted, as displayed in Fig. 9.8.

Figure 9.8 gives a good understanding about the venting area and its relation to the venting time. The venting time numbers aren't accuracte enough to use as a reference for future research as the model used assumes a linear volume decrease of the airbag. The entire deflation would only take about 10 ms, when maximizing the venting area. This is pretty fast as the time between the detection of a section to be vented and the opening of the valve itself is estimated to be 17 ms [28]. This consists of 4 ms electronics delay, 8 ms pyro activation and 5 ms for the valve deployment and opening. On the other hand, the faster the venting occurs, the quicker a counter-moment can be created to level the airbag in case of a perhaps inclined impact on a slope or a rock, therefore the maximum venting area has been chosen.

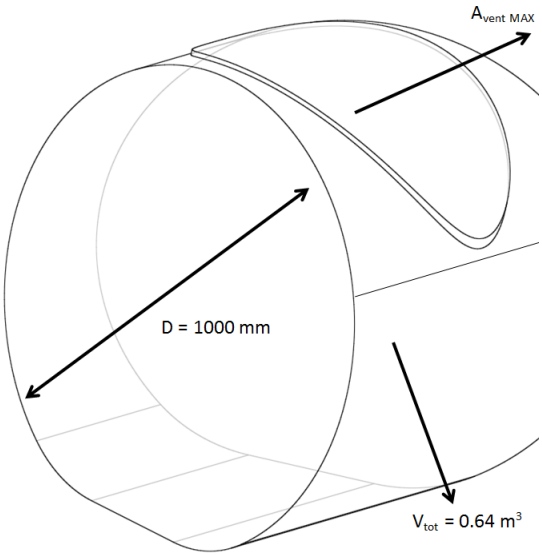

Figure 9.7: One section of the octagonal airbag illustrating the venting area.

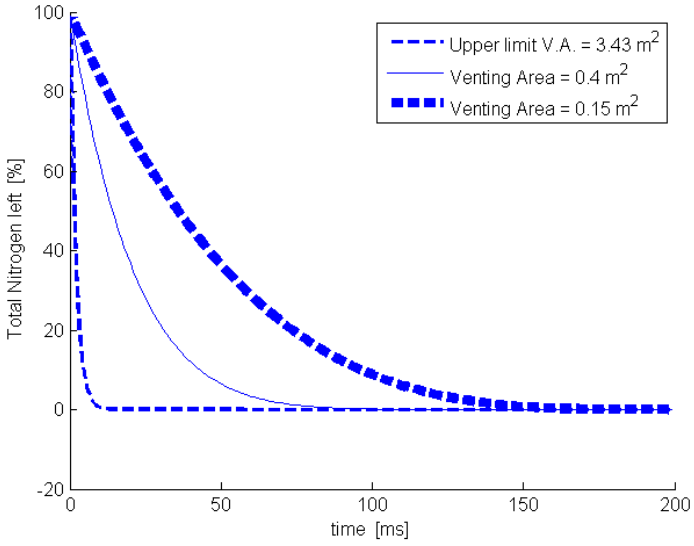

Figure 9.8: Venting of the entire airbag for 3 different venting area's.

Vent triggering

As mentioned before, separate venting of each section will be used in order to reduce the risk of tip-over.

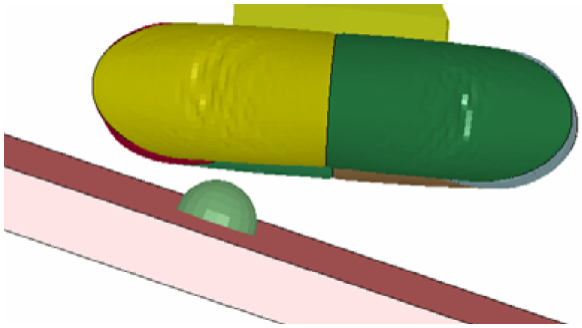

Figure 9.9: Impact simulation on an inclined surface with a rock [28]

Fig. 9.9 illustrates the need for separated venting. If the entire airbag would deflate during the first strike, the right part of the airbag would hit the ground without any pressure left inside. Furthermore, the situation in Fig. 9.9 will tend to induce a rotation/angular momentum. If no/limited pressure is present in that part of the airbag, the system will tend to tip-over.

An appropriate system must be chosen for this highly sensitive and accurate job. Research has shown that without a precise venting control strategy, the success probability was limited to about 81% [63]. The need for a complex control algorithm which vent each section separately is thus rather important. Pyrotechnics remain the best option for the opening of the vent valves, however an appropriate sensor hasn't been chosen yet as still some future research must still be done as discussed in subsection 9.3.3 between the use of strain gages and a proximity radar system.

9.2.3 Post landing of the LADS

In this section the post landing procedure is described in detail. After the LADS is on Mars surface the Zebro's need to be activated and then be able to get out of the lander.

The deployment happens in the following steps. The protective shell covering the Zebro's will be lifted, they will activated in an order depending on their position and walk out to the Mars surface. The main risks during this process are: failure of the hull lift, failure to activate some or all of the Zebro's, and Zebro's getting entangled in remains of the structure or the airbag.

Shell elevator

Each LADS has a structure specified in Sect. 8.1. The first thing that will happen after landing is lifting the shell. This is done by a mechanism as shown in Fig. 9.10 powered by small electric motor. Total energy required for this lift is estimated to be about 7 J. This is based on the weight of the structure, gravitational force acting on it and the distance it needs to cover. This energy requirement is an estimate as it does not take into account efficiency and friction. When the shell is lifted the Zebro's should be able to move out.

(a) Elevator mechanism (b) Open LADS

Figure 9.10: Illustration of the opening of the shell, releasing the Zebro's

Zebro activation

In collaboration with the Zebro design team it has been decided that the Zebro's can be activated by radio signal. After elevating the protective structure, the Zebro's at the top in the front can be activated. When the path is clear for the next row they can follow. This can happen by using a set time interval or letting the Zebro communicate about their position so that it is known whether they were able to clear away safely and perhaps what path not to take. The former is easier, but the latter is recommended since this communication needs to be set up anyway for the swarm to function.

Zebro departure

The height of each stack of Zebro's is approximately 30 cm. This means that each Zebro will fall at most a distance of 30 cm to the Martian surface. According to the Zebro design team, the Zebro structure should be able to withstand the loads that this fall incurs.

To check whether the Zebro's could walk over the airbag a test was performed. In reality a deflated airbag will look like Fig. 9.11a, in the test the Zebro walked over both large patches of polyester fabric and small patches of Vectran that were covering a rocky environment as can be seen in Fig. 9.11b. Polyester was used because it is cheap and easily available while having a similar surface quality as the considered weaves, the fibers just have a lower strength. This should not influence the results of this test. The test was completed successfully so it can be concluded that the Zebro's should have no problem traversing the airbag post landing. It should however be noted that the Zebro sunk into the sand easily which can pose problems when walking on the Martian surface where sand is much more fine. However this is outside the scope of this project and therefore will have to be dealt with by the Zebro designers.

(a) Vented Airbag test by Aerosekur [7]

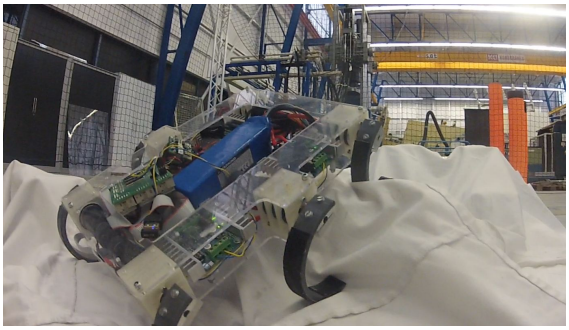

(b) Zebro's crawling over a Mars landscape + airbags

Figure 9.11: Illustration of testing the Zebro deployment

9.3 Touchdown system design

In this section the design of the airbag is given. It will start with the choice of shape and material for the airbag, then it will explain the gas generation system, control and sensors in the airbag and finally the physical system layout.

9.3.1 Airbag material and shape

The airbag shape and material have been largely determined in the midterm report [26] so just the conclusions will be repeated here. First the material is discussed and then the shape.

Airbag material

From the midterm report[26] it was concluded that the optimal fibers are Spectra 75 and Ventran HT. Spectra 75 comes with no real disadvantages and even an increased strength at low temperatures, 110% at 213 K[36], which gives it a higher specific strength than most all other eligible fibers in cold Martian atmosphere, however this fiber has not been used for this application. Vectran HT however has been used for previous Mars mission that utilized airbag landing systems and therefore can be recommended as a safe alternative to Spectra 75 in case it turns out to have unforeseen disadvantages.

The weight of the weave that will be used for the airbags cannot be easily determined from the specific strength of the fiber, different weave configurations should be tested to find the best solution. Options that should be considered are using a coating for additional protection and leak proofing of the airbag, and using ripstop layers for additional abrasion resistance and tear protection. For the weight estimation a conservative mass of 240 g m^{-2}[57] will be used which is comparable to Vectran HT with a silicon coating for leak tightness.

In order to determine the final fabric weave, thickness and coating, it is recommended that fabric tests are performed, which are to be followed up by full scale airbag tests. First, the optimum weave and seam structure should by determined. Then performing full scale drop tests including rocks to determine whether this weave actually performs up to expectations. For reference, the MER mission used six 100-denier layers of Vectran on the outside and two 200-denier layers on the inside[52] and the Pathfinder mission used a silicone coated Vectran airbag[20].

Airbag shape

From the midterm report the dimensions of the airbag were determined as given in Table 9.2. Three things have changed since the midterm: the reduction in amount of Zebro's taken means that the airbag inner radius could be decreased, the final shape selected is an octagonal planform for better manufacturability, and the payload mounting height has been increased to improve rock clearance and provide space for a bumper against rocks. The inner radius defines a circle that touches the inner midpoints of each section.

Fig. 9.12 illustrates the main design decisions of the airbag. The bottom view illustrates a new design change. The bottom section has been flattened in order to create a larger contact area at impact, thus reducing the pressures introduced at impact and the risk for tip-over.

Table 9.2: Airbag specifications

Specification	Midterm	Final
Airbag height	1 m	1 m
Airbag inner radius	0.6 m	0.5 m
Number of compartments	8	8
Payload mounting height	0.6 m	0.8 m

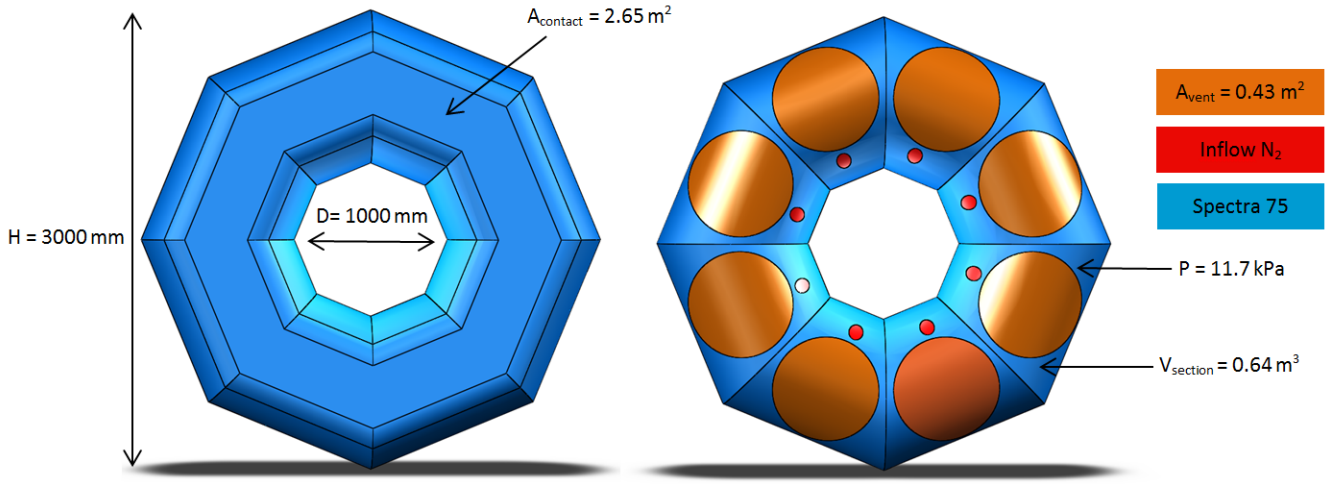

Figure 9.12: Design of the airbag, both top and bottom view

Airbag to payload plate connection

In order to connect the airbag to the payload mounting plate two options are considered: adhesive bonding of an extended piece of airbag fabric and a system of tendons wrapped around the airbag fastened to a type of ring bolts. The solution resulting in the lowest total mass is to be used, but the best solution cannot be determined analytically. For now the adhesive bonding method is chosen to finish the design, because the tendon system is more complicated to design. However it might be worthwhile to investigate this in greater detail.

9.3.2 Airbag inflation system

This section will discuss the design of the airbag inflation system. The airbag inflation system is primarily composed of a gas generation system. The requirements for this system are defined in subsection 9.2.2. In the midterm report [26] the gas is already chosen to be nitrogen and the type of gas generation system is also chosen.

Gas generation method

Three gas generation were considered in the midterm report [26]: Carbon fiber Overwrapped Pressure Vessels (COPV), Solid Propellant Gas Generators (SPGG) and Solid Propellant Cool Gas Generators (SPCGG or CGG). A trade-off based on mass and reliability led to the selection of CGG's as gas generation method, they are lighter than SPGG's and COPV's were discarded because their failure would be catastrophic for the whole mission due to the high pressure inside them.

Cool gas generator specifications

The CGG system will consist of 4 separate cylinders per lander, each cylinder connected to two airbag compartments. An overview of the specifications can be found in Table 9.3.

Table 9.3: Gas generation system specifications

Specifications[65]	
Number of cilinders	4
Cilinder diameter	85 mm
Cilinder height	205 mm
Total cilinder mass	1 kg
Nitrogen mass per cilinder	0.3125 kg
Gas purity	98%
Inflation time	< 3 s
Exit temperature	ambient

The initial design in the Midterm showed two CGG tanks located in the center of payload, in between the Zebro's. In order to increase packing inefficiency this has been changed to the configuration described below. The number of tanks has also been increased for three main reasons. First of all, increasing the amount of tanks, decreases the risk of failure of the inflation. Furthermore, each tank is connected to 2 sections of the airbag, this also brings a faster inflation process during free fall. Last of all, increasing the amount of cinders results in faster inflation times (Berry Zandbergen, CGG, mail contact 08-01-2014). The effect of smaller tanks on the inflation time is however still unknown.

Cilinder location and mounting

The cylinders are located on the protective hull that encapsulates the Zebro's. The mechanical interface provided for mounting the CGG is a clamp band that is clamped to the surrounding structure. Each tank will provide nitrogen for two airbag sections.

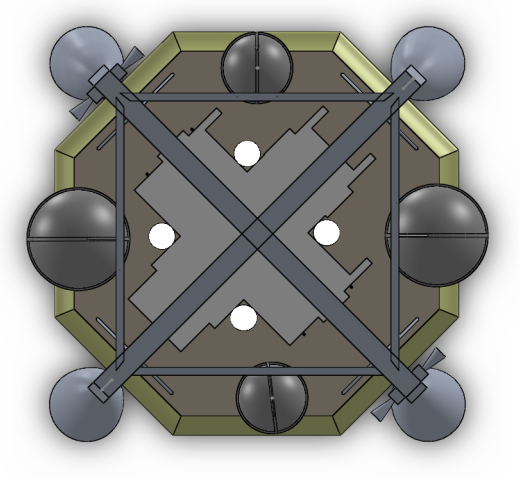

Figure 9.13: Top view illustrating the nitrogen tank position(in white) on the top view of the CAESAR

Inflation process

The total amount of nitrogen needed can be calculated using the ideal gas law:

$$P_{nit} \cdot v_{nit} = \frac{m_{nit}}{M_{nit}} \cdot R_u \cdot T_{nit} \tag{9.4}$$

Where

- Pressure $P_{nit} = 11.7$ kPa
- Volume $v_{nit} = 5.13$ m^3
- Molar mass Nitrogen-gas $M_{nit} = 28$ g mol^{-1}
- Universal gas constant $R_u = 8.314$ J K^{-1}mol^{-1}
- Temperature $T_{nit} = 193$ K

Using the given design parameters, one finds a required nitrogen mass of about 1.05 kg. Each nitrogen tank from CGG produces about 312 g of Nitrogen. Giving a total mass producible by the CGG system of 1.25 kg. This 200 g reserve nitrogen is used for coverage in the pipes and small possible leakages in the airbag fabric or connections.

9.3.3 Vent control

In this subsection the design of the vent control subsystem of the touchdown system is discussed. The function of this system is to open the venting valves and do this in such a way that tip-over risk is minimized. This can be done through control of the order and timing in which the compartments vent. This means that this system should somehow determine the optimal vent opening time for each different vent. This control is done through sensors in combination with pyrotechnics.

First sensor selection is done and then the control logic is defined.

Sensor selection

Fig. 9.14 illustrates the possible options for a vent triggering mechanism.

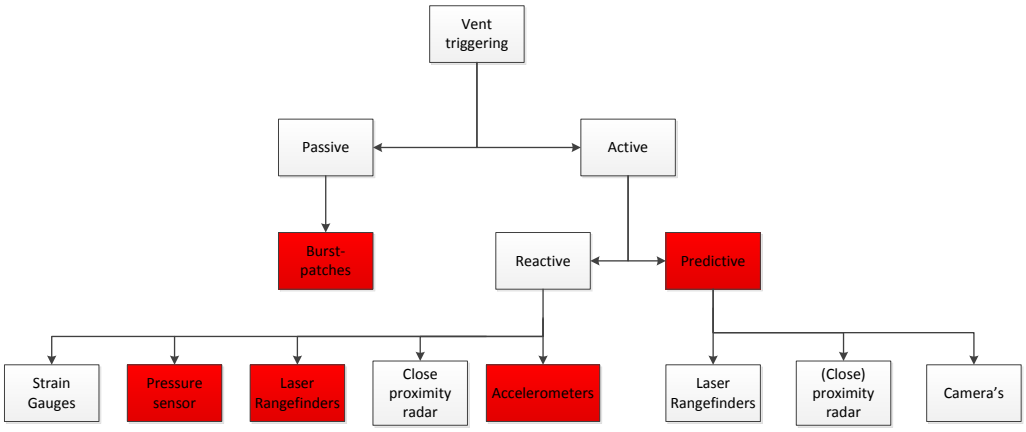

Figure 9.14: Vent triggering options

The simplest, cheapest and lightest method is the use of a passive system which is fully self-actuated by means of burst-patches which open at a certain pressure. Research however has learned that this method is unreliable and does not provide sufficient control of the entire system. Certain active sensors must thus be used either in a reactive or predictive mode.

The laser rangefinders, close proximity radar and pressure sensor will have to be placed inside the airbag, where the predictive systems must be placed outside the airbag. Longer sampling time, larger distances to measure and the limited view exactly under the airbag make all predictive sensors not feasible.

Accelerometers are excluded as impact on a certain section would affect the acceleration of the entire airbag, making it hard to have separated venting. Pressure sensors are not the best choice because of the long inflation time of the airbag, whereas the shape/volume is reached far faster. Single-beam laser rangefinders only send a single beam at a surface to be measured. This could create a time delay in the measurement if the airbag is hit by a rock at a different spot then the laser is pointing. See Fig. 9.15. Multiple beam lasers could fix this problem, but increases the size of the rangefinder.

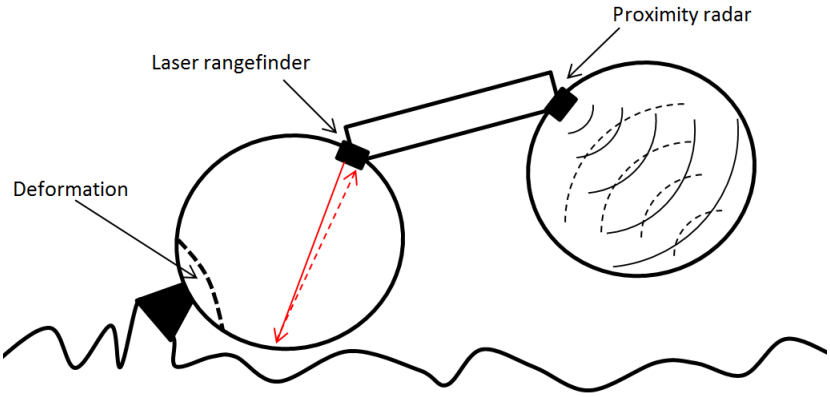

Figure 9.15: Laser rangefinder vs proximity radar system

A radar proximity system deals with this problem by emitting electromagnetic waves, covering a larger area in stead of a single point. It measures the changes in frequency of the reflected waves. The last option that might be a consideration is the use of strain gages. These must be placed at the lower half, because that is the part deforming most. As the airbag deforms during touchdown, the strain gage is deformed, causing a difference in electrical resistance.

Table 9.4: Trade-off between two remaining vent triggering options

Parameter	Strain gages	Radar/motion sensor
Unit Cost	++	-
Mass	++	-
Installation costs	–	++
Operating temperature range	+	-
Risk of failure	++	-

The above table illustrates a basic trade-off between both options. As seen from now, the strain gages seem to be the best option. However, further research is however still required in for instance wire-placement, amount of strain gages needed and the installation of the gages on the airbag fabric. See subsection 9.6.2

Finally the trigger mechanism for the vents is to be designed. Explosive pyrotechnic devices have proven their reliability and safety over several Space missions, ranging from separating the large Solid Rocket Boosters from the space shuttle to releasing small springs during the Curiosity mission, [23]. Pyrotechnics offer a self contained energy source that provides the a very high work potential for a very small volume and weight, only nuclear energy has a better performance. A pyrotechnical device could thus be placed on top of the vent, connecting straps and wires which hold the vent under constraint.

Control logic

For the venting system the control logic can be found in Fig. 9.16. The vent opening system is controlled by a pyrotechnic device. To prevent premature initiation of the pyrotechnic devices a safety and arming

system is used, when in safe position premature firing is made impossible. To ensure that the reliability of this system is acceptable NASA Standard Detonators (NSDs) can be used.

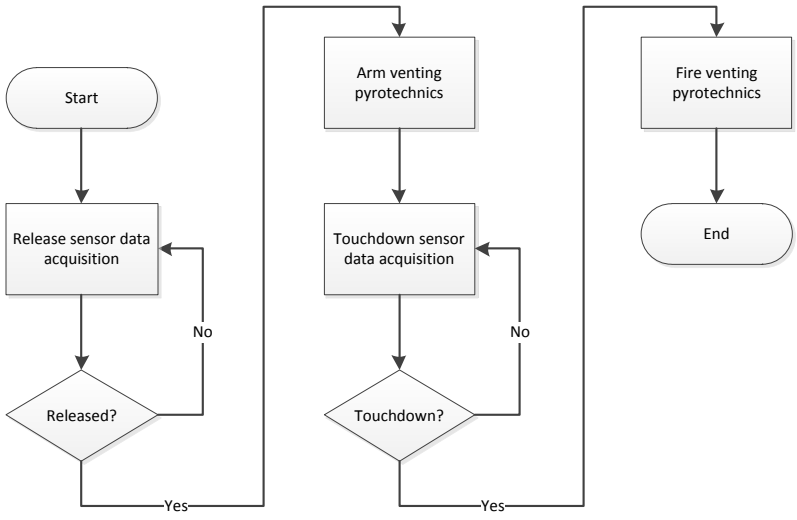

Figure 9.16: Venting control logic

9.3.4 Final touchdown system design

Finally the full system can be presented; in Fig. 9.17 CAESAR system is shown and in Fig. 9.18 the LADS sytem with inflated airbag is shown. Table 9.5 summarizes all previously determined design results.

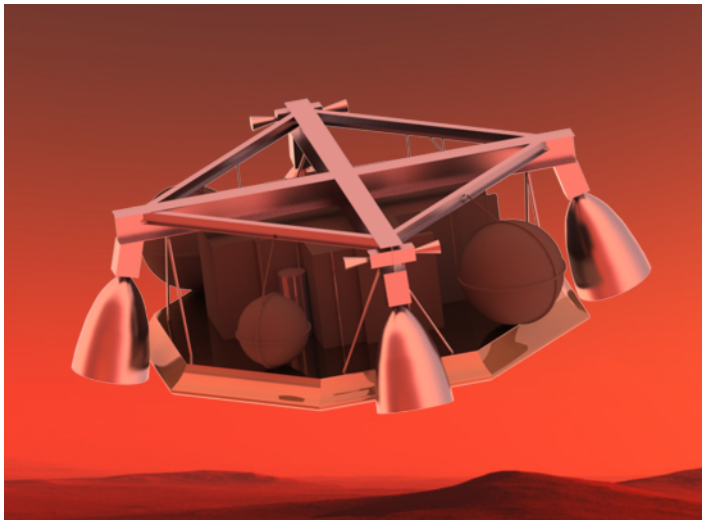

Figure 9.17: CAESAR system

Table 9.5: Design summary

Parameter	Value	Unit
Dimensions		
Airbag outside radius	1.5	m
Airbag inside radius	0.5	m
Airbag major radius	1	m
Airbag minor radius	0.5	m
Airbag surface area	26.61	m^2
Airbag venting area per vent	0.43	m^2
Airbag total vent area	5.12	m^2
Airbag volume	3.43	m^3
CCG Cilinder diameter	85	mm
CCG Cilinder height	205	mm
Masses		
Airbag fabric and coating	7.7	kg
Gas generation system	4	kg
Vents, pipework, valves, etc.	2.5	kg
Total system mass	14.2	kg
Operational		
Free fall time	4	s
Inflation time	3	s
Touchdown airbag pressure	11.7	kPa
Other		
Number of compartments	8	-

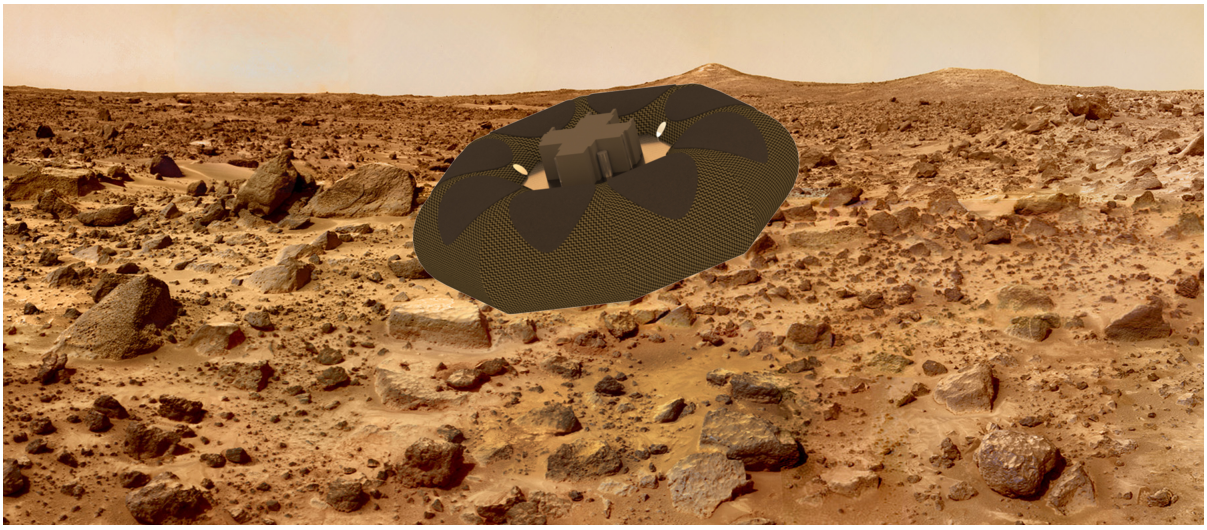

Figure 9.18: LADS system with inflated airbag

9.4 Verification and validation

Verification and validation will be discussed in this section. Verification is done by comparing the results of this study to another reference study and for validation recommendations and test setup proposals are given.

9.4.1 Verification

In order to verify that the results of this study are realistic, a reference study is chosen for comparison. The reference study chosen for comparison is a study done by Altair for the ExoMars mission[63]. This study is the most thoroughly reported study found on this topic and its results are based on extensive numerical optimization. In Table 9.6 key design parameters from both studies are listed.

Table 9.6: Design key parameter comparison with Altair

Parameter	MACHETE	Altair	Unit
Total system mass	14.2	18	kg
Total landed mass	154	385	kg
Airbag outside radius	1.5	2.205	m
Airbag height	1	1	m
Airbag total vent area	5.12	2.40	m^2
Touchdown airbag pressure	11.7	30.3	kPa

The first thing that should be noted is that Altair has a much higher landed mass than the MACHETE. The relative difference in system mass is not as large due to the fact that most subsystems hardly vary with changes in landed mass. This is mainly because of the 0.5 m rock clearance requirement, which is also the reason why the airbag height of both system is 1 m. What could be changed is the airbag outer radius, which leads to smaller volume and thus less gas required. The lower pressure also means that less gas is required, this combination of weight reduction in airbag fabric and the gas generation system is the source of the difference in system mass. For the vent area in this project the conclusion is that it should be as large as the geometry allows, see Sect. 9.2, also during the optimization of Altair the vent area was at its upper bound suggesting that the optimum is higher. The difference in airbag pressure is the only parameter for which the difference is not immediately clear, but it is suspected that this is due to the Altair airbag not having compartmentalized venting. Not having compartmentalized venting makes tip-over more likely and the higher pressure may compensate for this partly due to more pressure being left in the airbag at the point that full ground contact is made when landing on slopes.

9.4.2 Validation

For validation several tests have to be performed. One validation test was already done within this project, that is testing whether the zebros will be able to walk out of the lander over the airbags. The following validations are recommended for a follow-up project.

1. Testing the airbag fabric for tensile strength and puncture resistance.
2. Testing the CGGs for inflation time and exhaust temperature.
3. Performing full scale drop tests with simulated Martian surface including 0.5 m rocks and slopes.

For drop tests a structure similar to Fig. 9.19[57] can be used. The impact zone should also be able to have an inclination in order to test landing on different slopes.

Zebro egress test

For this test a rocky Martian environment with an airbag on it was simulated using samples of uncoated Vectran in one test and uncoated polyester fabric in another, polyester was chosen, because it is very similar to high strength fiber weaves in terms of surface quality, just the fibers are a lot weaker. This lower strength would only make it more likely for the zebro to get stuck, because it could for example tear it. An overview of the test setup can be in Fig. 9.21.

Conclusions from this test are that the zebro had no problems with airbag fabric as long as it did not turn upside down. Rocks too high for the zebro to climb may cause the zebro to flip itself and then the leg motion should be reversed otherwise it just grabs the airbag.

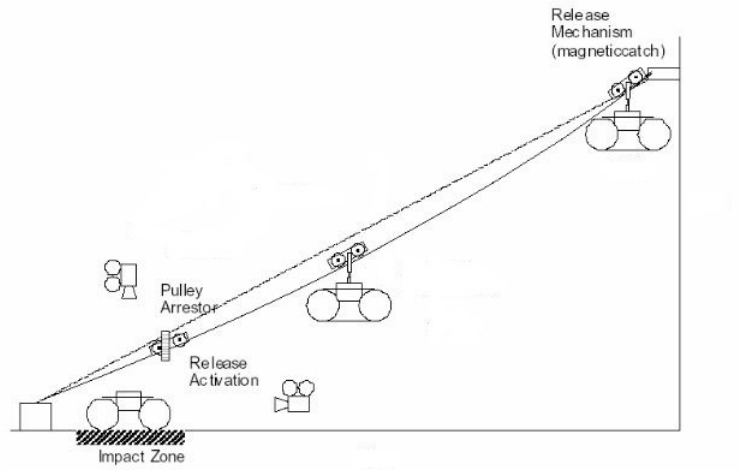

Figure 9.19: Example of an airbag drop test setup

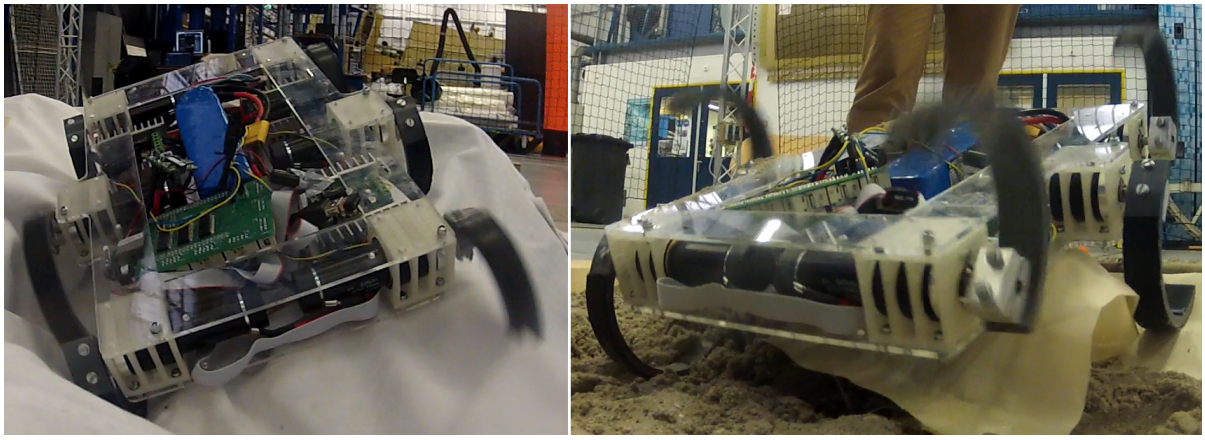

Figure 9.20: Zebro egress test, on the left walking on the polyester and on the right Vectran

9.5 Risk and sensitivity analysis

In this section the results of the touchdown system risk analysis and sensitivity analysis are given.

9.5.1 Risk analysis

In Table 9.8 the different identified risks with their possible measures are listed. In Table 9.7 an overview of the likelihood and severity of the different risks is given.

Table 9.7: This table shows the relative importance of all different risks for the touchdown system. Closer to the top right is more important. See Table 9.8 for the risk explanations.

Severity	Likelihood			
	Impossible	Improbable	Probable	Frequent
Catastrophic	11, 12	1, 2, 10	4	
Critical	6	5, 7, 8	3	
Marginal				
Negligible		9		

Risks in the top right quadrant of Table 9.7 will be examined more extensive. These risks are the the

Figure 9.21: An overview of the test setup

risk of too slow inflation and rocket engine exit flow hits airbag.

Too slow inflation time is a high risk event, because only four seconds are given for inflation and while the CGGs should require only three seconds they are a new technology and therefore it is an unproven system. Extensive testing should be done with the CGGs. Perhaps more smaller CGGs can be used, because the manufacturer suggested that with a lower capacity they would have a lower inflation time.

Rocket engine exihaust plume iteration is a high risk item, because it is not known exactly what the shape and temperature of the exit plume is. This must be researched as soon as possible and small adjustments to the design should be made if necessary.

Table 9.8: The risk analysis table shows all identified risks with 1 (high) to 4 (low) likelihood, severity and importance indicators.

ID	Risk	Effect	Likelihood	Severity	Importance	Action to minimize risk
1	Release failure	The touchdown system stuck, crash likely	3	1	2	Ensure high release system reliability
2	Release sensor failure	Airbag will not inflate, payload crashes	3	1	2	Use a fail-safe system, multiple sensors
3	Inflation too slow	Airbag pressure too low, dive-through likely	2	2	1	Use multiple smaller CGGs if needed
4	Rocket engine exit flow hits airbag	Airbag fabric decomposes at $T > 573$ K	2	1	1	Research flow shape and adjust design if needed
5	Vent sensor failure	Vents will not open, tip-over likely	3	2	2	Use a fail-safe system, multiple sensors
6	Pyrotechnic system failure	Vents will not open, tip-over likely	4	2	3	Use NASA standard equipment
7	Dive-through	Payload hits the surface with a too high velocity	3	2	2	Perform numerical simulations and full scale tests to optimize key design parameters
8	Tip-over	Payload hits the surface upside down, possibly hard	3	2	2	Perform numerical simulations and full scale tests to optimize key design parameters
9	Airbag puncturing	Venting area increased, dive through possible	3	4	4	Use a puncture proof tested outer layer
10	Shell elevator failure	Zebro's stuck inside shell	3	1	2	Test and design a redundant or more reliable system if required
11	Zebro activation failure	Zebro's not activated	4	1	3	Have multiple activation possibilities
12	Zebro departure failure	Zebro's stuck in touchdown system	4	1	3	Test zebros for entanglement and enable them to walk upside down

9.5.2 Sensitivity analysis

The touchdown system must as well be investigated for possible fluctuations and their impact. The one-by-one approach has been selected by varying each parameter one at a time, while keeping all the other set at their designed value. Only the impact and venting phase have been analyzed.

Impact

The sensitivity analysis is subdivided into two main categories, effect of mass changes and effect of size changes. Increasing masses do not have a high impact on the necessary pressure as seen in Fig. 9.22.

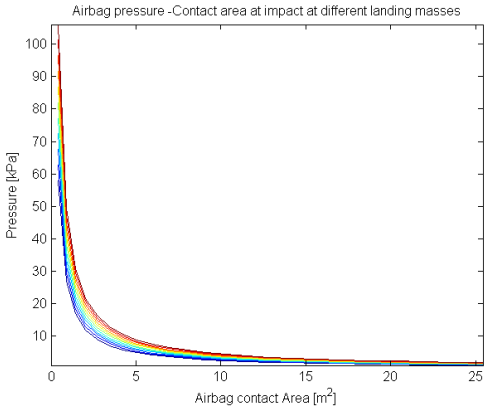

Figure 9.22: Airbag pressure in function of airbag contact area for masses from 200-400kg

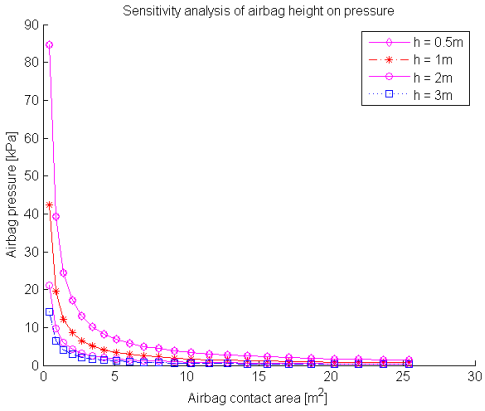

Figure 9.23: Pressure sensitivity for different airbag heights

Sensitivity on the airbag height on the airbag pressure has also been investigated. The results are illustrated in Fig. 9.23.

It appears that doubling the airbag height implies almost half of the pressure needed. This effect dies out eventually with increasing heights, but is rather sensitive for our range of airbag height.

Venting

The actual venting time was already determined in subsection 9.2.2. The inputs from the Wang-Nefske model were varied and it's results are summarized in Table 9.9.

Table 9.9: Sensitivity analysis on venting

Parameter	Effect on deflation time
Temperature increase	-
Pressure increase	-
Volume increase	+
Vent area decrease	++
Change in gas type	++

All parameters have minor changes on actual venting time of the airbag. Changing the venting area however seems to cause large differences in the deflation time as also already has been seen in Fig. 9.8. Changing the gas type has a large influence on the venting time as can been seen in Fig. 9.24. This is due to the extreme light molar mass of helium ($4\ g/mol$).

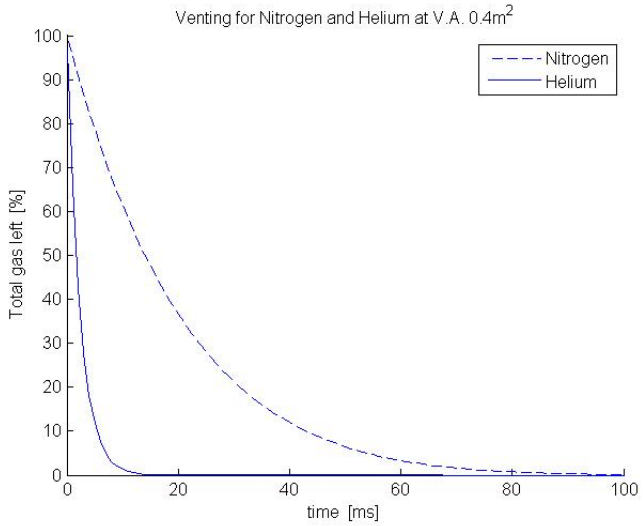

Figure 9.24: Comparison between helium and nitrogen venting at a venting area of 0.40 m^2

The actual venting of the airbag appears only to be highly sensitive for changes in vent area and gas type. This is however chosen in the design and will therefor not change during the mission.

9.6 Conclusions and Recommendations

In this section first conclusions are drawn about the touchdown system and then recommendations for continuation of this project are given.

9.6.1 Conclusions

The landing and deployment system plays a crucial role in the entire EDLD phase of the mission. It is the final step to a successful mission. After release from the CAESAR at 30 m altitude from the Martian surface, the 184 kg LADS will begin its 4 second free fall. The inflation of the octagonal shaped vented airbag will start after 1 second of free fall. The 5.13 cubic meter airbag will be inflated to a pressure of 11.7 kPa by means of 4 CGG tanks in the remaining 3 seconds. Directly after impact, the airbag will be entirely vented by means of eight 0.43 squared meter vents located on each section of the airbag. Vent control will be done using either a series of strain gages located on the bottom of the airbag or a radar/motion sensor on top of the airbag. This will prevent the airbag from tipping over in case of a unfavorable landing on rocks or a slope. Pyrotechnics will open the vents in a few milliseconds. The entire airbag will be made of Spectra 75, one of the toughest materials under cold Martian conditions.

9.6.2 Recommendations

The recommendations are made with continuation of this project in mind and will list steps necessary to finish the design.

Airbag material

For the airbag design different fabrics in different weaves with different coatings should be tested to determine their performance.

Rocket avoidance

Subsection 9.2.1 illustrated the verification of the rocket exhaust plume interaction. Fig. 9.6 shows that the airbag must not be inflated to it's full shape before 0.48 seconds of inflation. This can't be analytical

modeled as the airbag volume behaves non-linear during inflation. Therefore actual testing of inflation under Martian conditions must be done or using a FEM-analysis.

Touchdown failure

Possible failure modes of the airbag are tip-over, dive-through and puncture. Validation of the model for these failure modes should be done by means of real-life full-scale testing simulating the Martian surface with rocks and possible slopes. Tip-over can also be checked using a FEM-analysis like LS-DYNA.

Vent control sensor

As mentioned in subsection 9.3.3, still some research must be done over radar proximity radars and strain gages. As strain gages seem to be the best option, it must still be investigated whether the added complexity and weight of the wires and attachment to the airbag fabric does not exceed those of the radar system.

10 Power and command & data handling characteristics

An important factor within the whole spacecraft will be the power, command and data handling (PCADH) system. The other systems all require a reliable power source to function, even the structure subsystem needs power to deploy the Zebro's after touch-down. The data communication between the ADCS and propulsion group will be controlled by the data handling and processing unit. The data communications system will send the diagnostic data back to earth during descent, such that in case of mission failure, the causes can be investigated. This chapter will elaborate on the design choices that have been made in the midterm report, present the power and data connections within the system, and close off with an overview of the contents of these systems.

10.1 Electrical Power Subsystem

In the midterm report [26] various design choices were already made. These will be discussed below. If a more detailed elaboration is desired, the midterm report covers most of these topics in more detail.

In the entire system, three different batteries are required. One central battery during the parachute phase, one battery for each cluster during the rocket phase, and one battery for each cluster in the airbag compartments; this airbag compartment separates from the rocket during the landing phase, thus the need for a second battery. To protect the battery from failure on cell level, every cell is connected with a bypass diode so that, if a cell fails, only that cell is lost. Lastly, a redundant second battery will be available to each system to prevent the system from failing if the battery fails. The mass penalty is low since the mass of the batteries are low.

The battery in both the MACHETE and the CAESAR is a rechargeable $LiFePO_4$ battery because high power and relatively little energy is required. These batteries have a C-rate of C/35 and are environmental friendly and safe. They will be charged before entry by the accompanying transfer spacecraft to counteract the trickle discharge. For now, that spacecraft is assumed to use solar panels, but any energy source is of course accepted. In Fig. 10.1 and 10.2 an electrical block diagram is shown in which the connections between the subsystems and the EPS are displayed.

The battery in the LADS will be made of Lithium Thionyl Chloride ($LiSOCl_2$) because of its high specific energy which results in a very low mass. Both the airbag and deployment mechanism require significantly less power than the rocket phase system, which is why a high discharge rate is not an advantage anymore. $LiSOCl_2$ batteries are primary batteries which means they do not have to be charged. The connections between the battery and subsystems is shown in Fig. 10.3.

10.2 Command And Data Handling

The Command And Data Handling needs a CPU that does not fail in the radiation-high environment. Two methods exist for this: using radiation hardened CPU or ensure safety by redundancy. Radiation hardened hardware is very expensive and lacks computing power compared to 'normal' hardware. The second possibility employs a voting system between three CPU's to rule out bitflips. These normal CPU's are more powerful than radiation hardened CPU's and they cost less. That is why normal CPU's with a voting algorithm are chosen. Both Field Programmable Gate Arrays (FPGA's) and micro-controllers are viable options for a future team to decide on. Bitflips are more common in memory. Memory normally is either volatile, which means that if the power is lost for even a short time the entire memory is erased, or

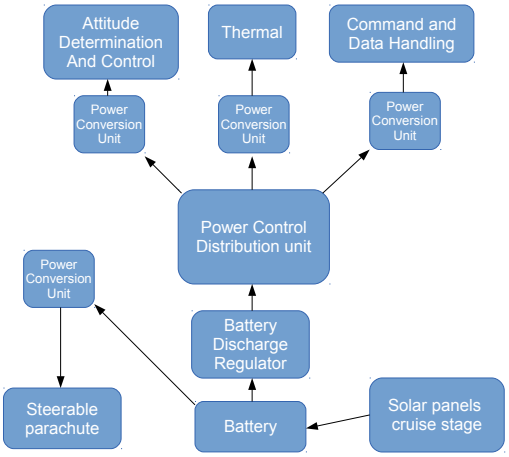

Figure 10.1: Electrical block diagram MACHETE

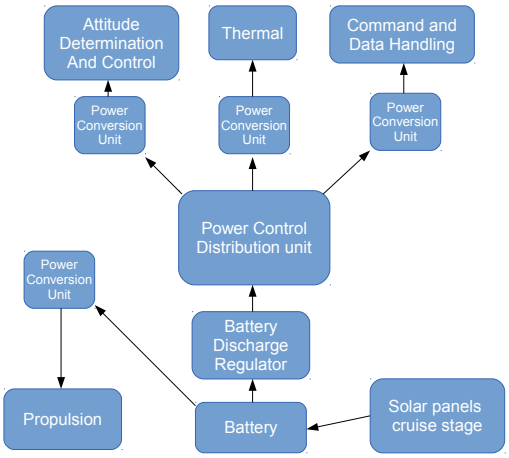

Figure 10.2: Electrical block diagram CAESAR

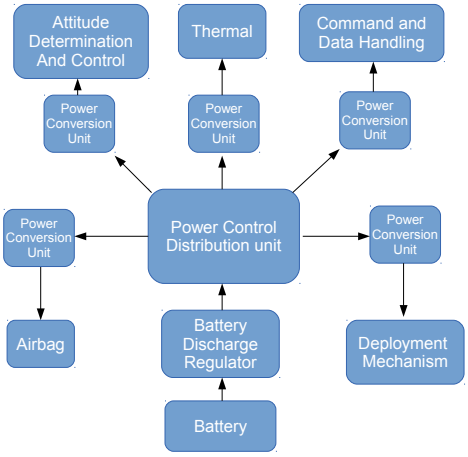

Figure 10.3: Electrical block diagram LADS

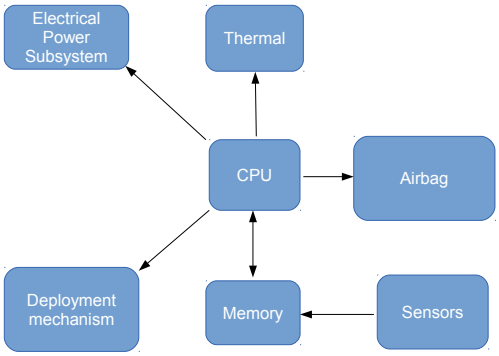

Figure 10.4: Data Handling block diagram LADS

requires a charge pump, which means that if the charge pump is struck by an ion the ability to write to or erase the memory. The most suited memory is F-RAM which is non-volatile but does not require a charge pump. The gathered data needs to be sent to Earth in order for the mission to have any functionality. This will be done with a direct connection via a low gain X-band antenna (which requires less accuracy than a high gain antenna) and with a relay via the Mars Reconnaissance Orbiter (MRO) or Mars Odyssey (MO) using an Ultra High Frequency (UHF) antenna. The data block diagrams for the LADS, CAESAR, and MACHETE are shown in Fig. 10.4, 10.5 and 10.6 respectively.

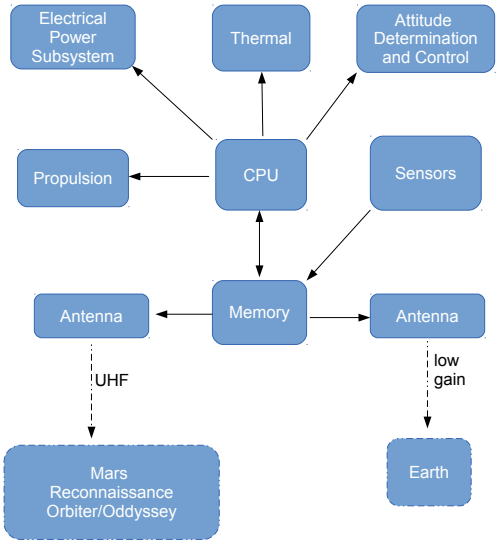

Figure 10.5: Data Handling block diagram CAE-SAR

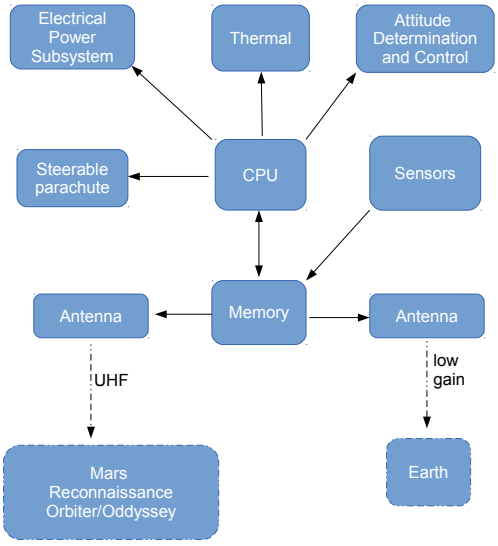

Figure 10.6: Data Handling block diagram MACHETE

10.3 Thermal control

These electronics need thermal protection from both high and low temperatures. Aerogel is chosen as isolation material between the electronics and the harsh Martian temperatures. It has a density that is close to air, but has high thermal insulation properties. Aerogel is still under development and has many different forms, which makes it difficult to give exact characteristics. As a reference, NASA has already released pictures of a slab of Aerogel of approximately 4 mm insulating a regular rose against the blue flame of a Bunsen burner. Naturally, high power electronics in a confined space tend to get warm. To counteract this Phase Change Material (PCM) is used to absorb the heat from the electronics. PCM works as a combination of sensible and latent heat. Below a certain temperature it absorbs heat and its temperature rises, but above this temperature it starts a phase change, absorbing heat without rising in temperature. This way the excess energy can be transferred from the electronics without the temperature inside the WEB rising to hazardous levels.

10.4 System overview

Now that all components of the system have been identified, a final overview can be presented. See Table 10.1 and 10.2 for an overview of the mass, power and energy budget for the entire combined system. For the relevant components also their operational time is stated. It should be noted that these numbers are rough estimations. Once a team starts physically selecting components these numbers will become more accurate. This table does not contain all parts requiring power, so adding the required energy of Table 10.1 will not equal the capacity of one of the batteries in Table 10.2.

Note that the final battery masses in the table have been obtained by dividing their capacity with their energy density, and then multiplying that value with a factor of two for the structure around the battery.

Of course, components like wires and converters will also have their place in the post-mission functionality. This is now not taken into consideration, but is easy for a future team to incorporate.

Table 10.1: Final mass and power budget for the PCADHTT

Component	Mass [kg]	Power [W]	Operational time [s]	Energy [Wh]
Aerogel	0	-	-	-
CPU	0.04	1.875	300	0.156
X-band Antenna	0.23	20	180	0.25
Phase change material	-	-	-	-
Power control and distribution unit	8.42	-	-	-
Power conversion unit	10.5	84.2	180	4.21
Ultra High Frequency Antenna	0.5	10	180	0.5
Wiring	5.8	16.84	500	2.34

Table 10.2: Final mass and power budget for the PCADHTT

Component	Power provided [W]	Operational time [s]	Capacity [Wh]	Mass [kg]
Battery CAESAR	425	180	21.25	0.35
Battery LADS	2	30	0.017	0.00011
Battery MACHETE	2000	120	66.7	1.11

10.5 Verification and validation

This section will discuss the verification and validation process of both the EPS and the CADH system.

10.5.1 Verification

For verification the following approach is used:

- Check the sources of the values and equations. Are they legitimate?
- Are the values and equations used in the right way, under the right circumstances?
- Are all requirements satisfied?

Verification EPS

Sources that are used for sizing of the EPS are mainly the highly respected SMAD, Spacecraft System Engineering and the website 'Battery University', which has a good reputation among scientists.

The equations used were specifically designed for use in space. The values were given by other departments, and were obtained specifically for this mission. This satisfies this criterion.

The requirements are satisfied. This is no surprise, since for the power subsystem it is only a matter of sizing the battery. This provided no problems.

Verification Command and Data Handling & Communication

The Command and Data Handling subsystem was designed with the help of the previously named sources, but also the Space Antenna Handbook and the world wide web, deploying a 'verification by numbers' method. This means all of the websites and papers that were found agreed with each other. The legitimacy of these sources is unknown, but a strong case can be made for them due to them all agreeing on the same numbers and formulas.

All of the equations used came from SMAD, which is designed for space missions.

The system logs everything the sensors measure, and relays that at a rate of 512 kbs^{-1}. The total dose of these electronics have been found to be about 10-15 krad. This satisfies this requirement by a factor of 100. Because of the triple-voting system the system will not fail due to bitflips.

10.5.2 Validation

For validation the following approach is used:

- Check if the obtained values are realistic.
- Do various tests to see if the actual outcome matches the theory.
- Does it perform as the customer intended?

Validation EPS

The mass of the batteries is somewhat small, but that is to be expected since not a lot of energy is required due to the relative small descent time.

Tests can easily be conducted by connecting the batteries to a similar load and checking the effects. The same goes for the CPU and memory. Lastly, the thermal control can be checked by creating the same confined space and coating it with aerogel. Then the electronics should be placed inside and covered with PCM. They should then be made to run for some minutes, closely monitoring any failure or complication.

To check if it performs as the customer intended, a test-model needs to be produced. From the resulting feedback, this criterion can be evaluated.

Validation Command and Data Handling & Communication

The obtained values follow directly from existing similar missions. Therefore the values are realistic.

Testing and customer satisfaction investigation would be performed with a similar approach as described in Subsect. 10.5.2.

10.6 Risk and sensitivity analysis

In this section the risk and sensitivity analysis will be performed. The risk analysis will show what the greatest identified risks for the subsystems are, while the sensitivity analysis will show in what way the output will change if the input is altered.

10.6.1 Risk analysis

In Table 10.3 the risk analysis of the power and command & data handling subsystem is displayed.

Table 10.3: This risk analysis table shows all identified risks valued from 1 (high) to 4 (low)

ID	Risk	Effect	Likelihood	Severity	Action to minimize risk
1	Battery cell failure	EPS will fail	4	1	Bypass diodes will be installed so that only the cell will fail
2	Battery failure	EPS will fail	4	1	A redundant battery will be installed for backup
3	CPU malfunction due to radiation (bitflips)	The entire lander will malfunction	2	2	A voting algorithm between multiple processors
4	Cable overheat	A fire could start in the system	4	1	The wires will be made extra thick, and will be supplied with high-voltage low-current electricity.

It can be concluded from this table that the risks involved for the PCADH are low and easily managed.

10.6.2 Sensitivity analysis

In this subsection the consequences of an increase of mass or power is discussed.

Mass increase When the mass of the spacecraft increases nothing changes for the power & command and data handling subsystem. One exception to this would be if it would be an increase in spacecraft dry mass, this would result in a proportional increase in the mass of the wiring, based on your preliminary estimation methods. Since this accounts for only 2.5% of the spacecraft dry mass, this sensitivity is clearly 'low'.

Power increase When the power demand doubles, the mass of the battery also doubles, and the power used by the system also doubles. Since the mass of the battery is insignificant compared to the entire spacecraft mass, this has a low sensitivity. The converters however do not handle this increase in power well, mainly because they have an estimated efficiency of only 80%. This means that when the spacecraft power doubles, 20% of that amount is lost due to conversion. So the power needs to increase even more to counter-act that, which again loses 20% due to conversion. Of course, with each iteration this difference becomes a factor 5 smaller. This sensitivity is 'medium'.

10.7 Conclusion

In this chapter a design has been made for the power, command and data handling, communication and thermal control system. First, the battery types have been chosen. After that, a fitting processor and memory were selected, together with an antenna to send out data. Finally, the right thermal solution is presented for ensuring safe temperature levels for the electronics.

The electronics have to endure two types of damage induced by ionizing radiation. First, the total dose effect. Which is determined to be insignificant. The dose sustained from one transfer to Mars is 66 $\pm$12 rad and electronics will start to fail at a dose of 10 krad. The second damage sustained are bit flips due to ionizing particles. The CPU-unit can sustain the bit flip errors by utilizing a very expensive radiation hardened processor. However, a cheaper, but likely reliable option exists by using processors in triple redundancy. A triple voting algorithm will be used to cancel errors. Both FPGA and micro-controllers are viable options for a future team to decide on. Minimizing the risk of memory failure will be achieved by applying F-RAM, a new technology which is less susceptible to ionizing particles because there is no charge pump present. F-RAM is also resistant to short power failures. For the communication during the descent it is not feasible to transmit directly to Earth. Pointing accuracy, bandwidth and line-of-sight problems prevent a feasible connection. A more feasible option is communication relayed through the Mars orbiter, using UHF, a data rate of 512 kbps is achieved. It should be noted that on top of this a direct connection will still be established using an X-band antenna, the mass-penalty for this is low.

For the battery design, multiple types of chemical compositions have been investigated. Two types of batteries are required, the first type is applied in the MACHETE and CAESAR's, the second is applied in the LADS. For the lander battery a $LiFePO_4$ battery is chosen due to its reliability, ability to discharge rapidly and lack of environmental impact. $LiFePO_4$ batteries are rechargeable, which means they need to be charged during the transfer stage. For the airbag system, a $LiSOCl_2$ battery has been selected. The LADS battery does not need a recharge option since the $LiSOCl_2$ battery has a small self-discharge. The $LiSOCl_2$ has a large specific energy which enables a lightweight design. $LiSOCl_2$ does not have a high discharge rate, but this is not required in the LADS. To protect the EPS against failure on battery cell-level, the battery will have built-in relays in the form of bypass diodes. This ensures functionality of the system even if one cell fails. A second redundant battery will also be present as backup. The batteries and electronics will be housed in a Warm Electronics Box (WEB) which is isolated using aerogel to ensure safe temperatures. To prevent the WEB from overheating the electronics will be covered with PCM to absorb all the excess heat.

I would recommend a future team to test these designs in practice, it should not cost a lot in terms of funds or labour to do so and it would give the most accurate results.

11 System layout

This chapter gives an summary of the system layout and its mass and power budgets. First, the subsystems will be defined and briefly described. Then the total system mass and power budgets will be given.

11.1 Subsystem definition

In this section MACHETE will be divided into subsystem based on their function. The subsystems identified are re-entry system,, electronics, propulsion, deployment, structures and Zebro containment, and the payload itself. A further breakdown and a more detailled description is given below.

Re-entry system This system primarily provides drag induced deceleration in the initial stage of atmospheric entry. It consists of the aeroshell that encloses the lander structure and a supersonic parachute.

- **Aeroshell** The aeroshell protects the other systems in the high speed deceleration phase. It contains a heatshield and a backshell, both aerodynamically shaped to provide a certain lift over drag ratio. With this lift over drag ratio the deceleration and heat generation can be controlled. This subsystem is not designed in the current project, but is still included in the system description as it poses significant constraints on the lander design in terms of mass and volume.
- **Parachute** A supersonic parachute is used in the secondary phase of deceleration. It should be noted that the parachute is attached to the aeroshell and the weight of that system must be taken into account when sizing the parachute.
- **Structure holding the CAESAR's** This structure holds the CAESAR's during all the trip to Mars. It is directly attached the aeroshell and won't be needed once the separation with CAESAR has been performed.

Electronics This system provides power to the other subsystems and contains the management systems required for this. Furthermore, the signal and data processing, storage, and communication is part of the electronics subsystem.

- **Energy management and storage** This system stores the energy required for the whole mission and provides the required power at the right voltage to other subsystems. The system controlling the temperature of the battery system is also part of this subsystem.
- **Sensors** This system contains all the sensors required for the ADCS, the parachute, and the vented airbag deployment system.
- **Signal and Data Processing** The sensor signals and data received via communication is processed by a central processing unit. This system has the control algorithms embedded and provides the autonomy required for the mission.
- **Data storage** The data storage contains the predetermined mission data and supports the data processing. The option to log data during the descent and store it for later communication to earth is still investigated.
- **Communication Hardware** Primary communication to earth is provided during the descent phase to indicate a possible cause when mission failure occurs. The same communication hardware could be used when a posed landing functionality is incorporated.

Propulsion system The propulsion system consists of the main thruster system as well as the actuators required for the attitude control.

- **Main thruster system** The main thruster system provides the ΔV required for the deceleration and navigation in the rocket powered descent phase. This subsystem also contains the propellant, tanks, fuel lines and valves, and propellant pressurizing system.
- **Attitude control actuators** The attitude control will have actuators either as gimballed main thrusters or as a separate system of smaller thruster.

Deployment system This system will make sure that the Zebro packages have a safe touchdown on the Martian surface. The vented airbag and supporting hardware are part of this subsystem.

- **Airbag** The vented air bag used will be inflated after the deployment from the rocket powered stage. On touchdown, the different sections of the airbag will deflate controllably to prevent tip over.
- **Gas generation** This system uses a cool gas generator to inflate and pressurize the airbag system right before touchdown.

Structures & Zero Containment The structure subsystem physically attaches all the subsystems and protects the Zebro's during the entire mission.

- **Main lander structure** The main landing structure rigidly connects the main thruster systems and contains the mechanism that deploys the airbag systems.
- **Deployed structure** This structure connects the airbag system to the Zebro containment packages.
- **Zebro containment** This system protects the Zebro's during the entire mission from launch till touchdown.

Payload The system has a payload of 224 Zebro's divided over 8 clusters. If different payloads are requested, for example a charge station, these systems can be taken at the expense of Zebro payload mass and volume.

11.2 Mass and power budget

In this section the mass and power budget from every department are gatered and presented in table 11.1. It has been stated in Chap. 5 that the total allowable mass of MACHETE including the aeroshell must not exceed 3300 kg. It can be seen that the current design is much lighter. Therefore it might be conceivable to have a heavier payload.

Table 11.1: System mass and power budget

Element	Mass [kg]	Power[W]
Re-entry vehicle	839.5	
Heatshield	385	
Backshell	349	
Parachute	86.5	
Structure holding CAESAR's	21.7	
Electronics	317.5	948
Batteries	3	
Power control unit	68	
Regulators & converters	84	672
Wiring	46	136
UHF Antenna	4	80
Sensor pack	88	88
CPU	0.5	16
Lidar	24	32
IMU		12
Propulsion system	786.5	2408
Main Thrusters	280	
Tanks	37	
Lines & Valves	58.5	
Propellant	400	
Attitude thrusters	11	168
Flow regulation		2240
Deployment	113	8
Airbag fabric & coating	61	
Gas & storage	32	
Vents & pipework	20	8
Structure	149.5	1
Zebro containment	22.5	
Main lander structure	52.5	
Deployed structure	65.5	
Release structure	3	1
Clamps	5	
Payload	846	
8x28 Zebro's	846	
Total	3052	3365

Part III: Post design operations

In the post design operations part of the report an analysis the compliance and risks of the design will be evaluated. In addition a future project plan is presented. Finally a conclusion will be given, and several recommendations are given.

Compliance is analysed using a compliance matrix. Each of the initial given requirements is treated and the compliance of the design to this requirement is scored. From all these results a compliance matrix is constructed which provides a complete overview of the performance of the design.

In order to characterize the design beyond compliance to the requirements, a risk analysis is presented. This risk analyses should provide valuable information on the quality of the current design, as well as providing a solid guideline for future design work. This aspect is expanded upon in the future project chapter in which a broad range of aspects related to future detail design, spacecraft construction and handling are touched upon. This chapter also includes a rough cost estimate.

12 Compliance matrix

In this chapter, the compliance matrix will be presented. All the requirements proposed in the mid-term report have been evaluated whether the requirement is met. When the requirement is met with a specific quantity, it is shown in the "Achieved value" column. Comments are given when applicable. When a requirement is not met, it might have been outdated or beyond the scope of this project and subject for further research.

Table 12.1: Compliance of the requirements established in the mid-term report.

Number	Requirement	Achieved value	Compliant	Comments
	Structural design & payload protection			
1.	The system should withstand loads associated with handling.		Yes	
2.	The system should withstand loads in the range of -1 g_E to -5 g_E associated with the launch.	10% safety margin	Yes	
3.	The system should withstand loads in the range of 2 g_E to 15 g_E associated with re-entry.	10% safety margin	Yes	
4.	The system should withstand loads in the range of 0.378 g_E to 11 g_E associated with touchdown.		Yes	Re-entry is driving
5.	The system should withstand temperatures in the range of 184 K to 242 K.		Yes	Aluminium
6.	The system should withstand radiations occurring in space travel and on Mars.		Yes	
7.	The Zebro's should be able to leave the system after deployment.		Yes	Experimental result

Table 12.2: Compliance of the requirements established in the mid-term report.

Number	Requirement	Achieved value	Compliant	Comments
	Flight and propulsion			
1.	The parachute system should decelerate a ΔV of 260 ms^{-1}.	260 ms^{-1}	Yes	Parachute design
2.	The rocket system should decelerate a ΔV of 100 ms^{-1}.	120 ms^{-1}	Yes	
3.	The system should provide a ΔV of 50 ms^{-1} for disposing or landing of the rocket stage.	92.68 - 339.51 ms^{-1}	Yes	A ΔV of 92.68 ms^{-1} for worst case scenario.
4.	The parachute system should have a navigational range of 1000 m.	2026 - 2929 m	Yes	
5.	The rocket system should have a navigational range of 3500 m.	3500 m	Yes	
6.	The system should be able to hover for 30 s during a deployment sequence once the destination is reached.		Yes	
	Touchdown system			
1.	During the first strike on a flat surface, the airbag shall touch the ground with at least 30% of it's total contact area.		Unknown	Experimental tests required
2.	The airbag system must be able to account for the impact imposed on the payload without exceeding the maximum allowable gravitational deceleration of 30 g_M or 11.4 g_E.	30 g_M	Yes	
3.	The airbag must be designed in such a way that it will not tip-over or dive-through at impact.		Unknown	Detailed FEM analysis required
4.	The lander structure and airbag must be designed in such a way that all Zebro's can be deployed on the Martian surface without problems.		Yes	Experimental result
5.	Maximum inclination of the lander+structure must not be more than 10 degrees at impact [60].		Yes	ADCS threshold
6.	Maximum horizontal velocity must less than 16 ms^{-1} [60].		Yes	ADCS threshold
7.	The airbag must be capable to protect the payload at impact for rocks up to 0.5 m [60].		Yes	Bumpers installed as backup system
8.	The airbag must be capable of housing the lander structure as specified in the midterm report [26].		Yes	Design

Table 12.3: Compliance of the requirements established in the mid-term report.

Number	Requirement	Achieved value	Compliant	Comments
	ADCS & navigation			
1.	The ADCS shall be operational in the Martian environment.		Yes	
2.	The ADCS shall provide attitude control of the entry vehicle, with respect to the yaw, pitch, and roll.		Yes	
3.	The ADCS shall be operational in the Martian environment.		Yes	
4.	The ADCS should be able to determine its velocity in the range of 10 ms^{-1} and 16 ms^{-1}		Yes	
5.	The ADCS shall determine the roll of the lander, not exceeding more that 10 deg from the horizontal.		Yes	
6.	The ADCS shall determine the pitch of the lander, not exceeding more that 10 deg deviation from the vertical.		Yes	
7.	The ADCS shall orient the lander with the beacon once the lander and entry vehicle are no longer in contact.		Not required	Omnidirectionality
8.	The ADCS shall control the yaw of the lander to keep in constant contact with the beacon.		Not required	Omnidirectionality
9.	The ADCS shall control the altitude so is does not fall below below 28 m.	20	Yes	Requirement updated
10.	The navigation system should be able to detect obstacles larger than 0.5 m in height while determining the landing spot.		Yes	LIDAR
11.	The navigation system should be able to detect slopes exceeding 10 deg while determining the landing spot.		No	Further development required
12.	The navigation system should be able to avoid obstacles larger than 0.5 m in height while determining the landing spot.		No	Further development required
13.	The navigation system should be able to avoid slopes exceeding 10 deg while determining the landing spot.		No	Further development required
14.	The navigation system should be able to autonomously detect the most optimal landing spot at the beacon.		Yes	
15.	The navigation system should be able to intercept the beacon signal.		Yes	
16.	The navigation system should be able to calculate the optimal glide slope to the beacon.		Yes	
17.	The navigation system should be able to determine the distance to beacon.		Yes	
18.	The navigation system should be able to operate under Martian conditions.		Yes	
19.	The navigation system should be able to calculate alternative landing scenarios.		No	Further development required
20.	The navigation system should be able to navigate with loss of beacon signal.		Yes	
21.	The navigation system will function under the constraints imposed by the ADCS.		No	Further development required
22.	The navigation system will make sure not collision with in air obstacles will happen.		Yes	

Table 12.4: Compliance of the requirements established in the mid-term report.

Number	Requirement	Achieved value	Compliant	Comments
	Command & data handling			
1.	The system should log altitude, velocity, attitude, and position data during descent for 150 s.	180 s	Yes	
2.	The CPU-system should work in real-time.		Yes	
3.	The CPU-system should generate commands for the propulsion actuators.		Yes	
4.	The CPU-system should keep track of the mission progress and activate critical deployment cues.		Yes	When goal is reached within threshold.
5.	The data storage modules should have a capacity of at least 64 Mb.	128 Mb	Yes	Higher capacity F-RAM in development.
6.	The data storage modules should retain data for at least 100 seconds during a power outage.		Yes	Data retention in order of years.
7.	The communication-system should send data at a rate of 512 Kbs^{-1}.	512 Kbs^{-1}	Yes	Relay through MRO
8.	The communication-system should send data at a frequency of 390-405 MHz.		Yes	
9.	The descent antenna should send data in the direction of 30 to 100 deg from the z-axis.		Yes	Dipole antenna
10.	The system should endure a total radiation dose of 117 rad.	10.000 rad	Yes	
11.	The system should not fail due to bit-flips during the mission.	Negligible	Yes	Triple redundancy & error detection and correction
	Power system			
1.	The system should provide power in the range of 150 to 200 W to the spacecraft in the case of one rocket.		No	Old scenario
2.	The system should provide power in the range of 450 to 480 W to the spacecraft in the case of clustered rockets.	2000 W	Yes	Upscaling causes no problems
3.	The system should have a protection built in against cell-failure.		Yes	Bypass diodes
4.	The system should store 21.6 Wh of energy for the spacecraft in the case of one rocket.		No	Old scenario
5.	The system should store 64.2 Wh of energy for the spacecraft in the case of clustered rockets.		Yes	Upscaling causes no problems

13 Risk management

13.1 Technical risk assessment

During the technical risk assessment, every step of the mission was evaluated to understand its impact on the mission and its probability to fail. The consequences of these failures as well as the actions to minimize the risk are presented in this risk map. Furthermore the responsibilities for preventing these risks have been distributed. The severity, likelihood and importance of every risk are rated using a scale of 1 to 4 in which 1 indicates the points where the most attention are needed and 4 are the points that can be ignored. In Table 13.1 the relative importance of all risks can be found.

Table 13.1: This table shows the relative importance of all different risks for the separated lander clusters case. Closer to the top right is more important. See Tables 13.2 and 13.3 for the risk explanations.

Severity	Likelihood			
	Impossible	Improbable	Probable	Frequent
Catastrophic		5, 6, 12,20		
Critical	3	10,13,19,22	1, 4, 8, 11	15
Marginal		9,16,17,18,21	7	2, 14
Negligible				

13.2 Reliability Availability Maintainability and Safety

This section will give a RAMS analysis of the system, which will mean that the system will be evaluated on its **R**eliability, **A**vailability, **M**aintainability, and **S**afety. The goal of a RAMS analysis is to make the coherency of the four elements of the RAMS clear for the system in design. It will also support in the decision process of choosing the final system. The RAMS analysis will be done for both the single cluster as well for the multiple cluster design.

13.2.1 RAMS analysis for a clustered lander system

In this section the RAMS for a clustered lander system is given, which is a system existing out of eight separate landers each responsible for delivering its package of Zebro's.

Reliability

As far reliability goes for the MACHETE mission it is mostly depend on the circumstances of the Martian conditions. Most of the techniques and materials used in the development of the system are off-the-shelf and are proven to work. The single cluster system could fail due to unfavourable Martian weather and terrain condition that where not anticipated for in the EDL.When for example the wind conditions are bad the system could have trouble to navigate to the beacon and thus reach the preferable landing ground.

The terrain also causes a unreliability in the deployment process. When the terrain is too rough the autonomous system may determine it is not safe to deploy close to the beacon, forcing the system to look for alternative landing spots which on its turn causes extra fuel consumption which ultimately may badly influence the mission profile of the lander. For the deployment it self the big advantage in reliability of a clustered system is that if one cluster fails only 12.5% of the swarm is lost. It is still a very considerable amount however there would be seven of the eight clusters ready to deploy. It can be stated that when no more then two clusters fail the mission can be called a success. The MACHETE is designed for a very short

life span: 7 minutes. So the failure distribution or the amount of time before failure is occurring, can be assumed to be low.

Availability

The system will be up and running continuously as long the battery power of the Zebros is sufficient or if recharging of the Zebros is possible. Availability in this context means the swarm of Zebros is ready for use. When the swarm stops communicating one could say the mission is over and the Zebros are not available any more.

In perspective of the launch one should take in account the availability of a launch vehicle, a suitable launch location, and personnel with expertise .

Maintainability

Since the mission takes place at the Martian surface maintainability of the system is impossible, unless in further stadia of the mission design a self repair function is incorporated by making use of for example 3D-printing . The system will fully depend on how it is engineered back on earth. Once the Zebros are loaded into the launch vehicle nothing can be done to repair them. The only maintenance that still can be done is reprogram/update the Zebros firmware once they are landed on the Martian surface.

Safety

Since this mission is supposed to be a precursor of a manned mission to Mars, one should think about the safety of the first men on Mars. No hazardous situation should be created when the lander vehicle dropped its cluster and is navigated down to land. The fuel tanks for example should be empty to reduce the risk of explosion. Also no lose parts caused by a possible crash landing should injure the astronauts. As far safety on the ground the most dangerous part will be the launch from earth, the normal regulations should apply there to minimize the risk of casualties.

Table 13.2: The risk analysis table shows all identified risks with 1 (high) to 4 (low) likelihood, severity and importance indicators.

ID	Risk	Effect	Likelihood Clustered	Severity Clustered	Importance Clustered	Action to minimize risk	Owner
1	System non-healthy	The system appears to have not survived the trip to Mars	2	2	1	Clear documentation	Mars transfer design team
2	Non-suitable atmospheric conditions	The spacecraft must delay the entry or find another place to land	1	3	2	Not relevant	Mars transfer design team
3	More heat generation during entry	The payload takes heat damages/ burns in the atmosphere	4	2	4	Not relevant	Mars transfer design team
4	Higher entry loads	The payload takes structural damages	3	2	2	Design the payload using safety factor	Nathan van Schoote, Marc Reijen
5	Failure of high speed deceleration system	Payload crashes on Mars	3	1	2	Use proven technology	Christ Akkermans, Ruben Grandia
6	Failure of low speed deceleration system	Payload crashes on Mars	3	1	2	Use proven technology	Christ Akkermans, Ruben Grandia
7	Failure of measurement system	The lander can not get flight informations	2	3	3	Use redundant instruments	George Galatis, Sjoerd Butter
8	Failure of separation system	Remain a single stage unit	2	2	2	Provide single lander deployment	Bastiaan Lagaune, Robert Crone
9	Unable to identify hazards at landing target	The lander must choose a landing place with insufficient data	3	3	4	Use proven technology	George Galatis, Sjoerd Butter
10	Unable to set up landing target	The lander must land blind	3	2	4	Use redundancy	George Galatis, Sjoerd Butter
11	Unable to communicate with other landers	The lander cannot control its distance to other landers	2	2	2	Use redundant systems	Bart Walgaard, Frerik Andriessen
12	Failure in attitude control system sensors	The lander becomes uncontrollable and unnavigable	3	1	1	Use redundancy and proven technology	George Galatis, Sjoerd Butter
13	Landing system fuel shortage	The lander performs a vertical uncontrolled landing in free fall	3	2	3	Provide excess fuel	Christ Akkermans, Ruben Grandia
14	Broken Zebro(s)	Zebro(s) cannot deploy	1	3	2	Design such that functional Zebros still can deploy	Bastiaan Lagaune, Robert Crone

Table 13.3: The risk analysis table shows all identified risks with 1 (high) to 4 (low) likelihood, severity and importance indicators.

ID	Risk	Effect	Likelihood Clustered	Severity Clustered	Importance Clustered	Action to minimize risk	Owner
15	Zebros outside communication range	Zebros cannot be controlled	1	2	1	Give initial commands	Bastiaan Lagaune, Robert Crone
16	Solar flare	Electronic system might burn out	3	3	4	Provide protection against solar flares	Bart Walgaard, Frerik Andriessen
17	Failure in attitude control system software	The lander becomes uncontrollable	4	1	2	Excessive testing of software in a lab	George Galatis, Sjoerd Butter
18	Failure in attitude control system actuators	The lander becomes uncontrollable	3	1	2	Use redundancy and proven technology	George Galatis, Sjoerd Butter
19	Failure in air bag deployment	The lander will crash	2	1	2	Use proven air bag technology	Bastiaan Lagaune, Robert Crone
20	Insufficient power	The system will stop working properly	4	2	2	Excessive testing of power supply to system in a lab	Bart Walgaard, Frerik Andriessen
21	Communication link failure	The system is unable to transmit data back to earth	3	1	1	Use extra (alternative) data transmitting systems	Bart Walgaard, Frerik Andriessen
22	Error in EDL and orbit entry calculations	The wrong orbit and/or EDL calculations where used for successfully deployment.	4	2	3	Double checking the calculations	Mars transfer design team

13.3 Market analysis

In the proceeding section a market analysis will be done that will investigate the potential use of the system for future scientific or commercial uses. It will present a trend line of similar system requirements as also the comparison between the existing systems and the use of swarm systems.

The market analysis is subdivided into the following aspects:

- Market size: A measure of the market potential of this system, based on supply and demand.
- Market trends: These trends are used as a tool to predict the market in the future.
- Market growth rate: Is a parameter of the market analysis that is used to estimate the demand trend.
- Market opportunity: will such a system will cover needs that are not covered yet?

In the following sections each aspect of the market analysis will be done in regard to the CAESAR.

Market size

Due to the irregularity of this system, segmentation of the market is extremely difficult to measure.

Market trends

The trends of the market are hand in hand with the trends of future concepts of space exploration. The trends in space exploration tend to systems that are versatile, cheap and can be used as a base for other systems to be built on. These future systems need to support and aid human space exploration, concepts such as the Zebro. Current missions are systems that are isolated from such an interaction, for example.

This group predicts that the trends of the market guides toward an increase of demand for systems that will be capable of deploying swarms of robots.

Market growth rate

The growth rate of the market is dependent on the need for development of systems with on-board autonomy capability, as reported by Dr. Richard J. Doyle [21]. These systems must be cheap, versatile and capable to cover a range of mission profiles. The market for such systems will grow in the proceeding years [13].

Market opportunity

The above mentioned system is an operating system that will be capable of autonomously dispersing a system of swarming robots. This will provide the capability to explore regions of our solar system that were previously unattainable, but a better cost efficiency will be needed. With some modifications, this system may be capable of supporting future NASA swarm missions [68] [71]:

Asteroid Missions The aim of these missions would be to explore the asteroid belt, by dispersing the swarm on several asteroids of interest and collecting specific data.

Saturn Ring Exploration The aim of these missions would be to explore Saturn's rings, by dispersing the swarm on several of Saturn's rings so as to understand their make up and how they are formed.

Lunar Applications With the use of miniaturized robotics the moon can be used as a platform for low frequency radio telescopes with the dispersion of several elements each weighing approximately 5 kg.[71]

13.3.1 Conclusion

Deep space exploration is having a turn over in its approach for exploration. Systems for exploration are needed to function autonomously while providing a multi-mission profile. Systems need to be cost efficient, this is why swarm exploration is the future of deep space exploration. These type of systems wide array of possible applications and are expected to be heavily invested in for development.

14 Future project

In this chapter the continuation of the MACHETE project is discussed. The current state as of delivering this report is that a detailed concept is available, the next step would be exact dimensioning of every part. Next steps in this process will require more resources as experiments have to be done.

This chapter starts with presenting the work breakdown structure and work flow diagram for a future project followed by a Gantt chart where very rough estimations of the time each phase will take are made. Then an equally rough cost estimation is made based on reference projects.

14.1 Work breakdown structure

The work breakdown structure is the collection of tasks that need completed in order to finish the project, it can be found in Fig. 14.1. It is divided into five phases of which each phase has separate tasks and at least one deliverable. The five phases are: finish detailed design, manufacturing and mission project startup, production and assembly, mission preparation and mission execution.

Finish detailed design

This phase is about finishing the design of the MACHETE, getting it ready for production. The technical chapters each have listed recommendations as guidelines on how to continue. When these are followed and every dimension, lay-up and fastener has been selected a detailed design report with all this information will be the result. From here production can start.

Manufacturing and mission startup

Now that the detailed design is finished production preparation can start. For every part a manufacturer or supplier needs to be selected and workspace for assembling and every required validation test is required. When this is done a detailed production plan can be made.

During this phase also logistical preparations for executing the mission can start. Possible mission dates and launch sites will have to be found, the astrodynamics research in this report should be a good starting point, see Sect. 5.5, and a launcher must be selected. Finishing all of this a launch plan can be made.

Production, assembly and testing

When thinking about manufacturing one should not only think about what production techniques and methods will be used, but also about the location(s) and manufacturing stations where the manufacturing process will take place. What is the most cost efficient and safe way of manufacturing the different pieces and subsystems of the complete system?

In the process of manufacturing for space systems a more secure and delicate process will be required than when manufacturing for, for example the automotive industry. While the main goal of the design of the MACHETE mission was to use off-the-shelf products which implies the largest part of all electronics will be already manufactured. One could invite tenders for the manufacturing of the aeroshell and the supporting structures of the lander and than select the best offer. For the production of the rocket engine it is important the right test facilities are present to develop, test and finally qualify the engine for use.

If and when different parts and structures are produced at different locations assembly at one central location will be needed. This for example can be done at the integrations facility of ESA. At this location the different parts can be tested before assembly, and the final assembly can be tested too. To get the different parts and structures to the integrations facility one should think about transporting logistics. Each and every part of the final system should be able to be transported with conventional transportation techniques to prevent trouble transporting the system to and from the integrations facility.

Mission preparation

This phase includes all logistical tasks that need to be completed to be able to launch the MACHETE and is finished when everything from launch day planning to mission control staffing is complete.

Mission execution

Finally the mission can be executed. It should be very interesting to see what information the Zebro swarm is able to find about the Martian environment.

14.2 Work flow diagram

The work flow diagram shows the order in which tasks can be completed for the future project, it can be seen in Fig. 14.2. It should be noted that due to this tasks division being very high level it is very often possible to start with part of a tasks while the previous task is not completely finished. For example, subsystem assembly can be done partly while still validating parts. Therefore this is more to be used as a guideline for the future project, when arriving at a next stage it is always necessary to take a closer look at the next steps and search for opportunities to do tasks parallel.

14.3 Gantt chart

This Gantt chart gives a very general overview of the timeframe in which the future project can be completed, see Fig. 14.3. The mission is planned backwards from the first possible date where conditions on Mars are good for launch as described in Table 5.2 to be April 2018. To increase the chance of project succes slack is planned at the end equal to 33% of estimated project duration. This percentage is chosen because there is a lot of uncertainty about project duration at this point.

This is done by estimating the time required for each phase using typical timings given in SMAD[42], for the time range a low end duration is chosen. While this is a large mission, the technology used is mostly proven to work so time estimates can be on the low side. Also the payload and Mars transfer are not designed and manufactured within this mission, which saves a lot of work compared to a full space mission. It is possible that design and preparation of the Zebros takes longer than finishing this mission.

It is estimated that to finish the design part of the mission 9 months of testing, designing and manufacturing planning is required. This is due to the expectation that the setup and processing of all test data, optimizing all dimensions and creating detailed product drawings is a time consuming process. Also, since mass and reliability are especially important in space missions it is worthwhile to spend time optimizing the design.

Part procurement, assembly and testing is estimated to take another 9 months. This is a relatively short amount of time compared to figures given in SMAD, but it is expected to be possible due to the payload being completely separate. It is recommended to take special care of the electronic equipment, because part procurement and testing of electronic parts is likely to take longer than mechanical parts[42].

Finally after being launched the MACHETE will be in transfer to Mars for about 8 months after which it will perform its function of safely landing Zebros to be deployed on the Martian surface. Having completed its mission it will continue to fulfill its post landing function for as long as possible.

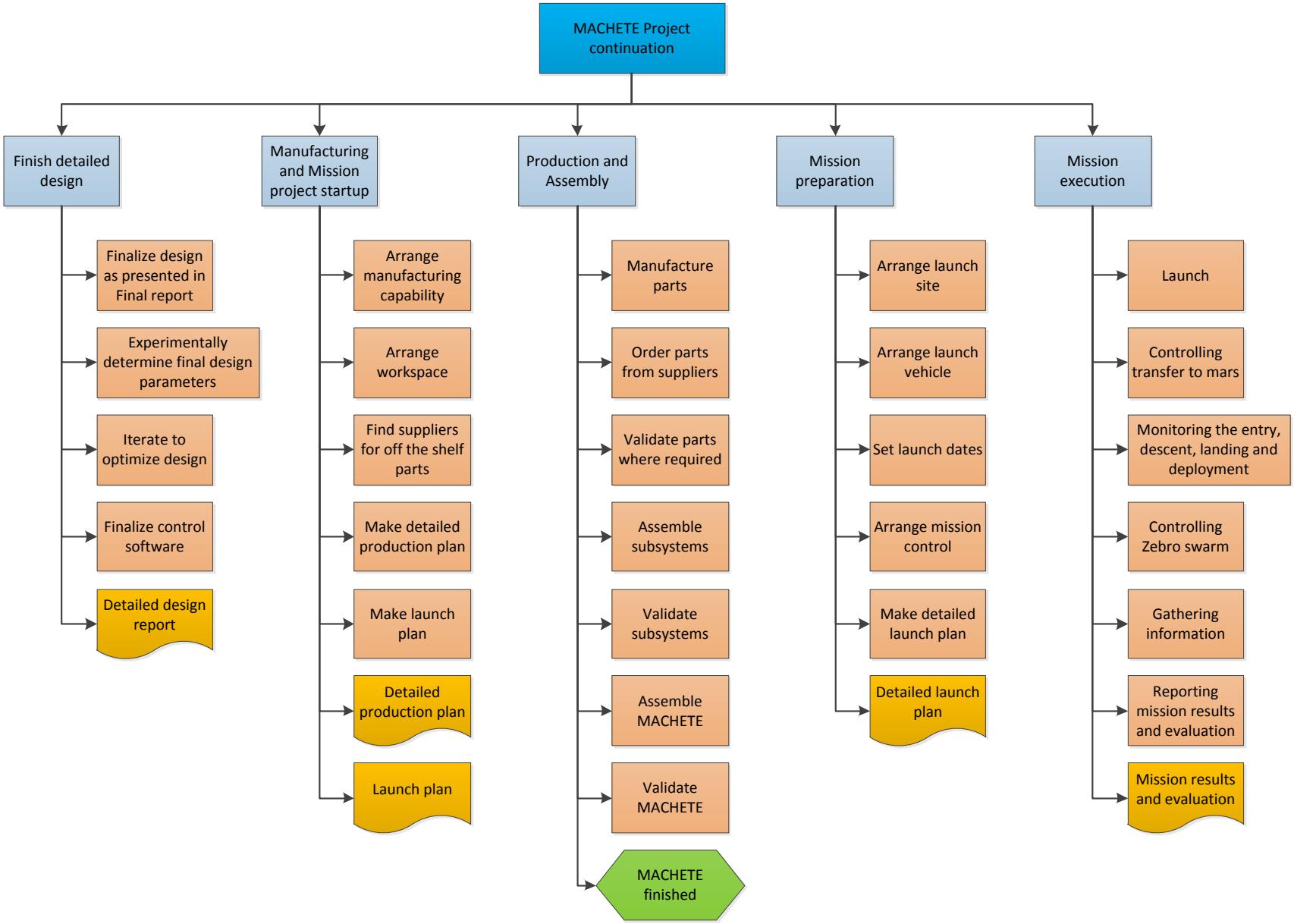

Figure 14.1: Future project work breakdown structure

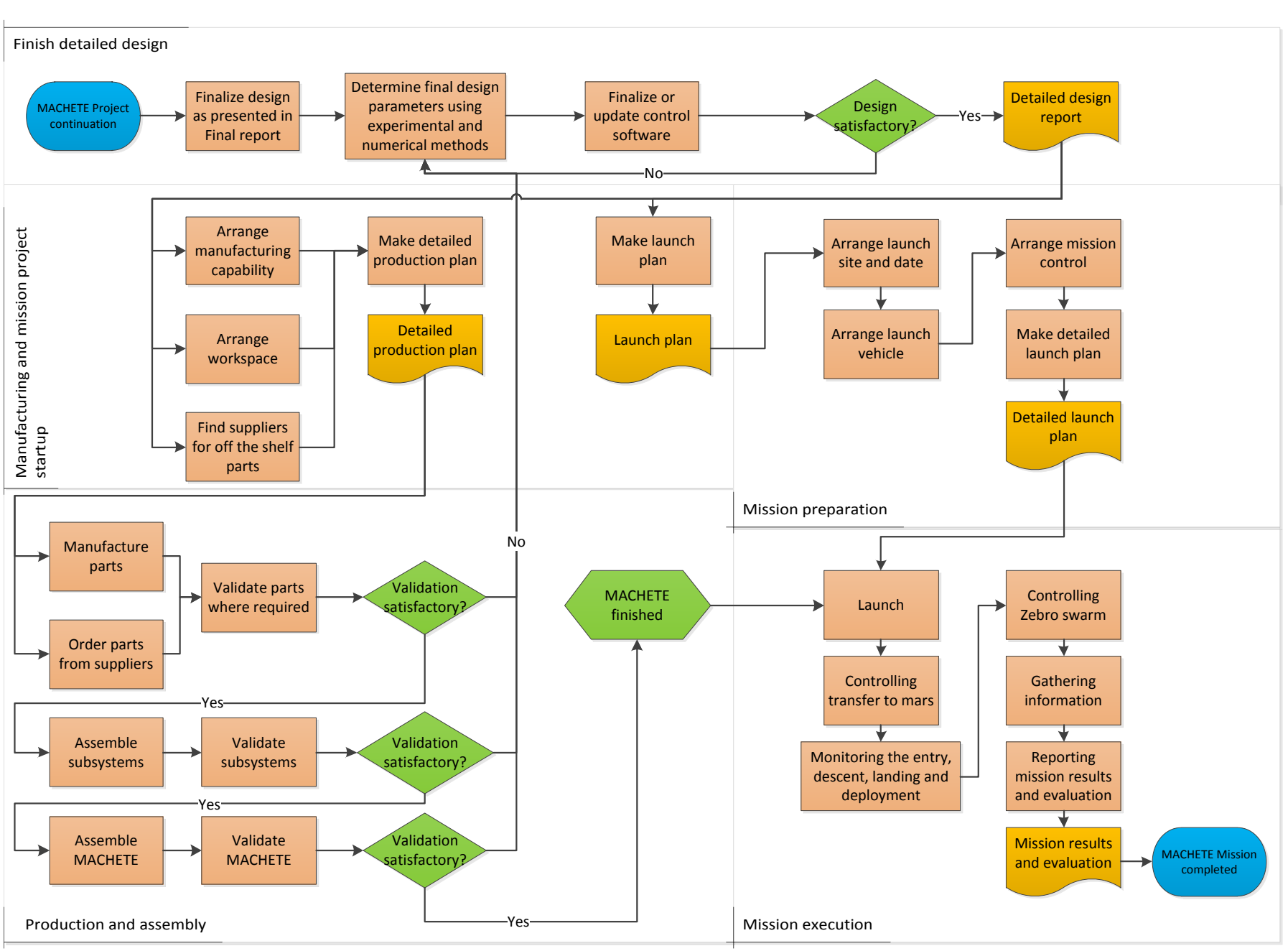

Figure 14.2: Future project work flow diagram

ID	Task Mode	Task Name	Duration	Start	Finish
1		**MACHETE project**	**640 days**	**Mon 30-5-16**	**Fri 9-11-18**
2		Finish detailed design	6 mons	Mon 30-5-16	Mon 14-11-16
3		Manufacturing and mission project startup	3 mons	Mon 14-11-16	Mon 6-2-17
4		Production and assembly	9 mons	Mon 6-2-17	Mon 16-10-17
5		Mission preparation	2 mons	Mon 21-8-17	Mon 16-10-17
6		Slack	6 mons	Mon 16-10-17	Mon 2-4-18
7		Launch	0 days	Mon 2-4-18	Mon 2-4-18
8		Mission execution	8 mons	Mon 2-4-18	Fri 9-11-18
9		Landing	0 days	Fri 9-11-18	Fri 9-11-18

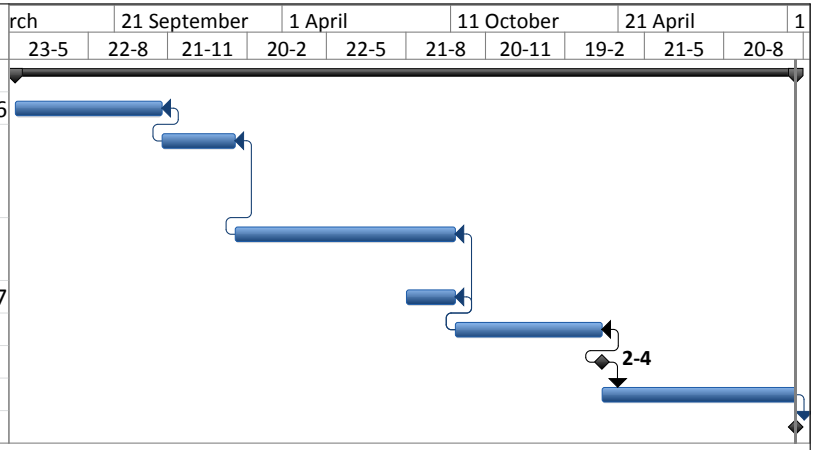

Project: Future project Gantt char
Date: Thu 23-1-14

Task		External Milestone		Manual Summary Rollup	
Split		Inactive Task		Manual Summary	
Milestone		Inactive Milestone		Start-only	
Summary		Inactive Summary		Finish-only	
Project Summary		Manual Task		Deadline	
External Tasks		Duration-only		Progress	

Page 1

Figure 14.3: Future project Gantt chart

14.4 Space logistics

This section will discuss the logistics of the project, another term would be space logistics which is defined by the AIAA as "The theory and practice of driving space system design for operability and managing the flow of material, services, and information needed throughout the system life-cycle" [8]. In a broader sense one could start thinking of acquisition, storage of materials and sub-assemblies, transport of materials and sub-assemblies, maintenance of production locations, personnel, and handling of space debris the mission may create. A brief explanation for the above mentioned aspects of the projects logistics will be given below.

14.4.1 Acquisition

In this context this mainly means acquiring the needed resources to successfully finance the project. For example: by collaborating with bigger companies to make use of their facilities, or get financing from them, or by acquiring government or private funding.

14.4.2 Storage of materials and sub-assemblies

In order to assemble the total system, sub-assemblies and materials needed for the total system will need storage while other parts of the system are still in production. Since most parts of a space system are very delicate special storing will be needed (e.g clean room storage, or special temperature regulated storage). The production plan should be set up such that the risk of damage due to storage is minimized.

14.4.3 Transport of materials and sub-assemblies

To effectively produce the parts of a system it is convenient to distribute production over several production plants. This distribution of production has as consequence that some of the materials and sub-assemblies have to be transported to the main assembly location. One should then take in account the size of the materials and sub-assemblies, but also their vulnerability for transporting. A convenient production plan should be made to reduce risk of transport damage to the materials and sub-assemblies.

14.4.4 Maintenance of production locations

The maintenance of the production locations is mainly an aspect of safety. By having all tools and devices checked on a regular basis the chance of failure is reduced, increasing the overall safety of the mission. Another aspect could be having an up-to-date alarm system to prevent valuable technologies to be stolen.

14.4.5 Personnel

To successfully perform a complex mission as going to Mars, specialists on many mission aspects (e.g structural mechanics, astrodynamics, programming etc.) will be needed. After the launch a specialized team will perform the task of mission ground control, monitoring the system's performance during the EDL and travel to Mars. At any time the safety of personnel must be guaranteed, this can be done by giving every person on the team an evacuation training, and have a strict safety regulation program.

14.4.6 Launch

Prior to launch the payload must be checked on any defects and then be loaded in to the protective structure of the launch vehicle. The spacecraft fuel tanks need to be filled at some point as well. Depending on the type of propulsion system, this may need to be done shortly before launch.

14.4.7 Handling of space debris/launch debris

With the launch of the system normal/space debris will exist, depending on the launcher type a pair of booster rockets will descent back to earth. With the help of scatter analyses the expected area of descent can be determined and be cleared for a while to minimize the risk of casualties or serious damage to property. After

touchdown the boosters can be picked up to prepare them for a next launch. Depending on the launch/travel scenario, debris in space may also exist, one should make sure that this debris does not form any hazard for any satellite orbiting the earth. After the EDL at Mars, only a parachute, a couple of air bag systems and thrusters will be left while all the fuel should have been burned up.

14.5 Cost analysis

A cost estimation is made based on reference Mars missions, especially MSL and future missions. Cost data is adjusted to fiscal year 2013 by US inflation[41]. A summary of past Mars lander missions can be found in Table 14.1

The idea of this project is to keep the costs low by using mostly proven technology. While having a mass similar to the MSL, at launch the mass is about equal to the launch mass of the MSL, the whole mission to get Zebros on Mars in expected to cost less than ExoMars. For the MSL the cost was greatly increased by missing the original launch date due to unacceptable technical risk. The 6 months slack planned in the Gantt chart is there to avoid these kind of costs altogether. Also in comparison to ExoMars this mission will have lower development costs, since the Zebro development is covered by other funds and all preliminary design work is already done by students. Therefore it is expected to be more in the range of the InSight and Geyser hopper mission costs, which also use mainly proven technology to keep the costs down, but because the mass of this mission will be slightly higher a cost estimate in the range of double an InSight mission seems fair and for a mission that would be allow unprecedented exploration possibilities this is a very reasonable cost.

Table 14.1: Cost comparison of previous and future Mars missions. Mission cost fiscal year is assumed to be launch year. S/C means spacecraft. *cost originally in euros, conversion factor €1 = $1.3543

Mission	Cost	Year	FY2013	Landed mass	Comments
Past missions					
Viking[43]	$1.0bn	1975	$4.3bn	1200 kg	Mission consisted of two 600 kg landers and two 900 kg orbiters
Pathfinder[31]	$265m	1997	$385m	264 kg	S/C development $150m, Rover $25m
MER[50]	$800m	2003	$1.0bn	539 kg	S/C development $625m, Launch $100m, Mission operations and processing $75m
Phoenix[51]	$457m	2007	$513m	343 kg	
MSL[69]	$2.5bn	2012	$2.5bn	899 kg	S/C development $1.8bn
Future missions					
InSight[49]	$425m	2013	$425m	350 kg	Cost is a cap, the costs are kept down by copying phoenix mission.
Geyser hopper[27]	$425m	2013	$425m	513 kg	Cost is a cap, the costs are kept down by copying phoenix mission
ExoMars[10]	$1.6bn*	2013	$1.6bn*	300 kg	
MACHETE	$850m	2014	$850m	1160 kg	

15 Conclusions and Recommendations

In this chapter, the conclusions and recommendations are presented. Conclusions are made for the project in general, as well as for the design of each subsystem. The recommendation section contains technical recommendations alongside recommendations for the planning of a future project.

15.1 Conclusions

The aim of this project is to research the technical feasibility of safely landing a swarm of Zebro's on the Martian surface. It is found that, within the limits of currently off-the-shelf and demonstrated technologies, it is possible to land a swarm of 224 Zebro's on Mars. With a total system mass of 3052 kg entering the atmosphere, and a total Zebro mass of 896 kg, the achieved payload ratio is 29%. The designed mission profile will be presented first. Conclusions involved with the technical design of each subsystem are presented in the subsequent paragraphs.

The mission profile is specifically designed to deliver a maximum payload within the required landing accuracy of 1 km around a target beacon; A steerable parachute is deployed at 7.5 km altitude. At an altitude of 2.5 km, eight rocket powered descent stages are deployed in pairs with 1.5 second intervals. Finally, each descent stage releases one package of 28 Zebro's, which is landed with a vented airbag system. Abbreviations are used to refer to each system; MACHETE for the first system, CAESAR for one rocket powered vehicle, and LADS for the landed airbag system.

As discussed with the customer, the MACHETE is sized such that the launch, interplanetary transfer, and hypersonic re-entry vehicles similar to that of the Mars science laboratory mission can be used. Consequently, for these phases, the technical feasibility is ensured and the development costs are minimized.

The mission is clustered after the MACHETE stage as opposed to after the CAESAR stage, because the former provides higher mission reliability. Furthermore, when landing eight systems in parallel instead of in series, more accurate and efficient landing spot determination can be performed. These advantages outweigh the mass penalty, which is in the order of few percent.

A ringsail parachute with a diameter of 20 m is required to give the MACHETE a terminal velocity of 100 m$\cdot$ s^{-1}. With AGAS, the US army's Affordable Guided Airdrop System, a glide range of 2 km can be achieved. Due to the entry uncertainty of 3.25 km and an estimated wind drift of 1 km, the required mission accuracy cannot be solely achieved by the parachute. It does, however, significantly reduce the fuel mass of the CAESAR stage.

Each CAESAR is deployed between a 2.5 and 2 km altitude, depending on its place in the release sequence. The system is sized to cope with an initial vertical velocity of 100 m$\cdot$ s^{-1} and a worst case navigation range of 2.25 km. With this profile, each of the four main thrusters is required to deliver a maximum thrust of 1200 N and provide a deep throttle setting to 5% of this.

Autonomous navigation and attitude control is provided by individually controlling the setting of each thruster. With differential thrusting, roll and pitch moments are created to point the fixed thrusters in the desired direction. Yaw rate control is facilitated by two dedicated smaller thruster pairs.

A bi-propellant combination of nitrous oxide and ethane is used in the main thrusters for both its high specific impulse and self pressurizing characteristic. Furthermore, its non toxic nature is in line with both the terrestrial and extraterrestrial sustainability goals.

A LADS is deployed at a 30 m altitude, resulting in a four second free fall. The inflation of the octagonal shaped vented airbags starts 1 second after release. In the remaining three seconds, four Cool Gas Generation tanks inflate the 5 m^3 airbag to a pressure of 12 kPa. Directly after impact the airbag will be entirely vented by means of eight 0.4 m^2 vents located on each section of the airbag. Vent control will be done using either a series of strain gages located on the bottom of the airbag or a radar/motion sensor on

top of the airbag. With this system the LADS can cope with 0.5 m high rocks and slopes up to 10 deg. Spectra 75 fibre is selected as the airbag material, as it provides the best puncture resistance under the low Martian atmospheric temperature. Also, it is shown that Zebro's can adequately crawl on this material after deployment.

Structural integrity during launch and re-entry, as well as release capabilities in MACHETE are provided by twelve vertical beams supported by sixteen horizontal rods. The rockets and fuel tanks are attached to a square shaped aluminium 7075-T6 I-beam structure that transfers the loads to the bottom plate. This bottom plate is an octagonal raster of I-beams covered by a magnesium plate. The Zebro's are packed in four columns of seven on the bottom plate with a magnesium top shell holding them in place. The airbag system is also attached to this bottom plate.

$LiFePO_4$ batteries are used to deliver 67 Wh at 2 kW to the MACHETE and 21 Wh at 425 W to each CAESAR. A $LiSOCl_2$ battery provides power to the LADS at 2 W for 17 mWh. Thermal protection of these batteries is secured by an aerogel insulated warm electronics box and by phase changing materials preventing overheating.

Communication to earth is relayed through the Mars orbiter by using an ultra high frequency antenna at a 512 kbps data rate. A low gain X-band antenna is installed as a direct link backup. To protect the electronic systems from bit flips, a triple voting algorithm is implemented. The communication equipment, as a post mission functionality, can be used for data relay by the Zebro swarm.

15.2 Recommendations

In the following paragraphs, several tests are recommended for each stage of the mission for validation purposes. Afterwards, a brief outline of a suggested future project is presented.

For the MACHETE stage it is recommended that the supersonic deployment of the parachute is tested in a supersonic windtunnel. The range and control of the steerable parachute can be validated by a high altitude atmospheric test. The CAESAR release sequence and specifically the risks of colliding has to be checked by extensively simulating this routine. The release mechanism should be physically tested.

For the CAESAR stage, it is recommended that a full size demonstrator is made, because the maximum thrust level is high enough to test hovering and some navigation on earth. In this sense, the beacon communication link can be tested together with the validation of the control stability, hardware, and software.

For the LADS stage, airbag inflation test have to be done to validate the inflation time. Also, it has to be verified that the inflated airbags do not come in contact rocket engine exhaust plumes. Furthermore, multiple airbag drop tests have to be done to validate the functioning of the vent system on various terrains.

The complete electronic power and data handling system should be tested in a thermal test facility. In this way, the performance of the warm electronic box and phase changing material can be validated.

For a future follow-up project, it is recommended that first the detailed design phase is concluded by translating the design into production drawings. Afterwards, manufacturing and mission planning should be started. A phase of assembly and execution of the proposed tests follows. When the design is validated, mission preparation can be started. Finally, the mission can be executed at the date picked in the mission planning.

Bibliography

[1] URL: http://www.iisd.org/sd/.

[2] URL: http://www2.sims.berkeley.edu/research/projects/how-much-info-2003/print.htm.

[3] URL: http://eetd.lbl.gov/paper/ideas/html/issues.htm.

[4] URL: http://www.mpoweruk.com/lithiumS.htm.

[5] URL: http://www.globalsecurity.org/military/systems/aircraft/systems/agas.htm.

[6] URL: http://www.european-test-services.net/services-mechanical-Hydra-Vibration.html.

[7] URL: http://www.aerosekur.com/Space/docs/2.mpg.

[8] AIAA. "Space Logistics Technical Committee: Space Logistics Definitions". In: (). URL: https://info.aiaa.org/tac/SMG/SLTC/Web%20Pages/Definitions.aspx.

[9] C. Akkermans. "Baseline report".

[10] J. Amos. "Europe's ExoMars missions 'on track'". In: *BBC News* (2013). URL: http://www.bbc.co.uk/news/science-environment-22914025.

[11] F. Amzajerdian et al. "Utilization of 3D imaging flash lidar technology for autonomous safe landing on planetary bodies". In: *OPTO*. International Society for Optics and Photonics. 2010, pp. 760828–760828. URL: http://proceedings.spiedigitallibrary.org/proceeding.aspx?articleid=746614.

[12] S. Bala. "Airbag Leakage Modeling in LSDYNA". In: *Livermore Software Technology Corporation* (2006).

[13] Y. Bar-Cohen et al. "Biomimetic Flying Swarm of Entomopters for Mars Extreme Terrain Science Investigations". In: *LPI Contributions*. NASA, 2012.

[14] E. M. Betts and R. A. Frederick Jr. "A Historical Systems Study of Liquid Rocket Engine Throttling Capabilities". In: (2010).

[15] B. Buyens. "Combustion characteristics of a nitrous oxide-ethane rocket engine". MA thesis. Delft University of technology, 2013.

[16] P. C. Calhoun and E. M. Queen. "ENTRY VEHICLE CONTROL SYSTEM DESIGN FOR THE MARS SMART LANDER". In: *AIAA Atmospheric Flight Mechanics Conference and Exhibit*. 5-8 August 2002, Monterey, California.

[17] J. Coffey. "Mars Dust Storm". In: *University Today* (2008).

[18] M. Dawson et al. "Monopropellant hydrazine 700 lbf throttling terminal descent engine for Mars Science Laboratory". In: *paper no. AIAA 2007-5481 presented at the 43rd AIAA/ASME/SAE/ASEE Joint Propulsion Conference and Exhibit. Cincinnati, OH, July* (2007), pp. 8–11.

[19] I. I. F. S. Development. *Business Strategy for Sustainable Development: Leadership and Accountability for the 90s*. World Business Council For Sustainable Development, 1992.

[20] I. Dover. "Mars Pathfinder & Mars Exploration Rover Airbags". In: *None* (Unknown).

[21] R. J. Doyle. *Autonomy Needs and Trends in Deep Space Exploration*. Tech. rep. DTIC Document, 2003.

[22] ectriFly. *ectriFly RimFire 50cc-65cc Brushless Motor*. URL: http://manuals.hobbico.com/gpm/gpmg4800-4805-manual.pdf.

[23] S. T. E.R. Lake and V. Drexelius. "A study of the role of pyrotechnic ssystem on the space shuttle program". In: *MCDONNELL DOUGLAS CORPORATION* (1973).

[24] European-Union. "Strategy For Sustainable Development". In: *EU Website* ().

[25] M. v. R. F.D. Andriessen. *SwAMP Vehicle*. Technical University of Delft, 2013.

[26] M. V. R. e. a. F.D. Andriessen. *MACHETE Vehicle*. Tech. rep. Delft University of Technology, 2013.

[27] S. J. O. Geoffrey A. Landis and M. McGuire. "Design Study for a Mars Geyser Hopper". In: *AIAA Aerospace Sciences Conference* (2012).

[28] G. Giovangrossi. "Vented AAirbag: a new promising technology for Mars Landers". In: *Aero Sekur* (2009).

[29] M. Golombek et al. "Rock size-frequency distributions on Mars and implications for Mars Exploration Rover landing safety and operations". In: *Journal of Geophysical Research: Planets (1991–2012)* 108.E12 (2003). URL: http://onlinelibrary.wiley.com/doi/10.1029/2002JE002035/full.

[30] K. C. Gonyea et al. "Aerodynamic Stability and Performance of Next-Generation Parachutes for Mars Descent". In: ().

[31] D. E. Grayzeck. "Mars Pathfinder". In: *none* (2013).

[32] H. Hargitai. "Mars Climate zone map based on TES data". In: *Planetologia* (2008).

[33] S. Harvey. "Planetary Seasons". In: *NASA, Educator Feutures* (2004).

[34] R. Herdy. "NITROUS OXIDE / HYDROCARBON FUEL ADVANCED CHEMICAL PROPULSION: DARPA CONTRACT OVERVIEW". In: *NASA Thermal & Fluids Analysis Workshop proceedings* (2006).

[35] C. Ho, N. Golshan, and A. Kliore. *Radio Wave Prpagation Handbook for Communication on and Around MArs*. Jet Propulsion Laboratory, National Aeronautics and Space Administration, 2002.

[36] Honeywell. "Honeywell Spectra Fiber". In: *None* (2013).

[37] Honeywell. "Honeywell spectra fiber capability guide brochure". In: *none* (2013).

[38] A. Hurlich. *Low Temperature Metals*. URL: http://www.bnl.gov/magnets/staff/gupta/Summer1968/0311.pdf.

[39] A. Karabeyoglu et al. "Modeling of N2O decomposition events". In: *AIAA* 4933 (2008), pp. 1–29.

[40] T. W. Knacke. *Parachute recovery systems design manual*. Tech. rep. DTIC Document, 1991.

[41] B. of Labor Statistics. "Consumer Price Index". In: *none* (2013). URL: http://www.bls.gov/cpi/home.htm.

[42] W. J. Larson and J. R. Wertz. *Space mission analysis and design*. Tech. rep. Torrance, CA (United States); Microcosm, Inc., 1992. URL: http://www.osti.gov/energycitations/product.biblio.jsp?osti_id7369177.

[43] R. D. Launius. *On Mars: Exploration of the Red Planet 1958-1978*. Ed. by C. J. Hamilton. National Aeronautics and Space Administration, 1984.

[44] Mathworks. *6DoF (Euler Angles)*. Mathworks. URL: http://www.mathworks.nl/help/aeroblks/6dofeulerangles.html.

[45] J. B. McKinney and C. H. Lowry. "Mars Precision Landing Using Guided Parachutes". In: *AIAA Annual Report* (2009).

[46] J. B. McKinney and C. H. Lowry. "Mars Precision Landing Using Guided Parachutes". In: *AIAA* 2983 (2009). URL: http://arc.aiaa.org/doi/pdf/10.2514/6.2009-2983.

[47] MOOG. URL: http://www.moog.com/products/propulsion-controls/spacecraft/components/thruster-valves/solenoid-actuated-thruster-valve/.

[48] NASA. "Greenspace". In: *Sustainable systems* (). URL: (%20http://www.nasa.gov/centers/ames/greenspace/sustainable-systems.html).

[49] NASA. "Insight". In: *none* (2014). URL: http://insight.jpl.nasa.gov/home.cfm.

[50] NASA. "Mars Exploration Rover Landings". In: *none* (2004). URL: http://marsrovers.jpl.nasa.gov/newsroom/merlandings.pdf.

[51] NASA. "Phoenix Landing". In: *none* (2008). URL: http://www.jpl.nasa.gov/news/press_kits/phoenix-landing.pdf.

[52] NASA. "Spacecraft: Airbags". In: *None* (Unknown). URL: http://marsrovers.jpl.nasa.gov/mission/spacecraft_edl_airbags.html.

[53] *NASA Tests Engine Technology for Landing Astronauts on the Moon*. NASA Newsroom, 2009. URL: http://www.nasa.gov/home/hqnews/2009/jan/HQ_09-005_Cryo_engine_test.html#.UrRX7-KoSPA.

[54] J. P. L. NASA. URL: http://marsrover.nasa.gov/home/.

[55] Nealson. "Biological contamination on MARS". In: (1992).

[56] NHS-England. "Sustainable Development Management Plan Guidance". In: *Sustainable Development Unit* ().

[57] M. G. D. Nicholas W. Brown. "Advanced Airbag Landing System for Planetary Landers". In: *AIAA* (2005).

[58] M. T. Z. Oded Aharonson and D. H. Rothman. "Statistics of Mars' topography from the Mars Orbiter Laser Altimeter:Slopes, correlations, and physical Models". In: *Department of Earth, Atmospheric and Planetary Sciences, Massachusetts Institute of Technology, Cambridge, Massachusetts* (2001).

[59] R. Prakash et al. "Mars Science Laboratory entry, descent, and landing system overview". In: *Aerospace Conference, 2008 IEEE*. IEEE. 2008, pp. 1–18.

[60] A. K. Richard Slade. "Design Optimization and Probalistic assement of a vented airbag landing system for the ExoMars Space Mission". In: *Altair ProductDesign* (2007).

[61] e. a. Saltelli. *Global sensitivity analysis: the primer*. Wiley. com, 2008.

[62] Scher. "Biological contamination of Mars. I. Survival of terrestrial microorganisms in simulated Martian environments." In: (1963). URL: http://www.ncbi.nlm.nih.gov/pubmed/11883443.

[63] R. Slade, A. Kiley, and V. Toropov. "Design Optimization and Probabilistic Assessment of a Vented Airbag Landing System for the ExoMars Space Mission". In: *Unknown* (2007).

[64] J. M. /. W. van Staveren / J.C. van der Vaart / E. de Weerdt / A.C. in t Veld / E. Mooij. *Flight Dynamics*. Delft University of Technology, 2013.

[65] C. Technologies. "Marslander Mars Airbag CGG Design". In: *CGG Technologies* (2013).

[66] *Test site explosion kills three* (2007). URL: http://articles.latimes.com/2007/jul/27/local/me-explode27.

[67] B. H. Thacker et al. *Concepts of model verification and validation*. Tech. rep. Los Alamos National Lab., Los Alamos, NM (US), 2004.

[68] W. Truszkowski et al. *Autonomous and Autonomic Systems: With Applications to NASA Intelligent Spacecraft Operations and Exploration Systems*. Springer, 2010.

[69] G. Webster. "Mars Science Laboratory Landing". In: *none* (2012). URL: http://www.jpl.nasa.gov/news/press_kits/MSLLanding.pdf.

[70] W. Weng, P. Taylor, and H. Savijarvi. "Modelling the martian boundary layer". In: *Mars Atmosphere Modelling and Observations*. Vol. 1. 2006, p. 123.

[71] G. Woan. "The Moon as a platform for radio telescopes: results of past ESA studies".

[72] E. M. Z. Papp. "Simulation, Veri?cation and Validation". Course Notes, February 2013.

[73] V. Zakirov et al. "Nitrous oxide as a rocket propellant". In: *Acta Astronautica* 48 (2001), pp. 353–362.

[74] B. Zandbergen. "Thermal rocket propulsion". In: *Delft University of Technology* (2003).